



Search for long-lived particles produced in pp collisions at $\sqrt{s} = 13$ TeV that decay into displaced hadronic jets in the ATLAS muon spectrometer

The ATLAS Collaboration

A search for the decay of neutral, weakly interacting, long-lived particles using data collected by the ATLAS detector at the LHC is presented. The analysis in this paper uses 36.1 fb^{-1} of proton–proton collision data at $\sqrt{s} = 13$ TeV recorded in 2015–2016. The search employs techniques for reconstructing vertices of long-lived particles decaying into jets in the muon spectrometer exploiting a two vertex strategy and a novel technique that requires only one vertex in association with additional activity in the detector that improves the sensitivity for longer lifetimes. The observed numbers of events are consistent with the expected background and limits for several benchmark signals are determined.

Contents

1	Introduction	3
2	ATLAS detector	3
3	Analysis strategy	5
4	Description of benchmark models	6
4.1	Scalar portal	7
4.2	Higgs portal baryogenesis	7
4.3	Stealth SUSY	8
5	Data and simulation samples	8
6	Trigger and event reconstruction	10
6.1	Reconstruction of prompt hadronic jets and missing transverse momentum	10
6.2	Muon RoI Cluster trigger	11
6.3	Reconstruction of MS vertices	11
6.3.1	Reconstructed objects for vertex isolation	12
7	Baseline event selection	13
8	Two-MS-vertex search	14
8.1	Event selection	15
8.2	MS vertex efficiency	15
8.3	Background estimation	16
9	Single-MS-vertex search	17
9.1	Event selection	17
9.1.1	1MSV _x +Jets strategy	17
9.1.2	1MSV _x + E_T^{miss} strategy	19
9.1.3	MS vertex efficiency	20
9.2	Background estimation	22
9.2.1	ABCD plane for 1MSV _x +Jets strategy	23
9.2.2	ABCD plane for 1MSV _x + E_T^{miss} strategy	23
10	Systematic uncertainties	25
10.1	Uncertainties in the signal predictions	25
10.2	Uncertainties in the background prediction	26
11	Results	27
12	Summary	31

1 Introduction

The discovery of the Higgs boson at the LHC completed the Standard Model (SM) of elementary particles and focused attention on the many central features of our universe that the SM does not address: dark matter (DM), neutrino mass, matter–antimatter asymmetry (baryogenesis), and the hierarchy problem (naturalness). Many Beyond the Standard Model (BSM) theoretical constructs proposed in the past few years that address these phenomena predict the existence of long-lived particles (LLPs) with macroscopic decay lengths that are limited only by Big Bang Nucleosynthesis to about $c\tau \lesssim 10^7\text{--}10^8$ m, where τ is the proper lifetime of the LLP [1]. Examples include: supersymmetric (SUSY) models such as mini split SUSY [2, 3], gauge-mediated SUSY breaking [4], R -parity-violating (RPV) SUSY [5, 6] and Stealth SUSY [7, 8]; models addressing the hierarchy problem such as Neutral Naturalness [9–12] and Hidden Valleys [13, 14]; models addressing dark matter [15–19], and the matter–antimatter asymmetry of the universe [20]; and models that generate neutrino masses [21, 22]. Many of these theoretical models result in neutral LLPs, which may be produced in the proton–proton collisions of the LHC and decay back into SM particles far from the interaction point (IP).

Searches for LLPs decaying into final states containing jets were carried out at the Tevatron ($\sqrt{s} = 1.96$ TeV) by both the CDF [23] and D0 [24] Collaborations, at the LHC by the ATLAS and LHCb Collaborations in proton–proton collisions at $\sqrt{s} = 7$ TeV [25, 26], by the ATLAS, CMS and LHCb Collaborations at $\sqrt{s} = 8$ TeV [27–32] and more recently by the CMS Collaboration at $\sqrt{s} = 13$ TeV [33]. To date, no search has observed evidence of BSM, neutral LLPs.

This paper describes a search for neutral LLPs produced in proton–proton interactions at $\sqrt{s} = 13$ TeV, using 36.1 fb^{-1} of data recorded by the ATLAS detector at the LHC during 2015 and 2016. Decays of LLPs can result in secondary decay vertices (displaced vertices) that are highly displaced from the IP. The present paper focuses on LLP decays reconstructed in the muon spectrometer. Three different analysis strategies are considered, with each strategy targeting a specific event topology. Two single-vertex strategies are based on methodologies presented in Ref. [34], and the third strategy is an inclusive search for two displaced vertices in the muon spectrometer.

This work significantly extends the mean proper lifetime ($c\tau$) range of the ATLAS search for a light scalar boson decaying into long-lived neutral particles beyond that at $\sqrt{s} = 8$ TeV in 20.3 fb^{-1} of 2012 proton–proton collision data [27], which covered the $c\tau$ region 1 to 100 m. Additionally, it extends the range of excluded proper lifetimes beyond that of a recent ATLAS analysis [30] that searches for displaced decays in the hadronic calorimeter and uses the same scalar boson model and mass points.

The paper first describes the ATLAS detector in Section 2, followed by the event selection strategy in Section 3, the benchmark models in Section 4, and the data and simulation samples in Section 5. The specialized trigger and reconstruction algorithms are discussed in Section 6, followed by a description of the baseline selection applied to all events in Section 7. The next two sections (8 and 9) outline the three search topologies. Systematic uncertainties are summarized in Section 10 and results for all three topologies are presented in Section 11. The summary and conclusions are given in Section 12.

2 ATLAS detector

The ATLAS detector [35], which has nearly 4π steradian coverage, is a multipurpose detector consisting of an inner tracking detector (ID) surrounded by a superconducting solenoid, electromagnetic and hadronic

calorimeters, and a muon spectrometer (MS) based on three large air-core toroidal superconducting magnets, each with eight coils. The ID covers the range $0.03 \text{ m} < r < 1.1 \text{ m}$ and $|z| < 3.5 \text{ m}$.¹ It consists of a silicon pixel detector, a silicon microstrip detector, and a straw-tube transition-radiation tracker. Together, the three systems provide precision tracking of charged particles for $|\eta| < 2.5$.

The calorimeter system covers the pseudorapidity range $|\eta| < 4.9$. It consists of a high-granularity lead/liquid-argon electromagnetic calorimeter (ECal) surrounded by a hadronic calorimeter (HCal). Within the region $|\eta| < 3.2$, the ECal comprises liquid-argon (LAr) barrel and endcap electromagnetic calorimeters with lead absorbers. An additional thin LAr presampler covering $|\eta| < 1.8$ is used to correct for energy loss in material upstream of the calorimeters. The ECal extends from 1.5 m to 2.0 m in r in the barrel and from 3.6 m to 4.25 m in $|z|$ in the endcaps. The HCal is a steel/scintillator-tile calorimeter that is segmented into three barrel structures within $|\eta| < 1.7$, and two copper/LAr hadronic calorimeters in the endcap ($1.5 < |\eta| < 3.2$). The HCal covers the region from 2.25 m to 4.25 m in r in the barrel (although the HCal active material extends only up to 3.9 m) and from 4.3 m to 6.05 m in $|z|$ in the endcaps. The solid angle coverage is completed with forward copper/LAr and tungsten/LAr calorimeter modules optimized for electromagnetic and hadronic measurements, respectively. Together the ECal and HCal have a thickness of 9.7 interaction lengths at $\eta = 0$.

The MS comprises three stations of separate trigger and tracking chambers that measure the deflection of muons in a magnetic field generated by the air-core toroid magnets. The barrel chamber system is subdivided into 16 sectors: 8 large sectors (between the magnet coils) and 8 small sectors (inside the magnet coils). Three stations of resistive plate chambers (RPC) and thin gap chambers (TGC) are used for triggering in the MS barrel and endcaps, respectively. The first two RPC stations, which are radially separated by 0.5 m, start at a radius of either 7 m (large sectors) or 8 m (small sectors). The third station is located at a radius of either 9 m (large sectors) or 10 m (small sectors). In the endcaps, the first TGC station is located at $|z| = 13 \text{ m}$. The other two stations start at $|z| = 14 \text{ m}$ and $|z| = 14.5 \text{ m}$, respectively. The muon trigger system covers the range $|\eta| < 2.4$. The muon tracking chamber system covers the region $|\eta| < 2.7$ with three layers of monitored drift tubes (MDT), complemented by cathode strip chambers (CSC) in the forward region. The MDT chambers consist of two multilayers separated by a distance ranging from 6.5 mm to 317 mm. Each multilayer consists of three or four layers of drift tubes. The individual drift tubes are 30 mm in diameter and have a length of 2–5 m depending on the location of the chamber in the spectrometer. In each multilayer the charged-particle track segment can be reconstructed by finding the line that is tangent to the drift circles. These segments are local measurements of the position and direction of the charged particle. Because the tubes are 2–5 m in length with a direction along ϕ , the MDT measurement provides only a very coarse ϕ position of the track hit. In order to reconstruct the ϕ position and direction, the MDT measurements are combined with the ϕ coordinate measurements from the trigger chambers.

The ATLAS trigger and data acquisition system [36] consists of a hardware-based first-level trigger (L1) followed by a software-based high-level trigger (HLT) that reduces the rate of recorded events for offline storage to 1 kHz.

The implementation of the L1 muon trigger logic is similar for both the RPC and TGC systems. Each of the three planes of the RPC system and the two outermost planes of the TGC system consist of a doublet of

¹ ATLAS uses a right-handed coordinate system with its origin at the nominal IP in the center of the detector and the z -axis along the beam pipe. The x -axis points from the IP to the center of the LHC ring, and the y -axis points upwards. Cylindrical coordinates (r, ϕ) are used in the transverse plane, where ϕ is the azimuthal angle around the z -axis. The pseudorapidity is defined in terms of the polar angle θ as $\eta = -\ln \tan(\theta/2)$. Angular distance is measured in units of $\Delta R \equiv \sqrt{(\Delta\eta)^2 + (\Delta\phi)^2}$.

independent detector layers. The first TGC plane contains three detector layers. A low- p_T (< 10 GeV) muon region-of-interest (RoI) is generated by requiring a coincidence of hits in at least three of the four layers of the two inner RPC planes for the barrel. In the endcaps, the trigger requires hits in the two outer TGC planes. A high- p_T muon RoI requires additional hits in at least one of the two layers of the outer RPC plane for the barrel, while for the endcaps, hits in two of the three layers of the innermost TGC layer are required. The muon RoIs have a spatial extent of 0.2×0.2 in $\Delta\eta \times \Delta\phi$ in the MS barrel and 0.1×0.1 in $\Delta\eta \times \Delta\phi$ in the MS endcaps. Only the two highest- p_T RoIs per MS sector are used by the HLT.

The L1 calorimeter trigger is based on information from the calorimeter elements within projective regions, called trigger towers. The trigger towers have a size of approximately 0.1 in $\Delta\eta$ and $\Delta\phi$ in the central part of the calorimeter, $|\eta| < 2.5$, and are larger and less uniform in the more forward region.

3 Analysis strategy

The analysis presented in this paper searches for events with two displaced vertices in the MS, or one displaced vertex in the MS in association with additional activity in the detector. Three separate strategies are studied, defined by the number of MS vertices and additional selection criteria. The benchmark models that motivate these strategies are discussed in detail in Section 4.

Candidate events are selected by the Muon RoI Cluster trigger [37] that requires a cluster of three (four) muon RoIs in the barrel (endcaps). No jet or track isolation requirements are applied at trigger level. Displaced vertices are then reconstructed using a dedicated MS vertex reconstruction algorithm [38].

The simplest strategy requires at least two MS vertices (2MSVx), and it is inclusive of any other activity in the event. The other two strategies require exactly one MS vertex, with additional requirements on associated objects (1MSVx+AO). The first requires exactly one MS vertex and two prompt jets (1MSVx+Jets), targeting models where prompt jets are produced together with the LLP, as expected in the Stealth SUSY scenarios. In these cases, the two prompt jets can also contribute to signal event selection. The second requires a small amount of missing transverse momentum (denoted by E_T^{miss}) in addition to the single displaced vertex (1MSVx+ E_T^{miss}) and targets models that do not predict significant activity in addition to LLPs, such as from decays of “SM-like” Higgs bosons into long-lived neutral scalar particle pairs. In fact, since the tracks originating from vertices in the MS are not considered in the E_T^{miss} computation, for these models the E_T^{miss} in signal events is sensitive to the Higgs boson p_T , which is typically of the order of tens of GeV. For signal vertices, if the second LLP has decayed in the ID or calorimeter the E_T^{miss} vector tends to be aligned with the direction of the displaced vertex, measured from the origin of the detector coordinate system. However, if the decay of the second LLP occur beyond the MS there is no missing energy. Therefore, the angle in the transverse plane between the vertex and the E_T^{miss} direction can contribute to the signal event selection. The three analysis strategies are summarized in Table 1, together with the theoretical benchmark models used in this paper.

The main source of background to LLPs decaying into hadronic jets in the MS is from hadronic or electromagnetic showers not contained in the calorimeter volume (*punch-through jets*) resulting in tracks reconstructed in the MS. Multijet events that contain vertices in the MS would have ID tracks and jets that point towards the displaced MS vertex as well as inwards to the IP. To reduce the acceptance of fake vertices from multijet events, vertices are required to be isolated from ID tracks and calorimeter jets. Additional background, referred to in this paper as *non-collision background*, can be generated by electronic noise in the MDT and RPC/TGC chambers, by cosmic-ray muons, by multijet events with mismeasured jets and by

Table 1: Topologies considered in this paper, corresponding basic event selection and benchmark models.

Strategy	Basic event selection	Benchmarks
2MSVx	At least 2 MS vertices	Scalar portal, Higgs portal baryogenesis, Stealth SUSY
1MSVx+Jets	Exactly 1 MS vertex At least 2 jets with $E_T > 150$ GeV	Stealth SUSY
1MSVx+ E_T^{miss}	Exactly 1 MS vertex $E_T^{\text{miss}} > 30$ GeV	Scalar portal with $m_\Phi = 125$ GeV, Higgs portal baryogenesis

machine-induced background [39]. This last contribution, usually referred to as *beam-induced background*, is composed of particles produced in the hadronic and electromagnetic showers caused by beam protons interacting with collimators or residual gas molecules inside the vacuum pipe.

To avoid unintended biasing of the results, the signal regions of the 2MSVx and 1MSVx+AO strategies were blinded during the analysis development.

4 Description of benchmark models

Although the event selections outlined in Section 3 are sensitive to a large variety of models, this paper interprets the results in terms of three different benchmark models. The first, shown in Figure 1(a), is a *scalar portal* model [14], where a SM-like Higgs or lower/higher-mass boson (Φ) decays into two long-lived scalars (s). Figure 1(b) shows the second model, *Higgs portal baryogenesis* [20], in which a SM-like Higgs boson (h) decays into long-lived Majorana fermions χ that decay into fermions, violating baryon and/or lepton number conservation. The last model, shown in Figure 1(c), is a *Stealth SUSY* model [7, 8] where the long-lived singlino (\tilde{S}) is produced by a gluino (\tilde{g}) in association with a prompt gluon-jet (g). The singlino decay produces two gluons and a light gravitino.

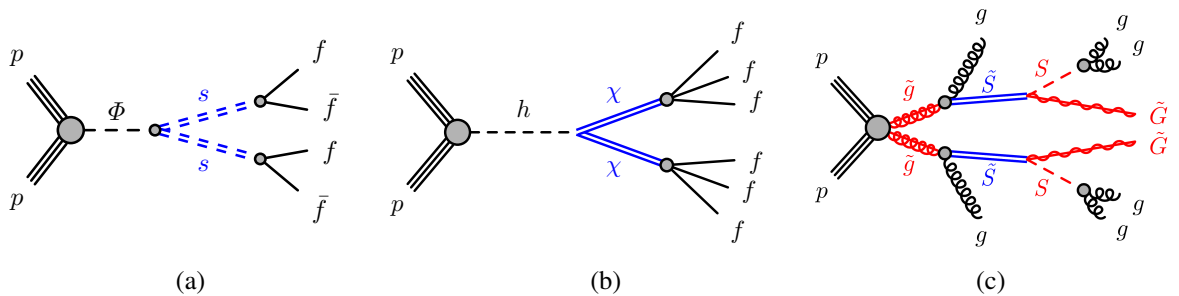


Figure 1: Diagrams of the benchmark models studied in this paper: (a) scalar portal model, (b) Higgs portal baryogenesis model, and (c) Stealth SUSY model. The LLPs in these processes are represented by double lines and labeled (a) s , (b) χ , and (c) \tilde{S} . In the Stealth SUSY model, \tilde{G} is the gravitino and S is the singlet. The final-state SM fermions are labeled as f , and the gluons as g .

The decay channels, the relative masses and lifetimes generated for each model, as well as details about the Monte Carlo (MC) event generation are described in Section 5.

4.1 Scalar portal

A theoretically popular way of introducing long-lived, neutral particles to the SM is through a hidden sector that weakly couples to the SM. For example, scalar (Higgs) portals [13, 14, 40], where the Higgs boson weakly mixes with a hidden-sector scalar, can result in pair production of hidden-sector scalars or pseudoscalars that carry no SM quantum numbers. The branching fraction limit for SM Higgs boson decays into undetected particles is currently at the 25% level [41] (assuming SM-like Higgs boson production and width), potentially allowing sizable branching fractions for decays into non-SM particles.

Moreover, models of neutral naturalness [42] are generic extensions of hidden-valley portal models where the scalar masses can be very low, typically 5 to 15 GeV. To date, no LHC analysis has explored this model.

The mechanism for LLP production in scalar decays is shown in Figure 1(a). Here, a scalar boson Φ decays with some effective coupling into a pair of long-lived scalars, s . The scalars s subsequently decay into SM particles. Since this model assumes that the couplings of the scalar to SM particles are determined by a Yukawa coupling, each long-lived scalar decays mainly into heavy fermions, $b\bar{b}$, $c\bar{c}$, and $\tau^+\tau^-$. The branching fractions of these decays depend on the mass of the scalar, m_s , but for $m_s \gtrsim 25$ GeV they are almost constant and equal to 85%, 5%, and 8%.

The branching fraction for Φ decaying into a pair of hidden-sector particles is not constrained in these models. It is therefore interesting to focus both on Higgs boson decays into LLPs, where Φ is a SM-like Higgs boson, and on other Φ mass regions previously unexplored for decays into LLPs.

4.2 Higgs portal baryogenesis

The origin of the cosmic asymmetric abundance of baryons remains one of the most prominent questions that demand physics beyond the SM. Several baryogenesis mechanisms have been proposed, but electroweak baryogenesis is one of the few with signatures that could be explored at the LHC energies. In addition to better testability, baryogenesis based on new weak-scale particles is also theoretically appealing since it can naturally connect new physics addressing the weak-scale hierarchy problem with the dynamics responsible for generating the baryon asymmetry. A few examples of low-scale (\lesssim TeV) baryogenesis models that generate the baryon asymmetry via the decays of weak-scale states have been shown to have direct testability at colliders [43–45].

In the baryogenesis model considered for this paper [20], the lowest-dimension operator coupling a singlet χ to the SM is the Higgs portal. The simplest realization of this interaction is with a scalar, Φ , that mixes with the SM Higgs boson [46]. If Φ has a Yukawa coupling to a pair of χ , this leads to the Higgs portal production of χ via exchange of a single SM-like Higgs boson after mixing, $pp \rightarrow h \rightarrow \chi\chi$, as shown in Figure 1(b). Since LHC experiments have established the existence of a SM-like Higgs boson with a mass of 125 GeV, while the other possibilities are more model-dependent, the model used here assumes the minimal spectrum where the Φ scalar is heavy and decouples, and focuses on the production channel via the SM Higgs portal.

For the production of the χ through the Higgs portal, two different regimes can be identified.

- $m_\chi < m_h/2$: in this region the dominant production mechanism is through an *on-shell* Higgs boson. The χ production at 13 TeV is expected to be copious, $O(10$ pb), and the constraints set by the current LHC searches are correspondingly strong. There are also indirect limits on the non-SM

decay branching fraction of the Higgs boson based on global fits [47, 48]. Despite all these strong constraints, the on-shell region is still very interesting due to the sizable branching fractions allowed for the Higgs decays into BSM particles [47, 48].

- $m_\chi > m_h/2$: in this region the Higgs boson is *off-shell* and the signal rate falls rapidly with increasing m_χ , even for large mixing. The cross section expected for a χ mass of 100 GeV is about 7 fb.

The decay modes of the χ must violate baryon and/or lepton number conservation, which generates the baryonic asymmetry. The lowest-dimensional interactions of this type allow χ to decay into three SM fermions. The decay channels used in this paper, $\chi \rightarrow \tau^+ \tau^- \nu_\ell$, $c b s$, $\ell^+ \bar{c} b$, $\nu b \bar{b}$, are examples of three types of couplings inspired by R -parity-violating SM fermion trilinear operators that can couple to χ [20]. The charge conjugates of these decay channels are also considered. Decays into final states as $c b b$ or $c s s$ are not possible since the R -parity-violating operator containing two down-type quarks with the same flavor is not allowed. Mixed cases such as $c b d$ or $c d s$ are possible, but they are not considered in this paper since their kinematics is similar to the $c b s$ channel and give similar results.

4.3 Stealth SUSY

Stealth SUSY models [7, 8] are a class of R -parity-conserving SUSY models that do not have large E_T^{miss} signatures. While this can be accomplished in many different ways, this search explores a model that involves adding a hidden-sector (stealth) singlet superfield S at the electroweak scale, which has a superpartner singlino \tilde{S} . By weakly coupling the hidden sector to the Minimal Supersymmetric Standard Model (MSSM) [49], the mass-splitting between S and \tilde{S} (δM) is small, assuming low-scale SUSY breaking. High-scale SUSY breaking also can be consistent with small mass splitting and Stealth SUSY, although this requires a more complex model and is not considered in this search [8].

The SUSY decay chain ends with the singlino decaying into a singlet plus a low-mass gravitino \tilde{G} , where the gravitino carries off very little energy and the singlet promptly decays into two gluons. The effective decay processes are $\tilde{g} \rightarrow \tilde{S} g$ (prompt), $\tilde{S} \rightarrow S \tilde{G}$ (not prompt), and $S \rightarrow g g$ (prompt), where the gravitino is treated as massless. This scenario results in one prompt gluon and two displaced gluons per gluino decay. Since R -parity is assumed to be conserved, each event necessarily produces two gluinos, resulting in two displaced vertices. A representative diagram of this process is shown in Figure 1(c). The simplified Stealth SUSY model considered in this paper assumes that all squarks are decoupled.

The decay width (and, consequently, the lifetime) of the singlino is determined by both the δM and the SUSY-breaking scale \sqrt{F} : $\Gamma_{\tilde{S} \rightarrow S \tilde{G}} \approx m_{\tilde{S}}(\delta M)^4/\pi F^2$ [7]. The SUSY-breaking scale \sqrt{F} is not a fixed parameter, and thus the singlino has the possibility of traveling an appreciable distance through the detector, leading to a significantly displaced vertex.

5 Data and simulation samples

The analysis presented in this paper uses $\sqrt{s} = 13$ TeV pp collision data recorded by the ATLAS detector with stable LHC beams during the 2015 and 2016 data-taking periods. After data quality requirements, the total integrated luminosity is 3.2 fb^{-1} and 32.9 fb^{-1} for 2015 and 2016, respectively.

Zero-bias data are used to estimate the expected background for the 2MSV_x strategy and potential contamination by non-collision background in the 1MSV_x+AO strategies. These data are acquired with a

Table 2: Mass parameters for the simulated scalar portal, Higgs portal baryogenesis, and Stealth SUSY models.

Model	m_ϕ [GeV]	m_s [GeV]
Scalar portal	100	8 , 25
	125	5 , 8 , 15 , 25 , 40
	200	8 , 25 , 50
	400	50 , 100
	600	50 , 150
	1000	50 , 150 , 400
<hr/>		
	m_χ [GeV]	χ decay channel
Higgs portal baryogenesis	10	
	30	$\tau^+ \tau^- \nu_\ell , c b s , \ell^+ \bar{c} b , \nu b \bar{b}$
	50	
	100	
<hr/>		
	$m_{\tilde{g}}$ [GeV]	$m_{\tilde{S}}, m_S$ [GeV]
Stealth SUSY	250	100 , 90
	500	
	800	
	1200	
	1500	
	2000	

special trigger which fires on the bunch crossing that occurs one LHC revolution after a low-threshold calorimeter-based trigger and therefore have a negligible signal contamination. The zero-bias trigger runs throughout ATLAS data taking, so these data are acquired with the same beam conditions present in normal physics data and can be used to study the expected background. Due to the very high output event rate, the zero-bias trigger is prescaled and only a fraction of the total events are recorded. For this reason, the integrated luminosity acquired is much lower than the total collected during 2015 and 2016 data taking and corresponds to $1.1 \mu\text{b}^{-1}$ and $12 \mu\text{b}^{-1}$ for the two periods, respectively.

Monte Carlo (MC) simulation samples were produced for all models considered in this paper. The masses, summarized in Table 2, were chosen to span the accessible parameter space. For the Stealth SUSY model, the singlino and singlet masses were set to 100 GeV and 90 GeV, respectively. These values were recommended by the authors of the model as a good representative choice [7]. The small mass-splitting between the singlino and singlet ensures that the gravitino carries off very little momentum. The *mean proper lifetime* of each sample is tuned to obtain a *mean lab-frame decay length* of 5 m. This choice maximizes the distribution of decays throughout the ATLAS detector volume. The mean proper lifetime used for the generation of the samples is within a range of 0.17–5.55 m, depending on the sample. For each MC sample, 400,000 events are produced.

Since the analysis is sensitive to a wide range of mean proper lifetimes, and the generation of many samples to cover a broad lifetime range would be extremely CPU-time consuming, a toy MC strategy was adopted to extrapolate the number of expected events to the range of mean proper lifetimes between 0 and 1000 m. For each LLP in the MC sample a random decay position sampled from an exponential distribution was generated. The physical decay position in the detector was then calculated for each particle using the LLP four-momenta from the simulated MC samples. The overall probability of the event to satisfy the selection

criteria was then evaluated from efficiencies to satisfy each selection criterion, parametrized as a function of the LLP decay position.

In order to validate the extrapolation procedure described above, another set of samples for only the scalar boson model with $m_s \geq 125$ GeV and with fewer (200,000) events was generated. The mean proper lifetime in each of these samples was tuned in order to have a slightly longer mean lab-frame decay length, corresponding to 9 m. The mean proper lifetimes in these MC samples span a range of 0.23–7.20 m, depending on the sample.

All MC samples described above were generated at leading order using MG5_aMC@NLO 2.2.3 [50] interfaced to PYTHIA 8.210 [51] parton shower model. The A14 set of tuned parameters [52] was used together with the NNPDF2.3LO parton distribution function (PDF) set [53]. The EVTGEN 1.2.0 program [54] was used for the properties of b - and c -hadron decays. The generated events were processed through a full simulation of the ATLAS detector geometry and response [55] using the GEANT4 [56] toolkit. The simulation includes multiple pp interactions per bunch crossing (pileup), as well as the effect on the detector response due to interactions from bunch crossings before or after the one containing the hard interaction. Pileup was simulated with the soft strong-interaction processes of PYTHIA 8.210 using the A2 set of tuned parameters [57] and the MSTW2008LO [58] PDF set. Per-event weights were applied to the simulated events to correct for inaccuracies in the pileup simulation.

6 Trigger and event reconstruction

Hadronic LLP decays in the MS typically produce narrow, high-multiplicity hadronic showers. Variations in track multiplicity and shower width depend on the mass and boost of the decaying LLP and the final states to which the LLP decays. Dedicated trigger [37] and vertex [38] algorithms were developed to select and reconstruct displaced decays in the MS. Due to the amount of material in the calorimeter, only decays occurring in or after the last sampling layer of the hadronic calorimeter will generally produce a significant number of hits in the MS and therefore were reconstructed.

6.1 Reconstruction of prompt hadronic jets and missing transverse momentum

Calorimeter jets with a E_T threshold greater than 10 GeV and $|\eta| < 4.9$ are constructed at the electromagnetic (EM) energy scale using the anti- k_t jet algorithm [59] with a radius parameter $R = 0.4$ using the FastJet 2.4.3 software package [60]. A collection of three-dimensional topological clusters of neighboring energy deposits in the calorimeter cells containing a significant energy above a noise threshold [61, 62] provide input to the anti- k_t algorithm. The calorimeter cell energies are measured at the EM scale, corresponding to the energy deposited by electromagnetically interacting particles. After reconstruction, jets are calibrated using the procedure outlined in Ref. [63].

The missing transverse momentum, E_T^{miss} , is defined as the magnitude of the negative vector sum of the transverse momenta of preselected electrons, muons, photons and jets, to which is added an extra term to account for energy deposits that are not associated with any of these selected objects [64]. This extra term was calculated from inner detector tracks matched to the PV to make it more resilient to contamination from pileup interactions. For the analysis presented in this paper, electrons, muons and photons were used only in the computation of E_T^{miss} , and their reconstruction is detailed in Refs. [65, 66]. Electrons were required to have a $p_T > 10$ GeV and $|\eta| < 2.47$ and also pass medium identification requirements [67].

Muons were required to have a $p_T > 10$ GeV and $|\eta| < 2.7$ with a matching track in the ID and pass a medium quality requirement [66]. Photons were selected using a tight identification requirement [68]. Since tracklets (defined in Section 6.3) are not used for the E_T^{miss} calculation, a displaced vertex from a signal event in the MS will contribute to the E_T^{miss} .

6.2 Muon RoI Cluster trigger

The Muon RoI Cluster trigger is a signature-driven trigger that selects candidate events for decays of LLPs particles in the MS: events must contain a cluster of muon RoIs within a $\Delta R = 0.4$ cone. The details of the performance and implementation of this trigger can be found in Ref. [37]. The isolation criteria for jets and tracks, discussed in Ref. [37] and used to reduce background punch-through jets, were not applied in the analysis presented in this paper. The trigger selects isolated, signal-like events and non-isolated, background-like events. The background-like events were then available to be used in control regions and for data-driven background estimations in signal regions.

The trigger efficiency, defined as the fraction of LLPs selected by the trigger as a function of the LLP decay position, is shown in Figure 2(a) and Figure 2(b) for four MC simulated benchmark samples with LLP decays in the MS barrel and endcap regions, respectively. The efficiency was parameterized as a function of the transverse decay position (L_{xy}) in the barrel and the longitudinal decay position ($|L_z|$) in the endcaps. The trigger is efficient for hadronic decays of LLPs that occur anywhere from the outer regions of the HCal to the middle stations of the MS. These efficiencies were obtained from the subset of events with only a single LLP decay in the muon spectrometer in order to ensure that the result of the trigger is due to a single burst of MS activity. The uncertainties shown are statistical only. The relative differences between the efficiencies of the benchmark samples are a result of the different masses of the LLPs, which in turn affect their momenta and consequently the opening angles of the decay products. The trigger efficiency is higher when the LLP decays close to the end of the hadronic calorimeter (barrel: $r \sim 4$ m, endcaps: $z \sim 6$ m) and it decreases substantially as the decay occurs closer to the middle station of the muon spectrometer (barrel: $r \sim 7$ m, endcaps: $z \sim 13$ m). For decays occurring close to the middle station, the charged hadrons and photons (and their EM showers) are not spatially separated and they are overlapping when they traverse the middle stations.

Scale factors were used in order to correct for mismodeling of the L1 muon trigger response in MC simulation and they were calculated by comparing the distributions of the average number of muon RoI clusters within a ΔR cone of 0.4 around the axis of a punch-through jet in multijet MC and data events. In fact, a high-energy jet has a high probability of punching through into the MS and creating a cluster of muon RoIs that can mimic the behavior of signal events. High-energy jets were selected using a jet trigger with a E_T threshold of 400 GeV. The scale factor is 1.13 ± 0.01 for the barrel and 1.04 ± 0.02 for the endcaps, and it does not depend on the η or the p_T of the jet.

6.3 Reconstruction of MS vertices

A dedicated algorithm [38], capable of reconstructing low-momentum tracks in a busy environment, was used to reconstruct the displaced MS vertices used in this search. The algorithm takes advantage of the spatial separation between the two multilayers inside a single MDT chamber. Single-multilayer straight-line segments that contain three or more MDT hits were reconstructed using a minimum χ^2 fit. Segments from multilayer-1 were then matched with those from multilayer-2. The paired set of single-multilayer

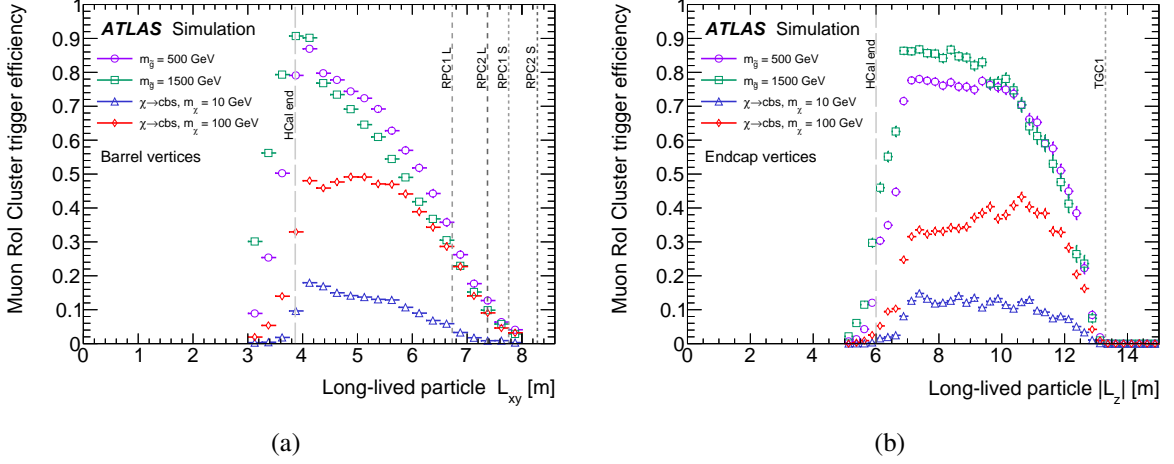


Figure 2: Efficiency for the Muon ROI Cluster trigger as a function of the decay position of the LLP for four simulated benchmark samples in the (a) MS barrel and (b) MS endcaps. The vertical lines show the relevant detector boundaries, where “HCal end” is the outer limit of the hadronic calorimeter, RPC 1/2 represent the first/second layer of RPC chambers, TGC 1 represents the first layer of TGC chambers and L/S indicate whether they are in Large or Small sectors.

segments and corresponding track parameters is called a *tracklet*. These tracklets are used to reconstruct the positions of MS vertices. This algorithm was previously used for both the 7 TeV [25] and 8 TeV [69] searches for displaced decays. Detectable decay vertices were located in the region between the outer edge of the HCal and the middle station of muon chambers. Due to the different detector technology (no spatially separated multilayers), the CSC chambers were not used for the MS vertex reconstruction.

6.3.1 Reconstructed objects for vertex isolation

In order to ensure sufficient signal acceptance and background rejection, a set of *vertex isolation criteria* for ID tracks and calorimeter jets was established in order to assist in determining whether or not a vertex is consistent with a displaced hadronic decay.

For track isolation, two separate criteria were used: one for high- p_T tracks which considers tracks with $p_T > 5$ GeV, and one for large multiplicities of low- p_T tracks which used the p_T vector sum of all tracks associated with the primary vertex (PV) with $p_T > 400$ MeV in a ΔR cone of 0.2 around the MS vertex axis². The two different isolations stem from the fact that some jets have most of their energy in a single hadron, while others can consist of multiple low- p_T tracks.

For the 2MSV χ and 1MSV χ +Jets strategies, all the jets considered for isolation must meet *jet quality criteria*. Jets must satisfy $E_T > 30$ GeV and $\log_{10}(E_{\text{HAD}}/E_{\text{EM}}) < 0.5$. The value $\log_{10}(E_{\text{HAD}}/E_{\text{EM}})$ quantifies the fraction of energy of the jet that is deposited in the HCal (E_{HAD}) with respect to the energy deposited in the ECal (E_{EM}). This requirement ensures that vertices originating from LLPs that decay near the outer edge of the hadronic calorimeter and also have significant MS activity were not rejected. In addition, in order to reduce the probability that a signal vertex fails to meet the isolation criteria due to pileup jets that do not have sufficient energy to create an MS vertex, jets with $20 < E_T < 60$ GeV

² The MS vertex axis is defined with respect to the detector coordinate system.

were required to be matched to the PV using a jet vertex tagger (JVT) discriminant [70]. Standard jet quality criteria [71] were not enforced because jets that do not fulfill these requirements can also produce a background MS vertex.

For the $1MSV_x + E_T^{\text{miss}}$ strategy a looser selection on the jets used for isolation was applied. The reason for this is that most of the background that enters the signal region of this strategy is generated by events where a jet satisfying the jet quality criteria is almost back-to-back with an MS vertex created by another jet that does not fulfill the jet quality criteria, but has enough energy to punch through into the muon spectrometer. Studies performed in data showed that there could be standard or pileup jets with a measured energy down to 15 GeV that can create a vertex in the MS. These jets would not be used to compute the isolation since they do not pass the E_T selection requirement present in jet quality criteria and the associated vertex would be incorrectly considered as a signal candidate. For these reasons, all jets above 15 GeV were considered in the isolation computation for the $1MSV_x + E_T^{\text{miss}}$ strategy. The looser selection on the jets used for isolation has negligible impact on the signal efficiency, according to simulation; in all the samples considered for the results presented in this paper there are no events rejected because of a jet below 20 GeV entering the isolation.

The same type of jet events could also affect the $2MSV_x$ and $1MSV_x + \text{Jets}$ strategies. For the former the jet quality criteria have no impact on the background estimation, while for the latter the effect is negligible because the additional selection on the energy of the two prompt jets strongly reduces this background contribution.

Vertex isolation criteria were optimized separately for each analysis strategy described in Section 3, and they are described in detail in Sections 8 and 9.

7 Baseline event selection

A common baseline selection was applied to the events considered in the three strategies described in Table 1. Events were required to pass the Muon RoI Cluster trigger and contain a PV with at least two tracks with $p_T > 400$ MeV. The vertex with the largest sum of the squares of the transverse momenta of all tracks associated with the vertex was chosen as the PV. This PV selection has no impact on the signal efficiency. In simulation, the selected PV corresponds to the signal interaction in about 95–99% of the cases, depending on the sample; even though the LLPs are invisible in the ID, the resonance (scalar, Higgs boson) is produced with a significant p_T .

An MS vertex due to a displaced decay typically has many more hits than an MS vertex from background; consequently a minimum number of MDT (n_{MDT}) and RPC/TGC ($n_{\text{RPC}}/n_{\text{TGC}}$) hits was required. The number of MDT hits was counted in the MDT chambers that have their center within $\Delta\phi = 0.6$ and $\Delta\eta = 0.6$ of the vertex (η, ϕ) position. The number of RPC or TGC hits is the sum of hits that are within $\Delta R = 0.6$ of the vertex position. A requirement on the maximum number of MDT hits was also applied to remove background events caused by coherent noise bursts in the MDT chambers. In addition to reducing the background, the minimum required number of RPC/TGC hits helps to further reject these noisy events, because a noise burst in the MDT system is not expected to be coherent with one in the muon trigger system.

A displaced decay that occurs in the transition region between MS barrel and endcaps results in hits in both regions. Vertex reconstruction was performed separately in the barrel and endcaps, and only the barrel (endcap) hits were used in the barrel (endcap) vertex reconstruction algorithm. Therefore, any vertices

reconstructed from either of the two algorithms have fewer hits, as they were reconstructed from a subset of the total hits. The result is a decrease in the reconstruction efficiency, and this also occasionally results in two vertices being reconstructed from a single LLP decay. Therefore, the MS vertices with pseudorapidity, $|\eta_{vx}|$, between 0.8 and 1.3 were not considered in the analysis. This has a negligible impact on the signal efficiency, since the average MS vertex efficiency in this region is less than 2%.

Background studies performed for the 1MSV_x+AO strategies using data showed that in the transition region between the barrel and the endcap hadronic calorimeters, $0.7 < |\eta_{vx}| < 1.2$, the probability of having a jet that does not fulfill the minimal selection criteria for being considered for isolation and that punches through into the MS is much higher than in other regions of the detector. This region overlaps the already excluded MS transition region, except for $0.7 < |\eta_{vx}| < 0.8$. The fraction of signal events removed was very small compared to the gain obtained by removing punch-through jet background that could affect the single-vertex analysis; therefore, vertices reconstructed in the MS region $0.7 < |\eta_{vx}| < 0.8$ were not considered either.

Table 3 summarizes the baseline criteria used to select “good” MS vertices.

Table 3: Summary of the baseline criteria used for the analysis presented in this paper. All selection criteria are also applied to signal MC events when determining the number of expected signal events in the dataset.

Event passes Muon RoI Cluster trigger	
Event has a PV with at least two tracks with $p_T > 400$ MeV	
Event has at least one MS vertex	
MS vertex matched to triggering muon RoI cluster ($\Delta R(\text{vertex}, \text{cluster}) < 0.4$). For 2MSV _x strategy: in the case of 2 muon RoI clusters, the second vertex should be matched to the second cluster.	
$300 \leq n_{\text{MDT}} < 3000$	
<i>Barrel</i>	<i>Endcaps</i>
MS vertex with $ \eta_{vx} < 0.7$ $n_{\text{RPC}} \geq 250$	MS vertex with $1.3 < \eta_{vx} < 2.5$ $n_{\text{TGC}} \geq 250$

8 Two-MS-vertex search

The two-MS-vertex strategy is designed to be sensitive to models where the LLP is pair-produced and decays hadronically between the outer region of the HCal and the middle station of the MS. Requiring two displaced vertices significantly reduces the expected background. In addition, background from punch-through jets was further reduced using the isolation criteria described in Section 6.3.1.

Residual background can arise from collision or non-collision processes and cannot be accurately simulated. Thus, data-driven methods were used to estimate the expected background, which also avoids systematic uncertainties due to the use of simulated events.

8.1 Event selection

In order to improve the rejection of background from punch-through jets, the isolation criteria using the reconstructed objects described in Section 6.3.1 were optimized for all the benchmark samples considered in this paper by comparing signal with multijet simulated events. The isolation criteria used for the 2MSVx strategy are summarized in Table 4, where ΔR is defined as the angular distance between the direction of the tracks or jets and the vertex axis. An MS vertex with tracks and/or jets satisfying these criteria was not considered in the analysis.

Table 4: Summary of the isolation criteria used to select signal events for the 2MSVx strategy in the barrel and endcaps regions. ΔR is defined as the angular distance between the direction of the tracks or jets and the vertex axis. MS vertices satisfying these criteria were not considered in the analysis.

Isolation requirements for 2MSVx strategy	Barrel	Endcaps
High- p_T track isolation, ($p_T > 5$ GeV)	$\Delta R < 0.3$	$\Delta R < 0.6$
Low- p_T track isolation, ($\Sigma p_T(\Delta R < 0.2)$)	$\Sigma p_T < 10$ GeV	$\Sigma p_T < 10$ GeV
Jet isolation	$\Delta R < 0.3$	$\Delta R < 0.6$

At least two isolated MS vertices must be present in the events. One MS vertex must be matched to the trigger-level muon RoI cluster [$\Delta R(\text{cluster}, \text{vertex}) < 0.4$]. If there were two distinct clusters, each MS vertex must be matched to one cluster. To ensure that the two MS vertices and/or two muon RoI trigger clusters do not come from the *same* background activity, the two vertices were required to be separated by at least $\Delta R = 1.0$, which has minimal impact on the overall signal acceptance.

8.2 MS vertex efficiency

The efficiency for vertex reconstruction is defined as the fraction of simulated LLP decays in the MS fiducial volume which match a reconstructed vertex passing the baseline event selection and satisfying the vertex isolation criteria [38]. A reconstructed vertex is considered matched to a displaced decay if the vertex is within $\Delta R = 0.4$ of the simulated decay position. The MS vertex efficiency was parameterized as a function of the transverse (L_{xy}) and longitudinal ($|L_z|$) LLP decay position in the barrel and endcaps, respectively. Figure 3(a) shows the efficiency for reconstructing a vertex in the MS barrel for a selection of benchmark samples. Figure 3(b) shows the efficiency for reconstructing a vertex in the MS endcaps.

The MS barrel vertex reconstruction efficiency is 30–40% near the outer edge of the hadronic calorimeter ($r \approx 4$ m) and it decreases substantially as the decay occurs closer to the middle station ($r \approx 7$ m). The decrease occurs because the charged hadrons and photons are not spatially separated and overlap when they traverse the middle station. This results in a reduction of the efficiencies for tracklet reconstruction and, consequently, vertex reconstruction. The efficiency for reconstructing vertices in the MS endcaps reaches 70% for higher-mass benchmark models. Because there is no magnetic field in the region in which endcap tracklets are reconstructed, the vertex reconstruction algorithm does not have the constraints on charge and momentum that are present in the barrel. Consequently, the vertex reconstruction in the endcaps is more efficient for signal, but also less robust in rejecting background events. More details are provided in Ref. [38].

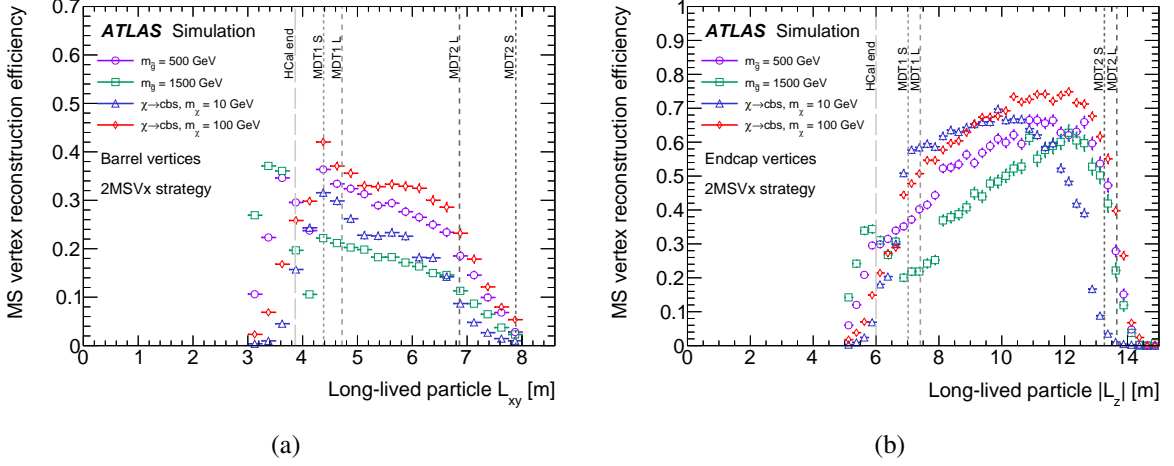


Figure 3: Efficiency to reconstruct an MS vertex for some of the Stealth SUSY and baryogenesis benchmark samples, for vertices that pass the baseline event selection and satisfy the vertex isolation criteria (no trigger selection is applied). (a): Barrel MS vertex reconstruction efficiency as a function of the transverse decay position of the LLP. (b): Endcap MS vertex reconstruction efficiency as a function of the longitudinal decay position of the LLP relative to the center of the detector. The vertical lines show the relevant detector boundaries, where “HCal end” is the outer limit of the hadronic calorimeter, MDT 1/2 represent the first/second layer of MDT chambers and L/S indicate whether they are in Large or Small sectors.

8.3 Background estimation

To estimate the expected background for the 2MSVx strategy it is necessary to quantify the frequency with which the MS vertex algorithm reconstructs isolated vertices for non-signal events. This number can be calculated from data using events with one isolated MS vertex which pass either the Muon RoI Cluster trigger or a zero-bias trigger. The expected background with two isolated MS vertices is calculated as follows:

$$N_{2Vx} = N^{1cl} \cdot P_{noMStrig}^{Vx} + N_{IUMBcl}^{2cl} \cdot P_{Bcl}^{Vx} + N_{IUMEcl}^{2cl} \cdot P_{Ecl}^{Vx}.$$

The events selected by the Muon RoI Cluster trigger and containing only one MS vertex are separated into those containing only one cluster of muon RoIs (N^{1cl}), and those containing two muon RoI clusters, where only one cluster is matched to the reconstructed MS vertex and the other is unmatched in the barrel or endcaps ($N_{IUMBcl}^{2cl}, N_{IUMEcl}^{2cl}$). The term $P_{noMStrig}^{Vx}$ is the probability of finding a vertex in events not selected by the Muon RoI Cluster trigger. This probability is determined from zero-bias events by dividing the number of good, isolated MS vertices not passing the muon RoI Cluster trigger by the total number of zero-bias events that satisfy standard event quality criteria. The terms P_{Bcl}^{Vx} and P_{Ecl}^{Vx} are the probabilities for finding an MS vertex given a muon RoI cluster in the barrel and endcaps, respectively. Since zero events are observed with two trigger clusters and one vertex, the contribution of the N^{2cl} terms is negligible.

Therefore, the number of two-MS-vertex events can be calculated as $N_{2Vx} = N^{1cl} \cdot P_{noMStrig}^{Vx}$.

Six good isolated MS vertices were found in 35,673,956 zero-bias triggered events, while 159,816 events with one isolated muon RoI cluster matched to a vertex were selected in the 2015 and 2016 datasets. The zero-bias sample has no overlap with the Muon RoI Cluster triggered events and contains zero events with more than one MS vertex. Contamination from signal events would result in overestimation of the probabilities and resulting background rates. The probability $P_{noMStrig}^{Vx}$ is thus estimated to be $6/35,673,956 = (1.7 \pm 0.7) \times 10^{-7}$,

where the uncertainty is statistical only. Therefore, the expected number of background events with one trigger cluster and two vertices is evaluated as $(159,816 \pm 400) \cdot (1.7 \pm 0.7) \times 10^{-7} = 0.027 \pm 0.011$, where the uncertainty is statistical only.

9 Single-MS-vertex search

For models with two LLPs, the probability of having both LLPs decay inside the detector decreases for mean lab-frame decay lengths greater than ~ 5 m. Thus, extending sensitivity to shorter and longer proper lifetimes for a given model also requires a strategy of using only one reconstructed displaced decay [34]. In the regime of long lifetimes the single-vertex analysis in the MS has unique sensitivity compared to other displaced searches, although it is affected by higher levels of background. For a search with only one displaced object, a background determination method similar to the two-vertex search does not work since the ensemble of events with one isolated vertex, used to estimate the background, already contains the signal region for the 1MSV_x+AO strategies. Instead, non-isolated vertices are used in a data-driven method to estimate the expected number of isolated fake vertices.

The following sections describe the event selection and background estimation for the 1MSV_x+Jets and 1MSV_x+ E_T^{miss} strategies. The events considered in these searches must satisfy the baseline selection criteria summarized in Section 7.

9.1 Event selection

Two separate signal selections are used for the two topologies that are considered in the single-MS-vertex search.

9.1.1 1MSV_x+Jets strategy

The main criterion that is used to distinguish a signal MS vertex from background is its degree of isolation as described in Section 8.1. To characterize the degree of isolation with a single value, the variable $\Delta R_{\text{min}} = \min(\Delta R(\text{vertex}, \text{closest jet}), \Delta R(\text{vertex}, \text{closest track}))$ was defined. Figures 4(a) and 4(b) show the distributions of the isolation variable used for 1MSV_x+Jets events for data and some of the MC benchmark samples for barrel and endcap vertices, respectively.

Another signal selection variable is the sum of the number of MDT hits and trigger hits (RPC and TGC in the barrel and endcaps, respectively) in a cone around an MS vertex, since a signal event is expected to leave more hits than a background one. Figures 5(a) and 5(b) present the distributions of the number of MS hits variable used for the 1MSV_x+Jets strategy for data collected during 2015 and 2016 and for some of the MC benchmark samples for barrel and endcap vertices, respectively.

Moreover, the two prompt jets produced by the gluino decays can be used to improve the signal selection for the Stealth SUSY analysis. The second-highest (subleading) jet E_T is generally above 150 GeV, though applying this requirement results in some loss of signal efficiency in the lowest-mass gluino sample ($m_{\tilde{g}} = 250$ GeV). For events with a barrel MS vertex the E_T of the leading and subleading jets was required to be above 150 GeV, while for events with an endcap MS vertex, a tighter requirement of 250 GeV was chosen due to the higher levels of background. Since the isolation variable depends on the ΔR between

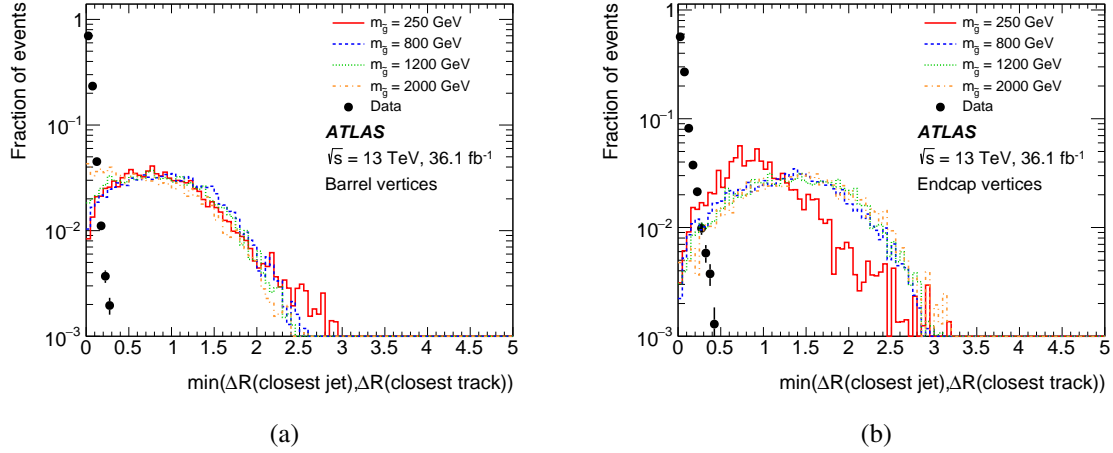


Figure 4: Distributions of the isolation variable used to select signal events for the 1MSV_x+Jet strategy, for the (a) barrel and (b) endcaps. The black points are data collected in 2015 and 2016, while the dashed and solid lines show the distributions for four of the MC Stealth SUSY signal samples. The events in the plots satisfy the baseline selection criteria described in Section 7. Distributions are normalized to unity.

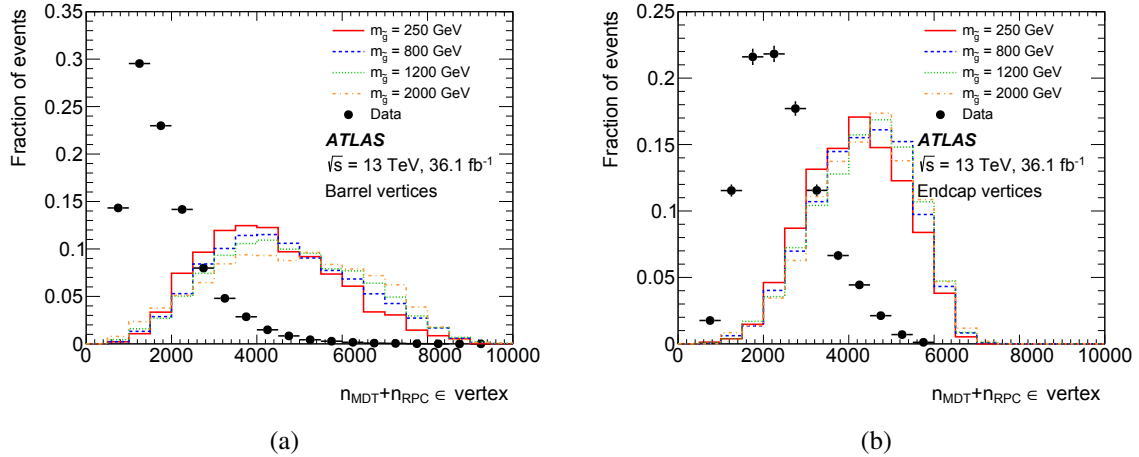


Figure 5: Distributions of the number of MS hits associated with the displaced vertex, used to select signal events for the 1MSV_x+Jet strategy, for the (a) barrel and (b) endcaps. The black points are data collected in 2015 and 2016, while the dashed and solid lines show the distributions for four of the MC Stealth SUSY signal samples. The events in the plots satisfy the baseline selection criteria described in Section 7. Distributions are normalized to unity.

a jet and the vertex, jets chosen for this selection must have $\Delta R(\text{jet}, \text{vertex}) > 0.7$. This prevents the selection of a sample containing punch-through jets that leave a vertex in the MS. In signal events, this requirement has minimal effect, since jets and vertices originate from different particles and thus tend to be well-separated. In data events, the main background is from multijet production, and thus if a jet is near a vertex it is generally well within $\Delta R = 0.7$. The selection on the two prompt jets described above is used to define two regions: one signal-dominated, and one background-dominated used to validate the data-driven background estimation.

The signal selection for the 1MSV_x+Jets strategy was optimized by examining the signal acceptance and background rejection using data from the background-dominated region defined by the E_T values of the two prompt jets. The minimum values required for isolation ΔR_{min} are 0.3 and 0.4 for the barrel and endcaps,

respectively; a minimum of 2000 MDT+RPC hits in the barrel and 2500 MDT+TGC hits in the endcaps is required. Table 5 summarizes the signal selection for the 1MSV_x+Jets strategy.

Table 5: Summary of the signal selection for the 1MSV_x+Jets strategy. An MS vertex satisfying these criteria is selected.

Event passes baseline selection	
<i>Barrel</i>	<i>Endcaps</i>
$n_{\text{MDT}} + n_{\text{RPC}} > 2000$	$n_{\text{MDT}} + n_{\text{TGC}} > 2500$
$\Delta R_{\text{min}} > 0.3$	$\Delta R_{\text{min}} > 0.4$
Two jets with $E_{\text{T}} > 150$ GeV, $\Delta R(\text{jet}, V_x) > 0.7$	Two jets with $E_{\text{T}} > 250$ GeV, $\Delta R(\text{jet}, V_x) > 0.7$

9.1.2 1MSV_x+ $E_{\text{T}}^{\text{miss}}$ strategy

The one-vertex searches for the scalar portal model with $m_{\phi} = 125$ GeV and the Higgs portal baryogenesis model are particularly challenging due to the absence of any distinctive associated objects produced with the LLPs, such as the two prompt jets in the Stealth SUSY model.

All the events used for the 1MSV_x+ $E_{\text{T}}^{\text{miss}}$ strategy are required to have a $E_{\text{T}}^{\text{miss}} > 30$ GeV, and in the endcaps, only vertices with at least five tracklets are considered, which further reduces the higher level of background present in this region.

The same isolation variable, ΔR_{min} , defined for the 1MSV_x+Jets strategy, is also used to select signal events for the 1MSV_x+ $E_{\text{T}}^{\text{miss}}$ strategy, although for the latter the isolation criteria are computed while placing a looser selection on the jets, as described in Section 6.3.1. Figures 6(a) and 6(b) show the distributions of the isolation variable used for the 1MSV_x+ $E_{\text{T}}^{\text{miss}}$ strategy for data and some of the MC benchmark samples for barrel and endcap vertices, respectively.

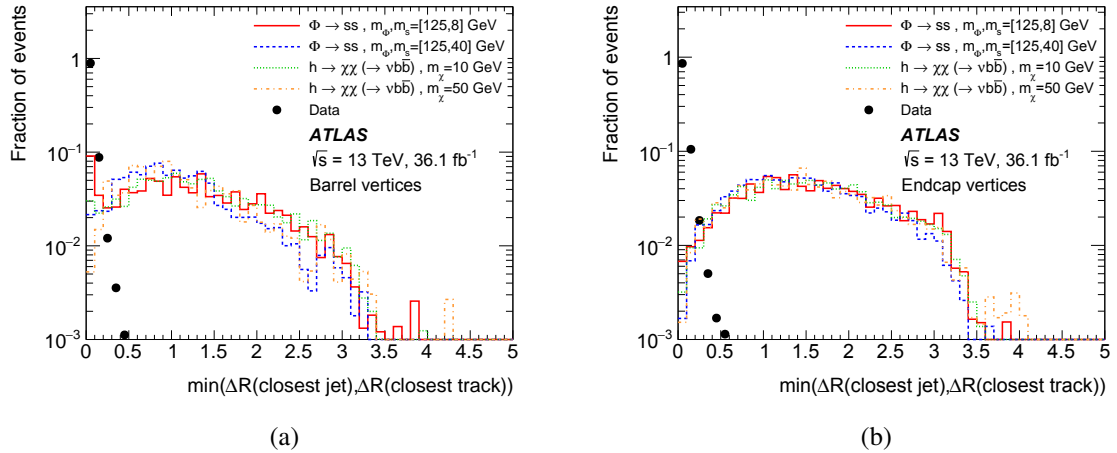


Figure 6: Distributions of the isolation variable used to select signal events for the 1MSV_x+ $E_{\text{T}}^{\text{miss}}$ strategy, for the (a) barrel and (b) endcaps. The black points are data collected in 2015 and 2016, while the solid lines show the distributions for four MC signal samples. The events in the plots satisfy the baseline selection criteria described in Section 7 and have $E_{\text{T}}^{\text{miss}} > 30$ GeV. Distributions are normalized to unity.

The angle in the transverse plane between the E_T^{miss} vector and the direction of the displaced vertex measured from the origin of the detector coordinate system, $|\Delta\phi(E_T^{\text{miss}}, \text{MSV}_x)|$, was also used to distinguish signal from background because for signal vertices the E_T^{miss} vector tends to be aligned with the direction of the displaced vertex. Figures 7(a) and 7(b) report the distributions of the $|\Delta\phi(E_T^{\text{miss}}, \text{MSV}_x)|$ variable, used to select signal events for the $1\text{MSV}_x + E_T^{\text{miss}}$ strategy, for data and some of the MC benchmark samples for barrel and endcap vertices, respectively.

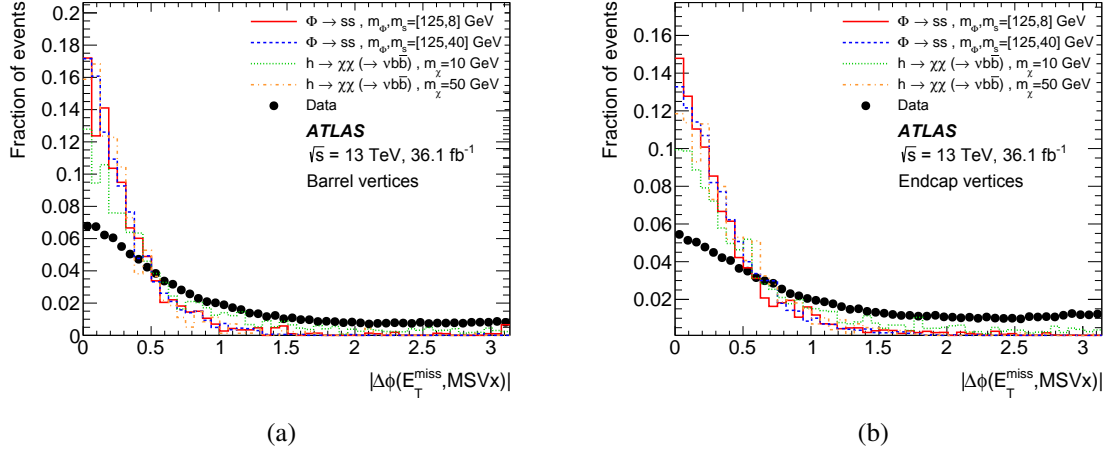


Figure 7: Distributions of the angle in the transverse plane between the E_T^{miss} and the displaced vertex $|\Delta\phi(E_T^{\text{miss}}, \text{MSV}_x)|$ used to select signal events for the $1\text{MSV}_x + E_T^{\text{miss}}$ strategy, for the (a) barrel and (b) endcaps. The black points are data collected in 2015 and 2016, while the dashed and solid lines show the distributions for four MC signal samples. The events in the plots satisfy the baseline selection criteria described in Section 7 and have $E_T^{\text{miss}} > 30$ GeV. Distributions are normalized to unity.

The number of MDT hits and trigger hits (RPC and TGC hits in the barrel and endcaps, respectively) in a ΔR cone around the MS vertex was used to define one signal-dominated region and one background-dominated region that was used to validate the data-driven background estimation. The selection requirements that define the two regions were optimized in order to ensure a sufficient signal acceptance and background rejection. For events with a barrel MS vertex the number of hits ($n_{\text{MDT}} + n_{\text{RPC}}$) is required to be greater than 1200, while for events with an endcap MS vertex, the number of hits ($n_{\text{MDT}} + n_{\text{TGC}}$) must exceed 1500.

The signal region selection for the $1\text{MSV}_x + E_T^{\text{miss}}$ strategy was optimized using signal acceptance versus background rejection estimated from data in the background-dominated region. The selection requires values of at least 0.8 for isolation ΔR_{min} and 1.2 for $|\Delta\phi(E_T^{\text{miss}}, \text{MSV}_x)|$, for both the barrel and endcaps. Due to the higher levels of background, the selection requirement imposed on the isolation is stricter than the ones used for the $1\text{MSV}_x + \text{Jets}$ strategy. Table 6 summarizes the signal selection for the $1\text{MSV}_x + E_T^{\text{miss}}$ strategy.

9.1.3 MS vertex efficiency

The efficiency for vertex reconstruction is defined as the fraction of simulated LLP decays in the MS fiducial volume which match a reconstructed vertex satisfying the signal selection criteria. A reconstructed vertex is considered matched to a displaced decay if the vertex is within $\Delta R = 0.4$ of the simulated decay position. Figures 8(a) and 8(b) show the efficiency for reconstructing a vertex for a selection of benchmark samples in the MS barrel and endcaps, respectively. Vertices selected for the Stealth SUSY and

Table 6: Summary of the signal selection for the $1MSV_x + E_T^{\text{miss}}$ strategy. An MS vertex satisfying these criteria is selected.

Event passes baseline selection	
$E_T^{\text{miss}} > 30 \text{ GeV}$	
$ \Delta\phi(E_T^{\text{miss}}, MSV_x) < 1.2$	
$\Delta R_{\text{min}} > 0.8$	
<i>Barrel</i>	<i>Endcaps</i>
$n_{\text{MDT}} + n_{\text{RPC}} > 1200$	$n_{\text{MDT}} + n_{\text{TGC}} > 1500$
	$n_{\text{tracklets}} \geq 5$

baryogenesis benchmark samples must satisfy the signal selection criteria described in Sections 9.1.1 and 9.1.2, respectively (no trigger selection is applied). The behavior of the MS vertex reconstruction efficiency as a function of the LLP proper lifetime is similar to that shown in Figure 3, although the efficiency values are different due to the different event selection. The MS barrel vertex reconstruction efficiency is 15–25% near the outer edge of the hadronic calorimeter ($r \approx 4 \text{ m}$) and it substantially decreases as the decay occurs closer to the middle station ($r \approx 7 \text{ m}$). The efficiency for reconstructing vertices in the MS endcaps reaches 40% for baryogenesis and Stealth SUSY high-mass gluino benchmark models. The lower efficiency for the Stealth SUSY sample with $m_{\tilde{g}} = 500 \text{ GeV}$ is due to the selection requirement on the E_T values of the two prompt jets, which is not optimal for the lower masses.

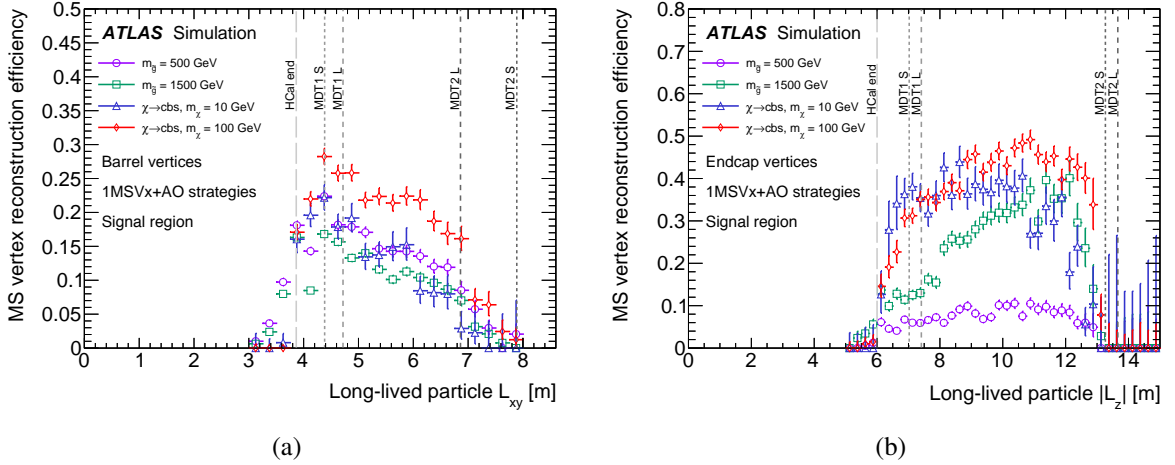


Figure 8: Efficiency to reconstruct an MS vertex for some of the Stealth SUSY and baryogenesis benchmark samples, for vertices that satisfy the signal selection criteria for the $1MSV_x + AO$ strategies (no trigger selection is applied). (a): Barrel MS vertex reconstruction efficiency as a function of the transverse decay position of the LLP. (b): Endcap MS vertex reconstruction efficiency as a function of the longitudinal decay position of the LLP. The vertical lines show the relevant detector boundaries.

9.2 Background estimation

The ABCD method developed for the $1MSV_X+AO$ strategies uses two, uncorrelated vertex-based variables to create a two-dimensional plane that is split into four parts: region A is where most signal events are located, and three control regions (B, C, and D) that contain mostly background. The number of background events in A can be predicted from the population of the other three regions: $N_A = N_B \times N_C / N_D$, assuming negligible leakage of signal into regions B, C and D. This calculation is performed in two separate regions: one background-dominated validation region (VR) and one signal region (SR). Two different ABCD planes were defined for the $1MSV_X+Jets$ and $1MSV_X+E_T^{miss}$ strategies. Figures 9(a) and 9(b) show the distribution of barrel vertices for data in the ABCD plane and the definition of the four subregions for the $1MSV_X+Jets$ and $1MSV_X+E_T^{miss}$ strategies, respectively.

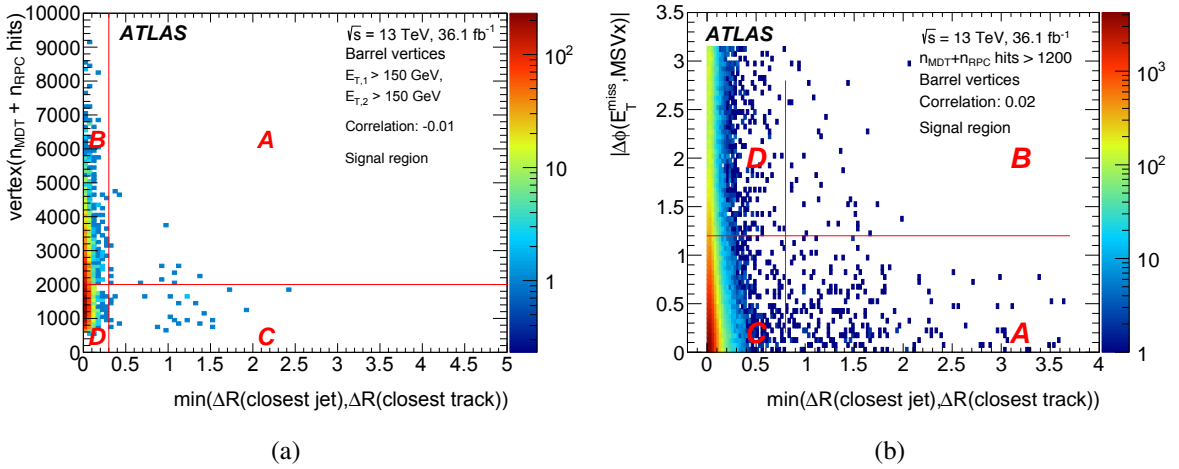


Figure 9: Distribution of barrel vertices in the ABCD plane for the SR and the definition of the four subregions for the (a) $1MSV_X+Jets$ strategy and (b) $1MSV_X+E_T^{miss}$ strategy.

The ABCD method relies on there being only one source of background, or multiple sources that have identical distributions in the ABCD plane. In general, non-collision background, which does not originate from the pp interaction point, will have a different distribution in the ABCD plane. To determine the non-collision background contamination, data collected in LHC empty bunch crossings throughout the 2016 data-taking period were used to estimate the number of non-collision background vertices in coincidence with events otherwise satisfying the single-vertex selection criteria. The empty bunch crossing trigger was not available in 2015, but the non-collision background's relative contribution is expected to be the same. The fraction of expected non-collision background vertices passing the final signal selection is negligible for the $1MSV_X+Jets$ strategy while for the $1MSV_X+E_T^{miss}$ strategy it corresponds to 0.8% (0.6%) of the total number of background events expected in the SR in the barrel (endcaps). Non-collision background events are equally distributed in the ABCD plane and they are taken into account as a systematic uncertainty.

Signal contamination in the VR, which can bias the ABCD method validation, was tested and found to be negligible for both the $1MSV_X+Jets$ and $1MSV_X+E_T^{miss}$ strategies.

9.2.1 ABCD plane for 1MSVx+Jets strategy

For Stealth SUSY-like events the ABCD plane for background estimation is constructed with the isolation ΔR_{\min} variable, and the sum of the numbers of MDT and trigger hits associated with the MS vertex, described in Section 9.1.1. These two variables form the x -axis and y -axis of the ABCD plane, respectively. The SR and the VR are built using the E_T values of the leading and subleading jets and their definition is summarized in Table 7.

Table 7: Summary of the definition of the VR and SR used for the ABCD method for the 1MSVx+Jets strategy.

Region	Criteria
Barrel	VR: $50 < E_{T,\text{subleading}} < 150 \text{ GeV}$, $E_{T,\text{leading}} > 150 \text{ GeV}$ SR: $E_{T,\text{leading}} > 150 \text{ GeV}$, $E_{T,\text{subleading}} > 150 \text{ GeV}$
Endcaps	VR: $100 < E_{T,\text{subleading}} < 250 \text{ GeV}$, $E_{T,\text{leading}} > 250 \text{ GeV}$ SR: $E_{T,\text{leading}} > 250 \text{ GeV}$, $E_{T,\text{subleading}} > 250 \text{ GeV}$

Signal contamination in regions B, C and D in the SR of the 1MSVx+Jets ABCD plane was found to be negligible. Signal contamination in the VR is negligible for benchmark samples with $m_{\tilde{g}} > 500 \text{ GeV}$, and for $m_{\tilde{g}} = 500 \text{ GeV}$ in the barrel region. However, the endcaps region for $m_{\tilde{g}} = 500 \text{ GeV}$ and both barrel and endcaps regions for $m_{\tilde{g}} = 250 \text{ GeV}$ have non-negligible signal contamination in the VR and thus are not included in the 1MSVx+Jets strategy. Both the VR and SR show very low linear correlation between the two variables: -0.01 (-0.03) for the VR, and -0.01 (-0.05) for the SR in the barrel (endcaps).

Table 8 summarizes the observed and expected numbers of events in the four regions of the ABCD plane constructed using events from the VR. The number of observed events in region A is 46 and 11 in the barrel and endcaps, respectively. These are in agreement with the 45 ± 5 (stat.) ± 9 (syst.) and 15 ± 3 (stat.) ± 12 (syst.) events predicted by the ABCD method in the barrel and endcaps, respectively. The systematic uncertainty associated with the background estimation reported above is described in detail in Section 10.2.

Table 8: Event counts in each of the four regions of the 1MSVx+Jets ABCD plane and expected number in region A obtained using 2015 and 2016 data from the VR. Both the statistical and systematic errors of the background expectation are reported.

VR	A	Expected background	B	C	D
Barrel	46	45 ± 5 (stat.) ± 9 (syst.)	7,748	90	15,620
Endcaps	11	15 ± 3 (stat.) ± 12 (syst.)	3,335	20	4,365

9.2.2 ABCD plane for 1MSVx+ E_T^{miss} strategy

For the 1MSVx+ E_T^{miss} strategy the two variables used to define the ABCD plane are the isolation ΔR_{\min} and the angle in the transverse plane between the E_T^{miss} vector and the displaced vertex $|\Delta\phi(E_T^{\text{miss}}, \text{MSVx})|$, described in Section 9.1.2. The SR and VR are defined using the sum of the numbers of MDT and trigger hits in a cone around the MS vertex and their definition is summarized in Table 9. Signal contamination in the VR is negligible.

Both the VR and SR show very low linear correlation between the two variables: 0.03 (0.01) for the VR, and 0.02 (−0.01) for the SR in the barrel (endcaps).

Table 9: Summary of the definition of the VR and SR used for the ABCD method for the $1MSV_X + E_T^{\text{miss}}$ strategy.

Region	Criteria
Barrel	VR: $n_{\text{MDT}} + n_{\text{RPC}} < 1200$ SR: $n_{\text{MDT}} + n_{\text{RPC}} > 1200$
Endcaps	VR: $n_{\text{MDT}} + n_{\text{TGC}} < 1500$ SR: $n_{\text{MDT}} + n_{\text{TGC}} > 1500$

Table 10 summarizes the observed and expected numbers of events in the four regions of the ABCD plane constructed using events from the VR. The number of observed events in region A is 334 ± 18 and 1107 ± 33 for the barrel and endcaps, respectively. These are in agreement with the 319 ± 29 (stat.) ± 38 (syst.) and 1153 ± 46 (stat.) ± 69 (syst.) events predicted by the ABCD method in the barrel and endcaps, respectively. The systematic uncertainty associated with the background estimation reported above is described in detail in Section 10.2.

Table 10: Event counts in each of the four regions of the $1MSV_X + E_T^{\text{miss}}$ ABCD plane and expected number in region A obtained using 2015 and 2016 data from the VR. Both the statistical and systematic errors of the background expectation are reported.

VR	A	Expected background	B	C	D
Barrel	334	319 ± 29 (stat.) ± 38 (syst.)	119	67,980	25,380
Endcaps	1,107	$1,153 \pm 46$ (stat.) ± 69 (syst.)	639	56,970	31,570

For the $1MSV_X + E_T^{\text{miss}}$ strategy the signal contamination in regions B, C and D of the SR ABCD plane is not negligible. The traditional method, which estimates the background in region A by taking the ratio of events in the adjacent regions, breaks down in the presence of signal in the control regions. An ABCD-likelihood method addresses this issue because it estimates the background in region A by fitting simultaneously background and expected signal events in the four regions of the ABCD plane. A likelihood function is formed from the product of four Poisson functions, one for each region A, B, C and D, describing signal and background expectations. The likelihood takes the form:

$$\mathcal{L}(n_A, n_B, n_C, n_D | s, b, \tau_B, \tau_C) = \prod_{i=A,B,C,D} \frac{e^{-N_i} N_i^{n_i}}{n_i!},$$

where n_A, n_B, n_C and n_D are the four observables that denote the number of events observed in each region in data. The N_i are linear combinations of the signal and background expectation in each region, defined as follow:

$$\begin{aligned} N_A &= s + b \\ N_B &= s \epsilon_B + b \tau_B \\ N_C &= s \epsilon_C + b \tau_C \\ N_D &= s \epsilon_D + b \tau_B \tau_C \end{aligned}$$

where s is the signal yield, b the estimated background in region A, ϵ_i the signal contamination derived from MC simulation, and τ_B and τ_C are the coefficients that relate the number of background events in region A to the other regions. The s , b and τ_i values are allowed to float in the simultaneous fit to the four data regions.

10 Systematic uncertainties

In this section, experimental and theoretical systematic uncertainties associated with the signal predictions and background estimation are described.

10.1 Uncertainties in the signal predictions

The signal efficiency systematic uncertainties are dominated by the modeling of the signal physics processes, pileup and detector response and the extrapolation of the expected number of signal events as a function of the LLP proper lifetime.

One of the sources of systematic uncertainty associated with the Muon RoI Cluster trigger stems from the trigger scale factors, and it was estimated by moving them up and down by their statistical uncertainty. The trigger efficiency values obtained with these modified MC samples were compared with the efficiency of the nominal sample, and the difference was taken as the systematic uncertainty. A similar strategy was also adopted to estimate the trigger systematic uncertainty associated with the modeling of the minimum-bias interactions used to emulate pileup and the systematic uncertainty due to the PDF used to generate signal MC events. For the latter, the PDF uncertainty was obtained by considering the envelope of the uncertainty of the PDF set. The total systematic uncertainty of the signal efficiency for passing the Muon RoI Cluster trigger was obtained by summing in quadrature the contributions described above and varies from 1% to 12%, depending on the sample and detector region. The total systematic uncertainty of the signal efficiency for reconstructing an MS vertex was obtained by summing in quadrature the contributions coming from pileup and PDF uncertainties (evaluated with the similar procedure described above) and varies from 0.07% to 5.5%, depending on the sample and detector region. The systematic uncertainty associated with the prompt jets used for the 1MSVx+Jets strategy originates from jet energy scale, PDF and pileup uncertainties, and was evaluated with the similar procedure described earlier. The overall systematic uncertainty of the two-jet efficiency was determined by adding each component in quadrature and varies from 0.3% to 9.8%, depending on the sample and detector region. Systematic uncertainties due to the E_T^{miss} computation for the 1MSVx+ E_T^{miss} strategy are negligible. By comparing the average number of muon segments in a cone around punch-through jets in data and MC simulation, systematic uncertainties associated with the mismodeling of the MS vertex reconstruction in signal events were found to be negligible.

For each of the scalar boson samples, excluding $m_s = 100$ GeV, two proper lifetime points were fully simulated: one nominal sample and a secondary sample with longer proper lifetime, as described in Section 5. The secondary sample is used to validate the extrapolation procedure, and a systematic uncertainty is assigned to each sample due to the non-closure of the extrapolation procedure. This is calculated by determining the fraction of events passing all analysis cuts in each MC sample generated with 9 m lab-frame decay length and comparing them to the expected global efficiencies obtained with the extrapolation procedure. The systematic uncertainty varies from 2% to 37%, depending on the sample.

Stealth SUSY benchmark samples have events with kinematic behavior similar to that of events in the high-mass scalar boson samples and they are thus assigned the average systematic uncertainty of those samples (11%). The kinematics of events in the baryogenesis samples is very close to the $\Phi(125) \rightarrow ss$ kinematics and a comparable systematic uncertainty related to the extrapolation procedure is assumed. For that reason, for all the baryogenesis benchmark samples the average systematic uncertainty of the five $\Phi(125) \rightarrow ss$ samples (32%) is used.

The uncertainty in the combined 2015+2016 integrated luminosity is 2.1%. It is derived, following a methodology similar to that detailed in Ref. [72], using the LUCID-2 detector for the baseline luminosity measurements [73], from calibration of the luminosity scale using x - y beam-separation scans.

10.2 Uncertainties in the background prediction

The systematic uncertainty associated with the background estimation of the ABCD method was evaluated using data events passing the validation region selection. Events falling in each of the two bands of the ABCD plane that surround region A, and that are shown in Figure 10 for the $1MSV_X + E_T^{\text{miss}}$ strategy in the barrel, were excluded and the expected background in the signal region was re-evaluated. The definition of region A was not modified in this procedure. The relative variation with respect to the observed events in region A was then evaluated. The size of the two bands is defined by the resolution of the two variables used to define the ABCD plane. The maximum value of the two results obtained by separately removing bands with widths of 1σ and 2σ was taken as the systematic uncertainty associated with the background estimation. Since the numbers of events in regions A and B are small, a bootstrap method [74, 75] was used to determine the statistical uncertainty of the background estimate.

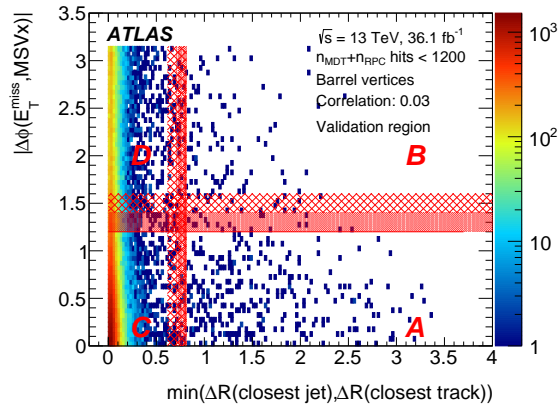


Figure 10: ABCD plane for the $1MSV_X + E_T^{\text{miss}}$ strategy in the barrel and definition of the regions excluded from the estimation of the background's systematic uncertainty.

For the $1MSV_X + \text{Jets}$ strategy the size of the two removed bands corresponds to 0.1 and 0.2 for the isolation and 100 and 200 for the number of MS hits. In the endcap validation region the uncertainty in the relative difference obtained from the bootstrap method is much higher than the statistical uncertainty of the background estimate in region A, while in the barrel the two are comparable. The final systematic uncertainty of the background estimate was taken to be the maximum of the statistical uncertainty from the bootstrap method and the statistical uncertainty from the background prediction in region A, and corresponds to 20% in the barrel and 81% in the endcaps.

For the $1MSV_x + E_T^{\text{miss}}$ strategy the size of the two removed bands corresponds to 0.1 and 0.2 for the isolation variable and 0.2 and 0.4 for $|\Delta\phi(E_T^{\text{miss}}, MSV_x)|$. The relative difference in the validation region is lower than the statistical uncertainty on the relative difference obtained from the bootstrap method in both the barrel and endcaps. The final systematic uncertainty of the background estimate is taken to be the maximum of the statistical uncertainty from the bootstrap method and the statistical uncertainty of the background prediction in region A, corresponding to 12% and 6% for barrel and endcaps, respectively. The small contribution from non-collision background was taken into account as a systematic uncertainty of the background estimate, as discussed in Section 9.2.

11 Results

For the 2MSV_x strategy, 0.027 ± 0.011 background events are expected. After unblinding, no events passing the full signal selection were found.

For the 1MSV_x+AO strategies, the number of observed events in the four regions of the ABCD plane and the background prediction in region A for events passing the SR selection are summarized in Table 11. No significant excess above the predicted number of background events is found.

Table 11: Event counts in each of the four regions of the ABCD plane and expected number in region A for the SR, using the 2015 and 2016 datasets. Both the statistical and systematic errors of the background expectation are reported.

Strategy	Region	A	Expected background	B	C	D
1MSV _x +Jets	Barrel	14	15 ± 3 (stat.) ± 3 (syst.)	2,057	25	3,414
	Endcaps	4	11 ± 3 (stat.) ± 9 (syst.)	560	15	761
1MSV _x + E_T^{miss}	Barrel	224	243 ± 38 (stat.) ± 29 (syst.)	42	132,000	22,800
	Endcaps	489	497 ± 51 (stat.) ± 30 (syst.)	94	165,800	31,390

Upper limits on the production cross section times branching fraction were derived using the CL_s prescription [76], implemented with the RooStat [77] and HistFactory [78] packages using a profile likelihood function [79]. For the 2MSV_x and 1MSV_x+Jets strategies the likelihood includes a Poisson probability term describing the total number of observed events. For the 1MSV_x+ E_T^{miss} strategy the likelihood described in Section 9.2.2 was used. For scalar boson benchmark samples with $m_\Phi \neq 125$ GeV, upper limits were set on $\sigma \times B$, where B represents the branching fraction for $\Phi \rightarrow ss$ assuming 100% branching fraction into fermion pairs. For scalar boson benchmark samples with $m_\Phi = 125$ GeV, upper limits were set on $\sigma/\sigma_{\text{SM}} \times B$, where σ_{SM} is the SM Higgs boson production cross section, 48.58 pb [80]. For the Stealth SUSY benchmarks, upper limits were set on $\sigma/\sigma_{\text{SUSY}} \times B$, where σ_{SUSY} is the SUSY production cross section for $pp \rightarrow \tilde{g}\tilde{g}$ [81] and B represents the branching fraction for $\tilde{g} \rightarrow \tilde{S}g$, assuming that both $\tilde{S} \rightarrow S\tilde{G}$ and $S \rightarrow gg$ have 100% branching fraction.

Figures 11, 12 and 13 show the observed limits for all the MC benchmark samples considered in this paper. The limits were obtained from the combination of 2MSV_x and 1MSV_x+AO strategies, performing a simultaneous fit of the 2MSV_x and 1MSV_x+AO likelihood functions, except for the scalar boson samples with $m_\Phi = 100$ GeV and $m_\Phi > 125$ GeV, Stealth SUSY with $m_{\tilde{g}} = 250$ GeV (both barrel and endcaps regions) and $m_{\tilde{g}} = 500$ GeV (endcaps region), baryogenesis with $m_\chi = 100$ GeV and baryogenesis $\chi \rightarrow \tau\tau\nu$ benchmark samples. In these cases, the ABCD method developed for the analysis reported in

this paper was found to be not optimal due to a large contamination by signal events in the VR or small signal-background separation for one of the variables of the ABCD plane. For those samples, the 2MSVx strategy provides strong limits and only those results are presented in this paper.

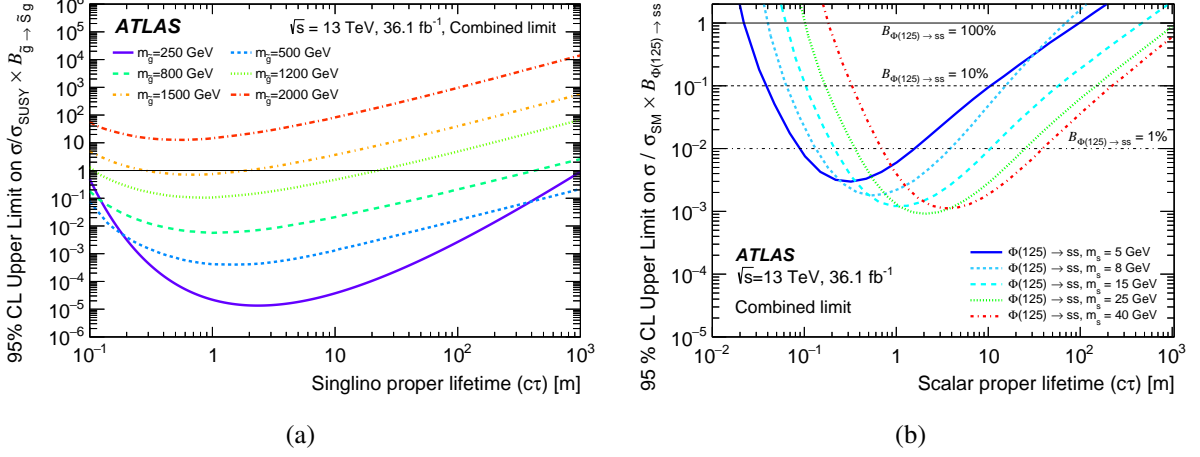


Figure 11: Observed limits for (a) Stealth SUSY and (b) $\Phi(125) \rightarrow ss$ benchmark samples obtained from the combination of 2MSVx and 1MSVx+AO strategies.

Table 12: Ranges of mean proper lifetime excluded at 95% CL for scalar boson benchmark models with $m_\Phi = 125$ GeV, assuming production cross-sections equal to 10% or 1% of the SM Higgs boson production cross-section [80] for the combination of 2MSVx and 1MSVx+ E_T^{miss} strategies.

$\Phi(125) \rightarrow ss$ m_s [GeV]	Excluded $c\tau$ range [m]	
	10%	1%
5	0.04–10.8	0.1–1.6
8	0.07–15	0.14–3.8
15	0.1–58	0.22–10.8
25	0.2–149	0.4–25
40	0.3–221	0.7–39

Table 12 summarizes the lifetime ranges excluded by the analysis presented in this paper for branching fractions of 10% and 1% for the scalar boson with $m_\Phi = 125$ GeV decaying into two long-lived scalars. The results are substantially improved compared to the Run 1 analysis, where for 25 GeV and 40 GeV long-lived scalar masses the $c\tau$ ranges excluded for 1% branching fraction were respectively 1.10–5.35 m and 2.82–7.45 m, while for lower long-lived scalar masses the Run 1 analysis did not have sensitivity at this level.

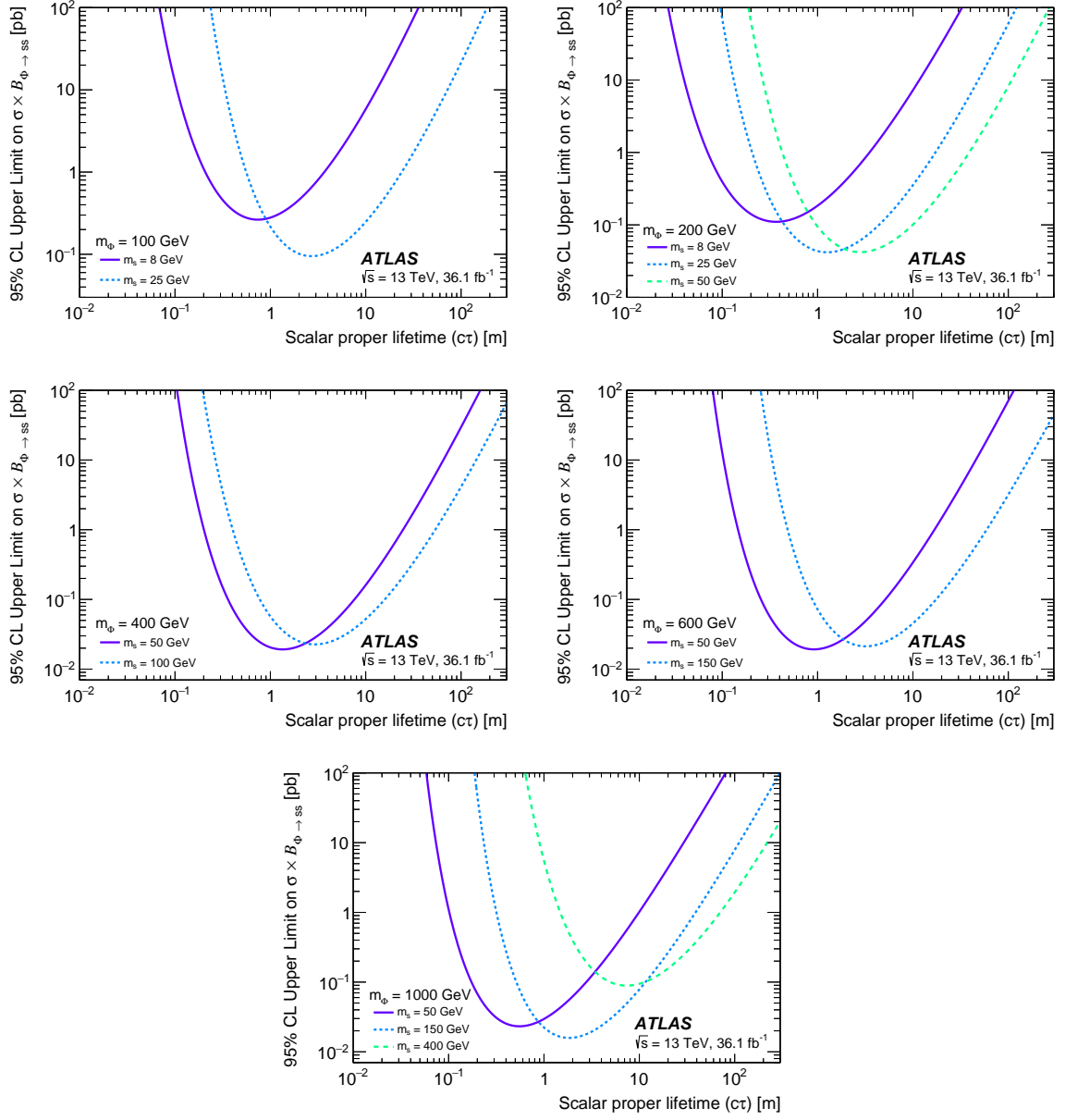


Figure 12: Observed limits for scalar boson benchmark samples with $m_\Phi = 100$ GeV and $m_\Phi > 125$ GeV. The different plots show the results obtained for different Φ mass points.

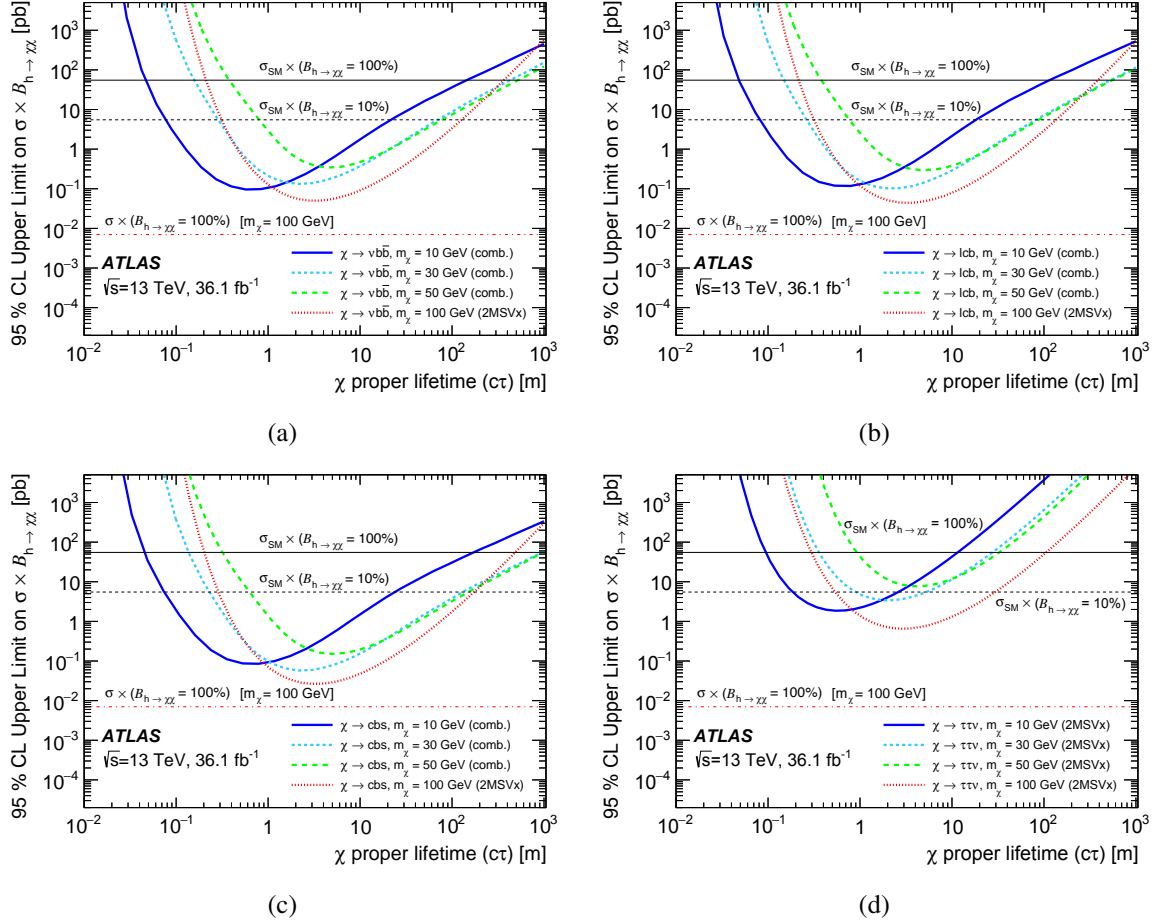


Figure 13: Observed limits obtained for all the baryogenesis benchmark samples. Limits for the on-shell $h \rightarrow \chi\chi$ production in (a), (b) and (c) are obtained from the combination of 2MSVx and 1MSVx+ E_T^{miss} strategies, while for the off-shell sample ($m_\chi = 100$ GeV) the limits shown are obtained from the 2MSVx strategy only. Limits for the $\chi \rightarrow \tau\tau\nu$ channel shown in (d) are obtained from the 2MSVx strategy only. For reference, the black solid and dashed lines show respectively the 100% and 10% $\sigma \times B$ assuming the SM Higgs boson total production cross section, while the red dash-dotted line reports the 100% $\sigma \times B$ for the off-shell $h \rightarrow \chi\chi$ production with $m_\chi = 100$ GeV, which is equal to 7 fb.

12 Summary

This paper presents the results of a search for long-lived neutral particles using 36.1 fb^{-1} of proton–proton collisions at $\sqrt{s} = 13 \text{ TeV}$ recorded at the LHC by the ATLAS detector in 2015 and 2016. Three separate strategies have been considered: two displaced vertices in the muon spectrometer (MS), one displaced vertex in the MS with two additional prompt jets, and one displaced vertex in the MS with $E_T^{\text{miss}} > 30 \text{ GeV}$. The observed number of events are consistent with the expected background and exclusion limits on the LLP production cross section as a function of its proper lifetime were computed for the theoretical benchmark models.

The results reported here are interpreted in terms of a scalar portal model similar to hidden-valley models where a boson can decay into two long-lived scalars, a Stealth SUSY model where each of the two long-lived singlino are produced from the gluino in association with a prompt jet, and a Higgs-boson-mediated baryogenesis model where the long-lived χ can decay into jets or leptons that violate the baryon and/or lepton number conservation.

The two-vertex search was performed with the same strategy as adopted in Run 1 and benefits from very low background, but at large $(c\tau)$ its sensitivity scales as $1/(c\tau)^2$, where τ is the proper lifetime of the LLP. The increased statistics and the analysis enhancements have improved the cross-section sensitivity for some of the $\Phi \rightarrow ss$ decays by about an order of magnitude compared to the ATLAS Run 1 analysis, and extended the sensitivity for the Stealth SUSY model to higher gluino masses that could not be reached with the Run 1 search.

The one-vertex search extends the sensitivity, which scales as $1/(c\tau)$ at large $(c\tau)$, to much longer lifetimes. For the low-mass samples ($\Phi(125) \rightarrow ss$ and Higgs portal baryogenesis) the sensitivity at shorter lifetimes is weaker than that attained with the two-MS-vertex search, while for the Stealth SUSY model in the high-mass regime ($m_{\tilde{g}} > 500 \text{ GeV}$) the contribution of the one-MS-vertex search is dominant in the whole spectrum of proper lifetimes.

Acknowledgments

We thank CERN for the very successful operation of the LHC, as well as the support staff from our institutions without whom ATLAS could not be operated efficiently.

We acknowledge the support of ANPCyT, Argentina; YerPhI, Armenia; ARC, Australia; BMWFW and FWF, Austria; ANAS, Azerbaijan; SSTC, Belarus; CNPq and FAPESP, Brazil; NSERC, NRC and CFI, Canada; CERN; CONICYT, Chile; CAS, MOST and NSFC, China; COLCIENCIAS, Colombia; MSMT CR, MPO CR and VSC CR, Czech Republic; DNRF and DNSRC, Denmark; IN2P3-CNRS, CEA-DRF/IRFU, France; SRNSFG, Georgia; BMBF, HGF, and MPG, Germany; GSRT, Greece; RGC, Hong Kong SAR, China; ISF and Benoziyo Center, Israel; INFN, Italy; MEXT and JSPS, Japan; CNRST, Morocco; NWO, Netherlands; RCN, Norway; MNiSW and NCN, Poland; FCT, Portugal; MNE/IFA, Romania; MES of Russia and NRC KI, Russian Federation; JINR; MESTD, Serbia; MSSR, Slovakia; ARRS and MIZŠ, Slovenia; DST/NRF, South Africa; MINECO, Spain; SRC and Wallenberg Foundation, Sweden; SERI, SNSF and Cantons of Bern and Geneva, Switzerland; MOST, Taiwan; TAEK, Turkey; STFC, United Kingdom; DOE and NSF, United States of America. In addition, individual groups and members have received support from BCKDF, CANARIE, CRC and Compute Canada, Canada; COST, ERC, ERDF, Horizon 2020, and Marie Skłodowska-Curie Actions, European Union; Investissements d'

Avenir Labex and Idex, ANR, France; DFG and AvH Foundation, Germany; Herakleitos, Thales and Aristeia programmes co-financed by EU-ESF and the Greek NSRF, Greece; BSF-NSF and GIF, Israel; CERCA Programme Generalitat de Catalunya, Spain; The Royal Society and Leverhulme Trust, United Kingdom.

The crucial computing support from all WLCG partners is acknowledged gratefully, in particular from CERN, the ATLAS Tier-1 facilities at TRIUMF (Canada), NDGF (Denmark, Norway, Sweden), CC-IN2P3 (France), KIT/GridKA (Germany), INFN-CNAF (Italy), NL-T1 (Netherlands), PIC (Spain), ASGC (Taiwan), RAL (UK) and BNL (USA), the Tier-2 facilities worldwide and large non-WLCG resource providers. Major contributors of computing resources are listed in Ref. [82].

References

- [1] A. Fradette and M. Pospelov, *BBN for the LHC: Constraints on lifetimes of the Higgs portal scalars*, *Phys. Rev. D* **96** (2017) 075033, arXiv: [1706.01920](#).
- [2] A. Arvanitaki, N. Craig, S. Dimopoulos, and G. Villadoro, *Mini-Split*, *JHEP* **02** (2013) 126, arXiv: [1210.0555 \[hep-ph\]](#).
- [3] N. Arkani-Hamed, A. Gupta, D. E. Kaplan, N. Weiner, and T. Zorawski, *Simply Unnatural Supersymmetry*, (2012), arXiv: [1212.6971 \[hep-ph\]](#).
- [4] G. F. Giudice and R. Rattazzi, *Theories with gauge mediated supersymmetry breaking*, *Phys. Rept.* **322** (1999) 419, arXiv: [hep-ph/9801271 \[hep-ph\]](#).
- [5] R. Barbier et al., *R-parity violating supersymmetry*, *Phys. Rept.* **420** (2005) 1, arXiv: [hep-ph/0406039 \[hep-ph\]](#).
- [6] C. Csaki, E. Kuflik, and T. Volansky, *Dynamical R-Parity Violation*, *Phys. Rev. Lett.* **112** (2014) 131801, arXiv: [1309.5957 \[hep-ph\]](#).
- [7] J. Fan, M. Reece, and J. T. Ruderman, *Stealth supersymmetry*, *JHEP* **11** (2011) 012, arXiv: [1105.5135](#).
- [8] J. Fan, M. Reece, and J. T. Ruderman, *A stealth supersymmetry sampler*, *JHEP* **07** (2012) 196, arXiv: [1201.4875](#).
- [9] Z. Chacko, D. Curtin, and C. B. Verhaaren, *A quirky probe of neutral naturalness*, *Phys. Rev. D* **94** (2016) 011504, arXiv: [1512.05782](#).
- [10] G. Burdman, Z. Chacko, H.-S. Goh, and R. Harnik, *Folded supersymmetry and the LEP paradox*, *JHEP* **0702** (2007) 009, arXiv: [hep-ph/0609152 \[hep-ph\]](#).
- [11] H. Cai, H.-C. Cheng, and J. Terning, *A quirky little Higgs model*, *JHEP* **0905** (2009) 045, arXiv: [0812.0843 \[hep-ph\]](#).
- [12] Z. Chacko, H.-S. Goh, and R. Harnik, *Natural Electroweak Breaking from a Mirror Symmetry*, *Phys. Rev. Lett.* **96** (2006) 231802, arXiv: [hep-ph/0506256 \[hep-ph\]](#).
- [13] M. J. Strassler and K. M. Zurek, *Echoes of a hidden valley at hadron colliders*, *Phys. Lett. B* **651** (2007) 374, arXiv: [hep-ph/0604261](#).
- [14] M. J. Strassler and K. M. Zurek, *Discovering the Higgs through highly-displaced vertices*, *Phys. Lett. B* **661** (2008) 263, arXiv: [hep-ph/0605193](#).

- [15] M. Baumgart, C. Cheung, J. T. Ruderman, L.-T. Wang, and I. Yavin, *Non-abelian dark sectors and their collider signatures*, [JHEP **04** \(2009\) 014](#), arXiv: [0901.0283 \[hep-ph\]](#).
- [16] D. E. Kaplan, M. A. Luty, and K. M. Zurek, *Asymmetric dark matter*, [Phys. Rev. **D79** \(2009\) 115016](#), arXiv: [0901.4117 \[hep-ph\]](#).
- [17] Y. F. Chan, M. Low, D. E. Morrissey, and A. P. Spray, *LHC signatures of a minimal supersymmetric hidden valley*, [JHEP **05** \(2012\) 155](#), arXiv: [1112.2705 \[hep-ph\]](#).
- [18] K. R. Dienes and B. Thomas, *Dynamical Dark Matter: I. Theoretical Overview*, [Phys. Rev. **D85** \(2012\) 083523](#), arXiv: [1106.4546 \[hep-ph\]](#).
- [19] K. R. Dienes, S. Su, and B. Thomas, *Distinguishing dynamical dark matter at the LHC*, [Phys. Rev. **D86** \(2012\) 054008](#), arXiv: [1204.4183 \[hep-ph\]](#).
- [20] Y. Cui and B. Shuve, *Probing baryogenesis with displaced vertices at the LHC*, [JHEP **02** \(2015\) 049](#), arXiv: [1409.6729 \[hep-ph\]](#).
- [21] J. C. Helo, M. Hirsch, and S. Kovalenko, *Heavy neutrino searches at the LHC with displaced vertices*, [Phys. Rev. **D89** \(2014\) 073005](#), [Erratum: [Phys. Rev. **D93**, no. 9, 099902 \(2016\)](#)], arXiv: [1312.2900 \[hep-ph\]](#).
- [22] B. Batell, M. Pospelov, and B. Shuve, *Shedding light on neutrino masses with dark forces*, [JHEP **08** \(2016\) 052](#), arXiv: [1604.06099 \[hep-ph\]](#).
- [23] CDF Collaboration, *Search for heavy metastable particles decaying to jet pairs in $p\bar{p}$ collisions at $\sqrt{s} = 1.96$ TeV*, [Phys. Rev. **D 85** \(2012\) 012007](#), arXiv: [1109.3136](#).
- [24] D0 Collaboration, *Search for Resonant Pair Production of Neutral Long-Lived Particles Decaying to $b\bar{b}$ in $p\bar{p}$ Collisions at $\sqrt{s} = 1.96$ TeV*, [Phys. Rev. Lett. **103** \(2009\) 071801](#), arXiv: [0906.1787](#).
- [25] ATLAS Collaboration, *Search for a Light Higgs Boson Decaying to Long-Lived Weakly Interacting Particles in Proton-Proton Collisions at $\sqrt{s} = 7$ TeV with the ATLAS Detector*, [Phys. Rev. Lett. **108** \(2012\) 251801](#), arXiv: [1203.1303](#).
- [26] LHCb Collaboration, *Search for long-lived particles decaying to jet pairs*, [Eur. Phys. J. C **75** \(2015\) 152](#), arXiv: [1412.3021](#).
- [27] ATLAS Collaboration, *Search for long-lived, weakly interacting particles that decay to displaced hadronic jets in proton-proton collisions at $\sqrt{s} = 8$ TeV with the ATLAS detector*, [Phys. Rev. **D. 92** \(2015\) 012010](#), arXiv: [1504.03634](#).
- [28] ATLAS Collaboration, *Search for massive, long-lived particles using multitrack displaced vertices or displaced lepton pairs in pp collisions at $\sqrt{s} = 8$ TeV with the ATLAS detector*, [Phys. Rev. **D 92** \(2015\) 072004](#), arXiv: [1504.05162 \[hep-ex\]](#).
- [29] CMS Collaboration, *Search for long-lived neutral particles decaying to quark-antiquark pairs in proton-proton collisions at $\sqrt{s} = 8$ TeV*, [Phys. Rev. **D 91** \(2015\) 012007](#), arXiv: [1411.6530](#).
- [30] ATLAS Collaboration, *Search for pair-produced long-lived neutral particles decaying in the ATLAS hadronic calorimeter in pp collisions at $\sqrt{s} = 8$ TeV*, [Phys. Lett. **B 743** \(2015\) 15](#), arXiv: [1501.04020](#).

- [31] LHCb Collaboration, *Updated search for long-lived particles decaying to jet pairs*, *Eur. Phys. J. C* **77** (2017) 812, arXiv: [1705.07332 \[hep-ex\]](#).
- [32] LHCb Collaboration, *Search for massive long-lived particles decaying semileptonically in the LHCb detector*, *Eur. Phys. J. C* **77** (2017) 224, arXiv: [1612.00945 \[hep-ex\]](#).
- [33] CMS Collaboration, *Search for new long-lived particles at $\sqrt{s} = 13$ TeV*, *Phys. Lett. B* **780** (2018) 432, arXiv: [1711.09120 \[hep-ex\]](#).
- [34] A. Coccaro, D. Curtin, H. J. Lubatti, H. Russell, and J. Shelton, *Data-driven model-independent searches for long-lived particles at the LHC*, *Phys. Rev. D* **94** (2016) 113003, arXiv: [1605.02742 \[hep-ph\]](#).
- [35] ATLAS Collaboration, *The ATLAS Experiment at the CERN Large Hadron Collider*, *JINST* **3** (2008) S08003.
- [36] ATLAS Collaboration, *Performance of the ATLAS trigger system in 2015*, *Eur. Phys. J. C* **77** (2017) 317, arXiv: [1611.09661 \[hep-ex\]](#).
- [37] ATLAS Collaboration, *Triggers for displaced decays of long-lived neutral particles in the ATLAS detector*, *JINST* **8** (2013) P07015, arXiv: [1305.2284](#).
- [38] ATLAS Collaboration, *Standalone vertex finding in the ATLAS muon spectrometer*, *JINST* **9** (2014) P02001, arXiv: [1311.7070](#).
- [39] R. Bruce et al., *Sources of machine-induced background in the ATLAS and CMS detectors at the CERN Large Hadron Collider*, *Nucl. Instrum. Methods Phys. Res. A* **729** (2013) 825.
- [40] M. J. Strassler, *Possible effects of a hidden valley on supersymmetric phenomenology*, (2006), arXiv: [hep-ph/0607160](#).
- [41] ATLAS and CMS Collaborations, *Measurements of the Higgs boson production and decay rates and constraints on its couplings from a combined ATLAS and CMS analysis of the LHC pp collision data at $\sqrt{s} = 7$ and 8 TeV*, *JHEP* **08** (2016) 045, arXiv: [1606.02266 \[hep-ex\]](#).
- [42] D. Curtin and C. B. Verhaaren, *Discovering uncolored naturalness in exotic Higgs decays*, *JHEP* **12** (2015) 072, arXiv: [1506.06141](#).
- [43] S. Blanchet, Z. Chacko, S. S. Granor, and R. N. Mohapatra, *Probing resonant leptogenesis at the LHC*, *Phys. Rev. D* **82** (2010) 076008, arXiv: [0904.2174](#).
- [44] C. S. Fong, M. Gonzalez-Garcia, E. Nardi, and E. Peinado, *New ways to TeV scale leptogenesis*, *JHEP* **08** (2013) 104, arXiv: [1305.6312](#).
- [45] H. An and Y. Zhang, *Direct detection of baryogenesis mechanism from squark decays at LHC*, *Phys. Rev. D* **89** (2014) 071902, arXiv: [1310.2608](#).
- [46] D. Curtin et al., *Exotic decays of the 125 GeV Higgs boson*, *Phys. Rev. D* **90** (2014) 075004, arXiv: [1312.4992](#).
- [47] C. Englert, T. Plehn, D. Zerwas, and P. M. Zerwas, *Exploring the Higgs portal*, *Phys. Lett B* **703** (2011) 298, arXiv: [1106.3097](#).
- [48] C. Englert, T. Plehn, M. Rauch, D. Zerwas, and P. M. Zerwas, *LHC: Standard Higgs and hidden Higgs*, *Phys. Lett. B* **707** (2012) 512, arXiv: [1112.3007](#).

- [49] C. Csáki, *The Minimal Supersymmetric Standard Model (MSSM)*, *Mod. Phys. Lett. A* **11** (1996) 599, arXiv: [arXiv:hep-ph/9606414 \[hep-ph\]](#).
- [50] J. Alwall et al., *The automated computation of tree-level and next-to-leading order differential cross sections, and their matching to parton shower simulations*, *JHEP* **7** (2014) 79, arXiv: [1405.0301](#).
- [51] T. Sjöstrand et al., *An Introduction to PYTHIA 8.2*, *Comput. Phys. Commun.* **191** (2014) 159, arXiv: [1410.3012](#).
- [52] ATLAS Collaboration, *ATLAS Pythia 8 tunes to 7 TeV data*, ATL-PHYS-PUB-2014-021, 2014, URL: <https://cds.cern.ch/record/1966419>.
- [53] R. D. Ball et al., *Parton distributions with LHC data*, *Nucl. Phys. B* **867** (2013) 244, arXiv: [1207.1303 \[hep-ph\]](#).
- [54] D. J. Lange, *The EvtGen particle decay simulation package*, *Nucl. Instr. Meth. A* **462** (2001) 152.
- [55] ATLAS Collaboration, *The ATLAS Simulation Infrastructure*, *Eur. Phys. J. C* **70** (2010) 823, arXiv: [1005.4568](#).
- [56] S. Agostinelli et al., *GEANT4 – a simulation toolkit*, *Nucl. Instrum. Meth. A* **506** (2003) 250.
- [57] ATLAS Collaboration, *Summary of ATLAS Pythia 8 tunes*, ATL-PHYS-PUB-2012-003, 2012, URL: <https://cds.cern.ch/record/1474107>.
- [58] A. Martin, W. Stirling, R. Thorne, and G. Watt, *Parton distributions for the LHC*, *Eur. Phys. J. C* **63** (2009) 189, arXiv: [0901.0002](#).
- [59] M. Cacciari, G. Salam, and G. Soyez, *The anti- k_t jet clustering algorithm*, *JHEP* **04** (2008) 063, arXiv: [0802.1189 \[hep-ex\]](#).
- [60] M. Cacciari, G. Salam, and G. Soyez, *FastJet user manual*, *Eur. Phys. J. C* **72** (2012) 1896, arXiv: [1111.6097 \[hep-ex\]](#).
- [61] ATLAS Collaboration, *Topological cell clustering in the ATLAS calorimeters and its performance in LHC Run 1*, *Eur. Phys. J. C* **77** (2017) 490, arXiv: [1603.02934 \[hep-ex\]](#).
- [62] ATLAS Collaboration, *Jet energy measurement with the ATLAS detector in proton-proton collisions at $\sqrt{s} = 7$ TeV*, *Eur. Phys. J. C* **73** (2013) 2304, arXiv: [1112.6426 \[hep-ex\]](#).
- [63] ATLAS Collaboration, *Jet energy scale measurements and their systematic uncertainties in proton-proton collisions at $\sqrt{s} = 13$ TeV with the ATLAS detector*, *Phys. Rev.* **D96** (2017) 072002, arXiv: [1703.09665](#).
- [64] ATLAS Collaboration, *E_T^{miss} performance in the ATLAS detector using 2015–2016 LHC pp collisions*, ATLAS-CONF-2018-023, 2018, URL: <https://cds.cern.ch/record/2625233>.
- [65] ATLAS Collaboration, *Electron and photon energy calibration with the ATLAS detector using data collected in 2015 at $\sqrt{s} = 13$ TeV*, ATL-PHYS-PUB-2016-015, 2016, URL: <https://cds.cern.ch/record/2203514>.
- [66] ATLAS Collaboration, *Muon reconstruction performance of the ATLAS detector in proton–proton collision data at $\sqrt{s} = 13$ TeV*, *Eur. Phys. J. C* **76** (2016) 292, arXiv: [1603.05598 \[hep-ex\]](#).
- [67] ATLAS Collaboration, *Electron identification measurements in ATLAS using $\sqrt{s} = 13$ TeV data with 50 ns bunch spacing*, ATL-PHYS-PUB-2015-041, 2015, URL: <https://cds.cern.ch/record/2048202>.

- [68] ATLAS Collaboration, *Photon identification in 2015 ATLAS data*, ATL-PHYS-PUB-2016-014, 2016, URL: <https://cds.cern.ch/record/2203125>.
- [69] ATLAS Collaboration, *Search for long-lived, weakly interacting particles that decay to displaced hadronic jets in proton–proton collisions at $\sqrt{s} = 8$ TeV with the ATLAS detector*, *Phys. Rev. D* **92** (2015) 012010, arXiv: [1504.03634](https://arxiv.org/abs/1504.03634) [hep-ex].
- [70] ATLAS Collaboration, *Performance of pile-up mitigation techniques for jets in pp collisions at $\sqrt{s} = 8$ TeV using the ATLAS detector*, *Eur. Phys. J. C* **76** (2016) 581, arXiv: [1510.03823](https://arxiv.org/abs/1510.03823) [hep-ex].
- [71] ATLAS Collaboration, *Selection of jets produced in 13 TeV proton–proton collisions with the ATLAS detector*, ATLAS-CONF-2015-029, 2015, URL: <https://cds.cern.ch/record/2037702>.
- [72] ATLAS Collaboration, *Luminosity determination in pp collisions at $\sqrt{s} = 8$ TeV using the ATLAS detector at the LHC*, *Eur. Phys. J. C* **76** (2016) 653, arXiv: [1608.03953](https://arxiv.org/abs/1608.03953) [hep-ex].
- [73] G. Avoni et al., *The new LUCID-2 detector for luminosity measurement and monitoring in ATLAS*, *JINST* **13** (2018) P07017.
- [74] B. Efron, *Bootstrap methods: Another look at the jackknife*, *The Annals of Statistics* **7** (1979) 1.
- [75] B. Efron and R. Tibshirani, *An Introduction to the Bootstrap*, Chapman & Hall/CRC, 1993.
- [76] A. L. Read, *Presentation of search results: the CL_S technique*, *J. Phys. G* **28** (2002) 2693.
- [77] L. Moneta et al., *The RooStats Project*, ACAT2010 Conference Proceedings (2010), arXiv: [1009.1003](https://arxiv.org/abs/1009.1003) [physics.data-an].
- [78] K. Cranmer, G. Lewis, L. Moneta, A. Shibata, and W. Verkerke, *HistFactory: A tool for creating statistical models for use with RooFit and RooStats*, CERN-OPEN-2012-016 (2012), URL: <http://cdsweb.cern.ch/record/1456844>.
- [79] G. Cowan, K. Cranmer, E. Gross, and O. Vitells, *Asymptotic formulae for likelihood-based tests of new physics*, *Eur. Phys. J. C* **71** (2011) 1554, [Erratum: *Eur. Phys. J. C* **73**, 2501 (2013)], arXiv: [1007.1727](https://arxiv.org/abs/1007.1727).
- [80] LHC Higgs Cross Section Working Group, *Handbook of LHC Higgs Cross Sections: 4. Deciphering the Nature of the Higgs Sector*, *J. Phys. G* **28** (2017) 2693, arXiv: [1610.07922](https://arxiv.org/abs/1610.07922).
- [81] LHC SUSY Cross Section Working Group, *Squark and gluino production cross sections in pp collisions at $\sqrt{s} = 13, 14, 33$ and 100 TeV*, *Eur. Phys. J. C* **74** (2014) 12, arXiv: [1407.5066](https://arxiv.org/abs/1407.5066).
- [82] ATLAS Collaboration, *ATLAS Computing Acknowledgements*, ATL-GEN-PUB-2016-002, URL: <https://cds.cern.ch/record/2202407>.

The ATLAS Collaboration

M. Aaboud^{34d}, G. Aad⁹⁹, B. Abbott¹²⁵, O. Abdinov^{13,*}, B. Abeloos¹²⁹, D.K. Abhayasinghe⁹¹, S.H. Abidi¹⁶⁴, O.S. AbouZeid³⁹, N.L. Abraham¹⁵³, H. Abramowicz¹⁵⁸, H. Abreu¹⁵⁷, Y. Abulaiti⁶, B.S. Acharya^{64a,64b,p}, S. Adachi¹⁶⁰, L. Adamczyk^{81a}, J. Adelman¹¹⁹, M. Adersberger¹¹², A. Adiguzel^{12c,aj}, T. Adye¹⁴¹, A.A. Affolder¹⁴³, Y. Afik¹⁵⁷, C. Agheorghiesei^{27c}, J.A. Aguilar-Saavedra^{137f,137a,ai}, F. Ahmadov^{77,ag}, G. Aielli^{71a,71b}, S. Akatsuka⁸³, T.P.A. Åkesson⁹⁴, E. Akilli⁵², A.V. Akimov¹⁰⁸, G.L. Alberghi^{23b,23a}, J. Albert¹⁷³, P. Albicocco⁴⁹, M.J. Alconada Verzini⁸⁶, S. Alderweireldt¹¹⁷, M. Aleksa³⁵, I.N. Aleksandrov⁷⁷, C. Alexa^{27b}, T. Alexopoulos¹⁰, M. Alhroob¹²⁵, B. Ali¹³⁹, G. Alimonti^{66a}, J. Alison³⁶, S.P. Alkire¹⁴⁵, C. Allaire¹²⁹, B.M.M. Allbrooke¹⁵³, B.W. Allen¹²⁸, P.P. Allport²¹, A. Aloisio^{67a,67b}, A. Alonso³⁹, F. Alonso⁸⁶, C. Alpigiani¹⁴⁵, A.A. Alshehri⁵⁵, M.I. Alstaty⁹⁹, B. Alvarez Gonzalez³⁵, D. Álvarez Piqueras¹⁷¹, M.G. Alviggi^{67a,67b}, B.T. Amadio¹⁸, Y. Amaral Coutinho^{78b}, L. Ambroz¹³², C. Amelung²⁶, D. Amidei¹⁰³, S.P. Amor Dos Santos^{137a,137c}, S. Amoroso⁴⁴, C.S. Amrouche⁵², C. Anastopoulos¹⁴⁶, L.S. Ancu⁵², N. Andari¹⁴², T. Andeen¹¹, C.F. Anders^{59b}, J.K. Anders²⁰, K.J. Anderson³⁶, A. Andreazza^{66a,66b}, V. Andrei^{59a}, C.R. Anelli¹⁷³, S. Angelidakis³⁷, I. Angelozzi¹¹⁸, A. Angerami³⁸, A.V. Anisenkov^{120b,120a}, A. Annovi^{69a}, C. Antel^{59a}, M.T. Anthony¹⁴⁶, M. Antonelli⁴⁹, D.J.A. Antrim¹⁶⁸, F. Anulli^{70a}, M. Aoki⁷⁹, J.A. Aparisi Pozo¹⁷¹, L. Aperio Bella³⁵, G. Arabidze¹⁰⁴, J.P. Araque^{137a}, V. Araujo Ferraz^{78b}, R. Araujo Pereira^{78b}, A.T.H. Arce⁴⁷, R.E. Ardell⁹¹, F.A. Arduh⁸⁶, J-F. Arguin¹⁰⁷, S. Argyropoulos⁷⁵, A.J. Armbruster³⁵, L.J. Armitage⁹⁰, A. Armstrong¹⁶⁸, O. Arnaez¹⁶⁴, H. Arnold¹¹⁸, M. Arratia³¹, O. Arslan²⁴, A. Artamonov^{109,*}, G. Artoni¹³², S. Artz⁹⁷, S. Asai¹⁶⁰, N. Asbah⁵⁷, E.M. Asimakopoulou¹⁶⁹, L. Asquith¹⁵³, K. Assamagan²⁹, R. Astalos^{28a}, R.J. Atkin^{32a}, M. Atkinson¹⁷⁰, N.B. Atlay¹⁴⁸, K. Augsten¹³⁹, G. Avolio³⁵, R. Avramidou^{58a}, M.K. Ayoub^{15a}, G. Azuelos^{107,av}, A.E. Baas^{59a}, M.J. Baca²¹, H. Bachacou¹⁴², K. Bachas^{65a,65b}, M. Backes¹³², P. Bagnaia^{70a,70b}, M. Bahmani⁸², H. Bahrasemani¹⁴⁹, A.J. Bailey¹⁷¹, J.T. Baines¹⁴¹, M. Bajic³⁹, C. Bakalis¹⁰, O.K. Baker¹⁸⁰, P.J. Bakker¹¹⁸, D. Bakshi Gupta⁹³, S. Balaji¹⁵⁴, E.M. Baldin^{120b,120a}, P. Balek¹⁷⁷, F. Balli¹⁴², W.K. Balunas¹³⁴, J. Balz⁹⁷, E. Banas⁸², A. Bandyopadhyay²⁴, S. Banerjee^{178,1}, A.A.E. Bannoura¹⁷⁹, L. Barak¹⁵⁸, W.M. Barbe³⁷, E.L. Barberio¹⁰², D. Barberis^{53b,53a}, M. Barbero⁹⁹, T. Barillari¹¹³, M-S. Barisits³⁵, J. Barkeloo¹²⁸, T. Barklow¹⁵⁰, R. Barnea¹⁵⁷, S.L. Barnes^{58c}, B.M. Barnett¹⁴¹, R.M. Barnett¹⁸, Z. Barnovska-Blenessy^{58a}, A. Baroncelli^{72a}, G. Barone²⁶, A.J. Barr¹³², L. Barranco Navarro¹⁷¹, F. Barreiro⁹⁶, J. Barreiro Guimarães da Costa^{15a}, R. Bartoldus¹⁵⁰, A.E. Barton⁸⁷, P. Bartos^{28a}, A. Basalae¹³⁵, A. Bassalat¹²⁹, R.L. Bates⁵⁵, S.J. Batista¹⁶⁴, S. Batlamous^{34e}, J.R. Batley³¹, M. Battaglia¹⁴³, M. Bauc^{70a,70b}, F. Bauer¹⁴², K.T. Bauer¹⁶⁸, H.S. Bawa^{150,n}, J.B. Beacham¹²³, T. Beau¹³³, P.H. Beauchemin¹⁶⁷, P. Bechtel²⁴, H.C. Beck⁵¹, H.P. Beck^{20,s}, K. Becker⁵⁰, M. Becker⁹⁷, C. Becot⁴⁴, A. Beddall^{12d}, A.J. Beddall^{12a}, V.A. Bednyakov⁷⁷, M. Bedognetti¹¹⁸, C.P. Bee¹⁵², T.A. Beermann³⁵, M. Begalli^{78b}, M. Begel²⁹, A. Behera¹⁵², J.K. Behr⁴⁴, A.S. Bell⁹², G. Bella¹⁵⁸, L. Bellagamba^{23b}, A. Bellerive³³, M. Bellomo¹⁵⁷, P. Bellos⁹, K. Belotskiy¹¹⁰, N.L. Belyaev¹¹⁰, O. Benary^{158,*}, D. Benchekroun^{34a}, M. Bender¹¹², N. Benekos¹⁰, Y. Benhammou¹⁵⁸, E. Benhar Noccioli¹⁸⁰, J. Benitez⁷⁵, D.P. Benjamin⁴⁷, M. Benoit⁵², J.R. Bensinger²⁶, S. Bentvelsen¹¹⁸, L. Beresford¹³², M. Beretta⁴⁹, D. Berge⁴⁴, E. Bergeaas Kuutmann¹⁶⁹, N. Berger⁵, L.J. Bergsten²⁶, J. Beringer¹⁸, S. Berlendis⁷, N.R. Bernard¹⁰⁰, G. Bernardi¹³³, C. Bernius¹⁵⁰, F.U. Bernlochner²⁴, T. Berry⁹¹, P. Berta⁹⁷, C. Bertella^{15a}, G. Bertoli^{43a,43b}, I.A. Bertram⁸⁷, G.J. Besjes³⁹, O. Bessidskaia Bylund¹⁷⁹, M. Bessner⁴⁴, N. Besson¹⁴², A. Bethani⁹⁸, S. Bethke¹¹³, A. Betti²⁴, A.J. Bevan⁹⁰, J. Beyer¹¹³, R.M. Bianchi¹³⁶, O. Biebel¹¹², D. Biedermann¹⁹, R. Bielski³⁵, K. Bierwagen⁹⁷, N.V. Biesuz^{69a,69b}, M. Biglietti^{72a}, T.R.V. Billoud¹⁰⁷, M. Bindi⁵¹, A. Bingul^{12d}, C. Bini^{70a,70b}, S. Biondi^{23b,23a}, M. Birman¹⁷⁷, T. Bisanz⁵¹, J.P. Biswal¹⁵⁸, C. Bittrich⁴⁶, D.M. Bjergaard⁴⁷, J.E. Black¹⁵⁰, K.M. Black²⁵, T. Blazek^{28a}, I. Bloch⁴⁴, C. Blocker²⁶, A. Blue⁵⁵, U. Blumenschein⁹⁰, Dr. Blunier^{144a}, G.J. Bobbink¹¹⁸, V.S. Bobrovnikov^{120b,120a},

S.S. Bocchetta⁹⁴, A. Bocci⁴⁷, D. Boerner¹⁷⁹, D. Bogavac¹¹², A.G. Bogdanchikov^{120b,120a}, C. Bohm^{43a},
 V. Boisvert⁹¹, P. Bokan¹⁶⁹, T. Bold^{81a}, A.S. Boldyrev¹¹¹, A.E. Bolz^{59b}, M. Bomben¹³³, M. Bona⁹⁰,
 J.S. Bonilla¹²⁸, M. Boonekamp¹⁴², A. Borisov¹²¹, G. Borissov⁸⁷, J. Bortfeldt³⁵, D. Bortoletto¹³²,
 V. Bortolotto^{71a,71b}, D. Boscherini^{23b}, M. Bosman¹⁴, J.D. Bossio Sola³⁰, K. Bouaouda^{34a}, J. Boudreau¹³⁶,
 E.V. Bouhova-Thacker⁸⁷, D. Boumediene³⁷, C. Bourdarios¹²⁹, S.K. Boutle⁵⁵, A. Boveia¹²³, J. Boyd³⁵,
 D. Boye^{32b}, I.R. Boyko⁷⁷, A.J. Bozson⁹¹, J. Bracini²¹, N. Brahimi⁹⁹, A. Brandt⁸, G. Brandt¹⁷⁹,
 O. Brandt^{59a}, F. Braren⁴⁴, U. Bratzler¹⁶¹, B. Brau¹⁰⁰, J.E. Brau¹²⁸, W.D. Breaden Madden⁵⁵,
 K. Brendlinger⁴⁴, L. Brenner⁴⁴, R. Brenner¹⁶⁹, S. Bressler¹⁷⁷, B. Brickwedde⁹⁷, D.L. Briglin²¹,
 D. Britton⁵⁵, D. Britzger^{59b}, I. Brock²⁴, R. Brock¹⁰⁴, G. Brooijmans³⁸, T. Brooks⁹¹, W.K. Brooks^{144b},
 E. Brost¹¹⁹, J.H. Broughton²¹, P.A. Bruckman de Renstrom⁸², D. Bruncko^{28b}, A. Bruni^{23b}, G. Bruni^{23b},
 L.S. Bruni¹¹⁸, S. Bruno^{71a,71b}, B.H. Brunt³¹, M. Bruschi^{23b}, N. Brusino¹³⁶, P. Bryant³⁶, L. Bryngemark⁴⁴,
 T. Buanes¹⁷, Q. Buat³⁵, P. Buchholz¹⁴⁸, A.G. Buckley⁵⁵, I.A. Budagov⁷⁷, M.K. Bugge¹³¹, F. Bühner⁵⁰,
 O. Bulekov¹¹⁰, D. Bullock⁸, T.J. Burch¹¹⁹, S. Burdin⁸⁸, C.D. Burgard¹¹⁸, A.M. Burger⁵, B. Burghgrave¹¹⁹,
 K. Burka⁸², S. Burke¹⁴¹, I. Burmeister⁴⁵, J.T.P. Burr¹³², V. Büscher⁹⁷, E. Buschmann⁵¹, P. Bussey⁵⁵,
 J.M. Butler²⁵, C.M. Buttar⁵⁵, J.M. Butterworth⁹², P. Butti³⁵, W. Buttinger³⁵, A. Buzatu¹⁵⁵,
 A.R. Buzykaev^{120b,120a}, G. Cabras^{23b,23a}, S. Cabrera Urbán¹⁷¹, D. Caforio¹³⁹, H. Cai¹⁷⁰, V.M.M. Cairo²,
 O. Cakir^{4a}, N. Calace⁵², P. Calafiura¹⁸, A. Calandri⁹⁹, G. Calderini¹³³, P. Calfayan⁶³, G. Callea^{40b,40a},
 L.P. Caloba^{78b}, S. Calvente Lopez⁹⁶, D. Calvet³⁷, S. Calvet³⁷, T.P. Calvet¹⁵², M. Calvetti^{69a,69b},
 R. Camacho Toro¹³³, S. Camarda³⁵, P. Camarri^{71a,71b}, D. Cameron¹³¹, R. Caminal Armadans¹⁰⁰,
 C. Camincher³⁵, S. Campana³⁵, M. Campanelli⁹², A. Camplani³⁹, A. Campoverde¹⁴⁸, V. Canale^{67a,67b},
 M. Cano Bret^{58c}, J. Cantero¹²⁶, T. Cao¹⁵⁸, Y. Cao¹⁷⁰, M.D.M. Capeans Garrido³⁵, I. Caprini^{27b},
 M. Caprini^{27b}, M. Capua^{40b,40a}, R.M. Carbone³⁸, R. Cardarelli^{71a}, F.C. Cardillo¹⁴⁶, I. Carli¹⁴⁰, T. Carli³⁵,
 G. Carlino^{67a}, B.T. Carlson¹³⁶, L. Carminati^{66a,66b}, R.M.D. Carney^{43a,43b}, S. Caron¹¹⁷, E. Carquin^{144b},
 S. Carrá^{66a,66b}, G.D. Carrillo-Montoya³⁵, D. Casadei^{32b}, M.P. Casado^{14g}, A.F. Casha¹⁶⁴, D.W. Casper¹⁶⁸,
 R. Castelijin¹¹⁸, F.L. Castillo¹⁷¹, V. Castillo Gimenez¹⁷¹, N.F. Castro^{137a,137e}, A. Catinaccio³⁵,
 J.R. Catmore¹³¹, A. Cattai³⁵, J. Caudron²⁴, V. Cavaliere²⁹, E. Cavallaro¹⁴, D. Cavalli^{66a},
 M. Cavalli-Sforza¹⁴, V. Cavasinni^{69a,69b}, E. Celebi^{12b}, F. Ceradini^{72a,72b}, L. Cerda Alberich¹⁷¹,
 A.S. Cerqueira^{78a}, A. Cerri¹⁵³, L. Cerrito^{71a,71b}, F. Cerutti¹⁸, A. Cervelli^{23b,23a}, S.A. Cetin^{12b},
 A. Chafaq^{34a}, D. Chakraborty¹¹⁹, S.K. Chan⁵⁷, W.S. Chan¹¹⁸, Y.L. Chan^{61a}, J.D. Chapman³¹,
 B. Chargeishvili^{156b}, D.G. Charlton²¹, C.C. Chau³³, C.A. Chavez Barajas¹⁵³, S. Che¹²³,
 A. Chegwidden¹⁰⁴, S. Chekanov⁶, S.V. Chekulaev^{165a}, G.A. Chelkov^{77,au}, M.A. Chelstowska³⁵,
 C. Chen^{58a}, C.H. Chen⁷⁶, H. Chen²⁹, J. Chen^{58a}, J. Chen³⁸, S. Chen¹³⁴, S.J. Chen^{15c}, X. Chen^{15b,at},
 Y. Chen⁸⁰, Y-H. Chen⁴⁴, H.C. Cheng¹⁰³, H.J. Cheng^{15d}, A. Cheplakov⁷⁷, E. Cheremushkina¹²¹,
 R. Cherkaoui El Moursli^{34e}, E. Cheu⁷, K. Cheung⁶², L. Chevalier¹⁴², V. Chiarella⁴⁹, G. Chiarelli^{69a},
 G. Chiodini^{65a}, A.S. Chisholm^{35,21}, A. Chitan^{27b}, I. Chiu¹⁶⁰, Y.H. Chiu¹⁷³, M.V. Chizhov⁷⁷, K. Choi⁶³,
 A.R. Chomont¹²⁹, S. Chouridou¹⁵⁹, Y.S. Chow¹¹⁸, V. Christodoulou⁹², M.C. Chu^{61a}, J. Chudoba¹³⁸,
 A.J. Chuinard¹⁰¹, J.J. Chwastowski⁸², L. Chytka¹²⁷, D. Cinca⁴⁵, V. Cindro⁸⁹, I.A. Cioară²⁴, A. Ciocio¹⁸,
 F. Ciotto^{67a,67b}, Z.H. Citron¹⁷⁷, M. Citterio^{66a}, A. Clark⁵², M.R. Clark³⁸, P.J. Clark⁴⁸, C. Clement^{43a,43b},
 Y. Coadou⁹⁹, M. Cobal^{64a,64c}, A. Coccaro^{53b,53a}, J. Cochran⁷⁶, H. Cohen¹⁵⁸, A.E.C. Coimbra¹⁷⁷,
 L. Colasurdo¹¹⁷, B. Cole³⁸, A.P. Colijn¹¹⁸, J. Collot⁵⁶, P. Conde Muiño^{137a,i}, E. Coniavitis⁵⁰,
 S.H. Connell^{32b}, I.A. Connelly⁹⁸, S. Constantinescu^{27b}, F. Conventi^{67a,aw}, A.M. Cooper-Sarkar¹³²,
 F. Cormier¹⁷², K.J.R. Cormier¹⁶⁴, L.D. Corpe⁹², M. Corradi^{70a,70b}, E.E. Corrigan⁹⁴, F. Corriveau^{101,ae},
 A. Cortes-Gonzalez³⁵, M.J. Costa¹⁷¹, F. Costanza⁵, D. Costanzo¹⁴⁶, G. Cottin³¹, G. Cowan⁹¹, B.E. Cox⁹⁸,
 J. Crane⁹⁸, K. Cranmer¹²², S.J. Crawley⁵⁵, R.A. Creager¹³⁴, G. Cree³³, S. Crépe-Renaudin⁵⁶,
 F. Crescioli¹³³, M. Cristinziani²⁴, V. Croft¹²², G. Crosetti^{40b,40a}, A. Cueto⁹⁶, T. Cuhadar Donszelmann¹⁴⁶,
 A.R. Cukierman¹⁵⁰, S. Czekierda⁸², P. Czodrowski³⁵, M.J. Da Cunha Sargedas De Sousa^{58b}, C. Da Via⁹⁸,
 W. Dabrowski^{81a}, T. Dado^{28a,z}, S. Dahbi^{34e}, T. Dai¹⁰³, F. Dallaire¹⁰⁷, C. Dallapiccola¹⁰⁰, M. Dam³⁹,

G. D'amen^{23b,23a}, J. Damp⁹⁷, J.R. Dandoy¹³⁴, M.F. Daneri³⁰, N.P. Dang^{178,1}, N.D. Dann⁹⁸, M. Danning¹⁷², V. Dao³⁵, G. Darbo^{53b}, S. Darmora⁸, O. Dartsis⁵, A. Dattagupta¹²⁸, T. Daubney⁴⁴, S. D'Auria⁵⁵, W. Davey²⁴, C. David⁴⁴, T. Davidek¹⁴⁰, D.R. Davis⁴⁷, E. Dawe¹⁰², I. Dawson¹⁴⁶, K. De⁸, R. De Asmundis^{67a}, A. De Benedetti¹²⁵, M. De Beurs¹¹⁸, S. De Castro^{23b,23a}, S. De Cecco^{70a,70b}, N. De Groot¹¹⁷, P. de Jong¹¹⁸, H. De la Torre¹⁰⁴, F. De Lorenzi⁷⁶, A. De Maria^{51,u}, D. De Pedis^{70a}, A. De Salvo^{70a}, U. De Sanctis^{71a,71b}, M. De Santis^{71a,71b}, A. De Santo¹⁵³, K. De Vasconcelos Corga⁹⁹, J.B. De Vivie De Regie¹²⁹, C. Debenedetti¹⁴³, D.V. Dedovich⁷⁷, N. Dehghanian³, M. Del Gaudio^{40b,40a}, J. Del Peso⁹⁶, Y. Delabat Diaz⁴⁴, D. Delgove¹²⁹, F. Deliot¹⁴², C.M. Delitzsch⁷, M. Della Pietra^{67a,67b}, D. Della Volpe⁵², A. Dell'Acqua³⁵, L. Dell'Asta²⁵, M. Delmastro⁵, C. Delporte¹²⁹, P.A. Delsart⁵⁶, D.A. DeMarco¹⁶⁴, S. Demers¹⁸⁰, M. Demichev⁷⁷, S.P. Denisov¹²¹, D. Denysiuk¹¹⁸, L. D'Eramo¹³³, D. Derendarz⁸², J.E. Derkaoui^{34d}, F. Derue¹³³, P. Dervan⁸⁸, K. Desch²⁴, C. Deterre⁴⁴, K. Dette¹⁶⁴, M.R. Devesa³⁰, P.O. Deviveiros³⁵, A. Dewhurst¹⁴¹, S. Dhaliwal²⁶, F.A. Di Bello⁵², A. Di Ciaccio^{71a,71b}, L. Di Ciaccio⁵, W.K. Di Clemente¹³⁴, C. Di Donato^{67a,67b}, A. Di Girolamo³⁵, B. Di Micco^{72a,72b}, R. Di Nardo¹⁰⁰, K.F. Di Petrillo⁵⁷, R. Di Sipio¹⁶⁴, D. Di Valentino³³, C. Diaconu⁹⁹, M. Diamond¹⁶⁴, F.A. Dias³⁹, T. Dias Do Vale^{137a}, M.A. Diaz^{144a}, J. Dickinson¹⁸, E.B. Diehl¹⁰³, J. Dietrich¹⁹, S. Díez Cornell⁴⁴, A. Dimitrievska¹⁸, J. Dingfelder²⁴, F. Dittus³⁵, F. Djama⁹⁹, T. Djobava^{156b}, J.I. Djuvland^{59a}, M.A.B. Do Vale^{78c}, M. Dobre^{27b}, D. Dodsworth²⁶, C. Doglioni⁹⁴, J. Dolejsi¹⁴⁰, Z. Dolezal¹⁴⁰, M. Donadelli^{78d}, J. Donini³⁷, A. D'onofrio⁹⁰, M. D'Onofrio⁸⁸, J. Dopke¹⁴¹, A. Doria^{67a}, M.T. Dova⁸⁶, A.T. Doyle⁵⁵, E. Drechsler⁵¹, E. Dreyer¹⁴⁹, T. Dreyer⁵¹, Y. Du^{58b}, F. Dubinin¹⁰⁸, M. Dubovsky^{28a}, A. Dubreuil⁵², E. Duchovni¹⁷⁷, G. Duckeck¹¹², A. Ducourthial¹³³, O.A. Ducu^{107,y}, D. Duda¹¹³, A. Dudarev³⁵, A.C. Dudder⁹⁷, E.M. Duffield¹⁸, L. Duflo¹²⁹, M. Dührssen³⁵, C. Dülzen¹⁷⁹, M. Dumancic¹⁷⁷, A.E. Dumitriu^{27b,e}, A.K. Duncan⁵⁵, M. Dunford^{59a}, A. Duperrin⁹⁹, H. Duran Yildiz^{4a}, M. Düren⁵⁴, A. Durglishvili^{156b}, D. Duschinger⁴⁶, B. Dutta⁴⁴, D. Duvnjak¹, M. Dyndal⁴⁴, S. Dysch⁹⁸, B.S. Dziedzic⁸², C. Eckardt⁴⁴, K.M. Ecker¹¹³, R.C. Edgar¹⁰³, T. Eifert³⁵, G. Eigen¹⁷, K. Einsweiler¹⁸, T. Ekelof¹⁶⁹, M. El Kacimi^{34c}, R. El Kosseifi⁹⁹, V. Ellajosyula⁹⁹, M. Ellert¹⁶⁹, F. Ellinghaus¹⁷⁹, A.A. Elliot⁹⁰, N. Ellis³⁵, J. Elmsheuser²⁹, M. Elsing³⁵, D. Emeliyanov¹⁴¹, Y. Enari¹⁶⁰, J.S. Ennis¹⁷⁵, M.B. Epland⁴⁷, J. Erdmann⁴⁵, A. Ereditato²⁰, S. Errede¹⁷⁰, M. Escalier¹²⁹, C. Escobar¹⁷¹, O. Estrada Pastor¹⁷¹, A.I. Etienve¹⁴², E. Etzion¹⁵⁸, H. Evans⁶³, A. Ezhilov¹³⁵, M. Ezzi^{34e}, F. Fabbri⁵⁵, L. Fabbri^{23b,23a}, V. Fabiani¹¹⁷, G. Facini⁹², R.M. Faisca Rodrigues Pereira^{137a}, R.M. Fakhruddinov¹²¹, S. Falciano^{70a}, P.J. Falke⁵, S. Falke⁵, J. Faltova¹⁴⁰, Y. Fang^{15a}, M. Fanti^{66a,66b}, A. Farbin⁸, A. Farilla^{72a}, E.M. Farina^{68a,68b}, T. Farooque¹⁰⁴, S. Farrell¹⁸, S.M. Farrington¹⁷⁵, P. Farthouat³⁵, F. Fassi^{34e}, P. Fassnacht³⁵, D. Fassouliotis⁹, M. Faucci Giannelli⁴⁸, A. Favareto^{53b,53a}, W.J. Fawcett³¹, L. Fayard¹²⁹, O.L. Fedin^{135,q}, W. Fedorko¹⁷², M. Feickert⁴¹, S. Feigl¹³¹, L. Feligioni⁹⁹, C. Feng^{58b}, E.J. Feng³⁵, M. Feng⁴⁷, M.J. Fenton⁵⁵, A.B. Fenyuk¹²¹, L. Feremenga⁸, J. Ferrando⁴⁴, A. Ferrari¹⁶⁹, P. Ferrari¹¹⁸, R. Ferrari^{68a}, D.E. Ferreira de Lima^{59b}, A. Ferrer¹⁷¹, D. Ferrere⁵², C. Ferretti¹⁰³, F. Fiedler⁹⁷, A. Filipčić⁸⁹, F. Filthaut¹¹⁷, K.D. Finelli²⁵, M.C.N. Fiolhais^{137a,137c,a}, L. Fiorini¹⁷¹, C. Fischer¹⁴, W.C. Fisher¹⁰⁴, N. Flaschel⁴⁴, I. Fleck¹⁴⁸, P. Fleischmann¹⁰³, R.R.M. Fletcher¹³⁴, T. Flick¹⁷⁹, B.M. Flierl¹¹², L.M. Flores¹³⁴, L.R. Flores Castillo^{61a}, F.M. Follega^{73a,73b}, N. Fomin¹⁷, G.T. Forcolin^{73a,73b}, A. Formica¹⁴², F.A. Förster¹⁴, A.C. Forti⁹⁸, A.G. Foster²¹, D. Fournier¹²⁹, H. Fox⁸⁷, S. Fracchia¹⁴⁶, P. Francavilla^{69a,69b}, M. Franchini^{23b,23a}, S. Franchino^{59a}, D. Francis³⁵, L. Franconi¹³¹, M. Franklin⁵⁷, M. Frate¹⁶⁸, M. Fraternali^{68a,68b}, A.N. Fray⁹⁰, D. Freeborn⁹², S.M. Fressard-Batraneanu³⁵, B. Freund¹⁰⁷, W.S. Freund^{78b}, E.M. Freundlich⁴⁵, D.C. Frizzell¹²⁵, D. Froidevaux³⁵, J.A. Frost¹³², C. Fukunaga¹⁶¹, E. Fullana Torregrosa¹⁷¹, T. Fusayasu¹¹⁴, J. Fuster¹⁷¹, O. Gabizon¹⁵⁷, A. Gabrielli^{23b,23a}, A. Gabrielli¹⁸, G.P. Gach^{81a}, S. Gadatsch⁵², P. Gadow¹¹³, G. Gagliardi^{53b,53a}, L.G. Gagnon¹⁰⁷, C. Galea^{27b}, B. Galhardo^{137a,137c}, E.J. Gallas¹³², B.J. Gallop¹⁴¹, P. Gallus¹³⁹, G. Galster³⁹, R. Gamboa Goni⁹⁰, K.K. Gan¹²³, S. Ganguly¹⁷⁷, J. Gao^{58a}, Y. Gao⁸⁸, Y.S. Gao^{150,n}, C. García¹⁷¹, J.E. García Navarro¹⁷¹, J.A. García Pascual^{15a}, M. Garcia-Sciveres¹⁸, R.W. Gardner³⁶, N. Garelli¹⁵⁰, V. Garonne¹³¹,

K. Gasnikova⁴⁴, A. Gaudiello^{53b,53a}, G. Gaudio^{68a}, I.L. Gavrilenko¹⁰⁸, A. Gavrilyuk¹⁰⁹, C. Gay¹⁷²,
 G. Gaycken²⁴, E.N. Gazis¹⁰, C.N.P. Gee¹⁴¹, J. Geisen⁵¹, M. Geisen⁹⁷, M.P. Geisler^{59a}, K. Gellerstedt^{43a,43b},
 C. Gemme^{53b}, M.H. Genest⁵⁶, C. Geng¹⁰³, S. Gentile^{70a,70b}, S. George⁹¹, D. Gerbaudo¹⁴, G. Gessner⁴⁵,
 S. Ghasemi¹⁴⁸, M. Ghasemi Bostanabad¹⁷³, M. Ghneimat²⁴, B. Giacobbe^{23b}, S. Giagu^{70a,70b},
 N. Giangiacomi^{23b,23a}, P. Giannetti^{69a}, A. Giannini^{67a,67b}, S.M. Gibson⁹¹, M. Gignac¹⁴³, D. Gillberg³³,
 G. Gilles¹⁷⁹, D.M. Gingrich^{3,av}, M.P. Giordani^{64a,64c}, F.M. Giorgi^{23b}, P.F. Giraud¹⁴², P. Giromini⁵⁷,
 G. Giugliarelli^{64a,64c}, D. Giugni^{66a}, F. Giuli¹³², M. Giulini^{59b}, S. Gkaitatzis¹⁵⁹, I. Gkialas^{9,k},
 E.L. Gkoukousis¹⁴, P. Gkountoumis¹⁰, L.K. Gladilin¹¹¹, C. Glasman⁹⁶, J. Glatzer¹⁴, P.C.F. Glaysher⁴⁴,
 A. Glazov⁴⁴, M. Goblirsch-Kolb²⁶, J. Godlewski⁸², S. Goldfarb¹⁰², T. Golling⁵², D. Golubkov¹²¹,
 A. Gomes^{137a,137b}, R. Goncalves Gama^{78a}, R. Gonçalo^{137a}, G. Gonella⁵⁰, L. Gonella²¹, A. Gongadze⁷⁷,
 F. Gonnella²¹, J.L. Gonski⁵⁷, S. González de la Hoz¹⁷¹, S. Gonzalez-Sevilla⁵², L. Goossens³⁵,
 P.A. Gorbounov¹⁰⁹, H.A. Gordon²⁹, B. Gorini³⁵, E. Gorini^{65a,65b}, A. Gorišek⁸⁹, A.T. Goshaw⁴⁷,
 C. Gössling⁴⁵, M.I. Gostkin⁷⁷, C.A. Gottardo²⁴, C.R. Goudet¹²⁹, D. Goujdami^{34c}, A.G. Goussiou¹⁴⁵,
 N. Govender^{32b,c}, C. Goy⁵, E. Gozani¹⁵⁷, I. Grabowska-Bold^{81a}, P.O.J. Gradin¹⁶⁹, E.C. Graham⁸⁸,
 J. Gramling¹⁶⁸, E. Gramstad¹³¹, S. Grancagnolo¹⁹, V. Gratchev¹³⁵, P.M. Gravila^{27f}, F.G. Gravili^{65a,65b},
 C. Gray⁵⁵, H.M. Gray¹⁸, Z.D. Greenwood^{93,al}, C. Grefe²⁴, K. Gregersen⁹⁴, I.M. Gregor⁴⁴, P. Grenier¹⁵⁰,
 K. Grevtsov⁴⁴, N.A. Grieser¹²⁵, J. Griffiths⁸, A.A. Grillo¹⁴³, K. Grimm^{150,b}, S. Grinstein^{14,aa}, Ph. Gris³⁷,
 J.-F. Grivaz¹²⁹, S. Groh⁹⁷, E. Gross¹⁷⁷, J. Grosse-Knetter⁵¹, G.C. Grossi⁹³, Z.J. Grout⁹², C. Grud¹⁰³,
 A. Grummer¹¹⁶, L. Guan¹⁰³, W. Guan¹⁷⁸, J. Guenther³⁵, A. Guerguichon¹²⁹, F. Guescini^{165a}, D. Guest¹⁶⁸,
 R. Gugel⁵⁰, B. Gui¹²³, T. Guillemin⁵, S. Guindon³⁵, U. Gul⁵⁵, C. Gumpert³⁵, J. Guo^{58c}, W. Guo¹⁰³,
 Y. Guo^{58a,t}, Z. Guo⁹⁹, R. Gupta⁴¹, S. Gurbuz^{12c}, G. Gustavino¹²⁵, B.J. Gutelman¹⁵⁷, P. Gutierrez¹²⁵,
 C. Gutschow⁹², C. Guyot¹⁴², M.P. Guzik^{81a}, C. Gwenlan¹³², C.B. Gwilliam⁸⁸, A. Haas¹²², C. Haber¹⁸,
 H.K. Hadavand⁸, N. Haddad^{34e}, A. Hadeef^{58a}, S. Hageböck²⁴, M. Hagihara¹⁶⁶, H. Hakobyan^{181,*},
 M. Haleem¹⁷⁴, J. Haley¹²⁶, G. Halladjian¹⁰⁴, G.D. Hallewell⁹⁹, K. Hamacher¹⁷⁹, P. Hamal¹²⁷,
 K. Hamano¹⁷³, A. Hamilton^{32a}, G.N. Hamity¹⁴⁶, K. Han^{58a,ak}, L. Han^{58a}, S. Han^{15d}, K. Hanagaki^{79,w},
 M. Hance¹⁴³, D.M. Handl¹¹², B. Haney¹³⁴, R. Hankache¹³³, P. Hanke^{59a}, E. Hansen⁹⁴, J.B. Hansen³⁹,
 J.D. Hansen³⁹, M.C. Hansen²⁴, P.H. Hansen³⁹, K. Hara¹⁶⁶, A.S. Hard¹⁷⁸, T. Harenberg¹⁷⁹, S. Harkusha¹⁰⁵,
 P.F. Harrison¹⁷⁵, N.M. Hartmann¹¹², Y. Hasegawa¹⁴⁷, A. Hasib⁴⁸, S. Hassani¹⁴², S. Haug²⁰, R. Hauser¹⁰⁴,
 L. Hauswald⁴⁶, L.B. Havener³⁸, M. Havranek¹³⁹, C.M. Hawkes²¹, R.J. Hawkings³⁵, D. Hayden¹⁰⁴,
 C. Hayes¹⁵², C.P. Hays¹³², J.M. Hays⁹⁰, H.S. Hayward⁸⁸, S.J. Haywood¹⁴¹, M.P. Heath⁴⁸, V. Hedberg⁹⁴,
 L. Heelan⁸, S. Heer²⁴, K.K. Heidegger⁵⁰, J. Heilman³³, S. Heim⁴⁴, T. Heim¹⁸, B. Heinemann^{44,aq},
 J.J. Heinrich¹¹², L. Heinrich¹²², C. Heinz⁵⁴, J. Hejbal¹³⁸, L. Helary³⁵, A. Held¹⁷², S. Hellesund¹³¹,
 S. Hellman^{43a,43b}, C. Helsens³⁵, R.C.W. Henderson⁸⁷, Y. Heng¹⁷⁸, S. Henkelmann¹⁷²,
 A.M. Henriques Correia³⁵, G.H. Herbert¹⁹, H. Herde²⁶, V. Herget¹⁷⁴, Y. Hernández Jiménez^{32c}, H. Herr⁹⁷,
 M.G. Herrmann¹¹², G. Herten⁵⁰, R. Hertenberger¹¹², L. Hervas³⁵, T.C. Herwig¹³⁴, G.G. Hesketh⁹²,
 N.P. Hesse^{165a}, J.W. Hetherly⁴¹, S. Higashino⁷⁹, E. Higón-Rodríguez¹⁷¹, K. Hildebrand³⁶, E. Hill¹⁷³,
 J.C. Hill³¹, K.K. Hill²⁹, K.H. Hiller⁴⁴, S.J. Hillier²¹, M. Hils⁴⁶, I. Hinchliffe¹⁸, M. Hirose¹³⁰,
 D. Hirschbuehl¹⁷⁹, B. Hiti⁸⁹, O. Hladik¹³⁸, D.R. Hlaluku^{32c}, X. Hoad⁴⁸, J. Hobbs¹⁵², N. Hod^{165a},
 M.C. Hodgkinson¹⁴⁶, A. Hoecker³⁵, M.R. Hoferkamp¹¹⁶, F. Hoenig¹¹², D. Hohn²⁴, D. Hohov¹²⁹,
 T.R. Holmes³⁶, M. Holzbock¹¹², M. Homann⁴⁵, S. Honda¹⁶⁶, T. Honda⁷⁹, T.M. Hong¹³⁶, A. Hönle¹¹³,
 B.H. Hooberman¹⁷⁰, W.H. Hopkins¹²⁸, Y. Horii¹¹⁵, P. Horn⁴⁶, A.J. Horton¹⁴⁹, L.A. Horyn³⁶,
 J-Y. Hostachy⁵⁶, A. Hostiuc¹⁴⁵, S. Hou¹⁵⁵, A. Hoummada^{34a}, J. Howarth⁹⁸, J. Hoya⁸⁶, M. Hrabovsky¹²⁷,
 I. Hristova¹⁹, J. Hrivnac¹²⁹, A. Hrynevich¹⁰⁶, T. Hryn'ova⁵, P.J. Hsu⁶², S.-C. Hsu¹⁴⁵, Q. Hu²⁹, S. Hu^{58c},
 Y. Huang^{15a}, Z. Hubacek¹³⁹, F. Hubaut⁹⁹, M. Huebner²⁴, F. Huegging²⁴, T.B. Huffman¹³², E.W. Hughes³⁸,
 M. Huhtinen³⁵, R.F.H. Hunter³³, P. Huo¹⁵², A.M. Hupe³³, N. Huseynov^{77,ag}, J. Huston¹⁰⁴, J. Huth⁵⁷,
 R. Hyneman¹⁰³, G. Iacobucci⁵², G. Iakovidis²⁹, I. Ibragimov¹⁴⁸, L. Iconomidou-Fayard¹²⁹, Z. Idrissi^{34e},
 P. Iengo³⁵, R. Ignazzi³⁹, O. Igonkina^{118,ac}, R. Iguchi¹⁶⁰, T. Iizawa⁵², Y. Ikegami⁷⁹, M. Ikeno⁷⁹,

D. Iliadis¹⁵⁹, N. Ilic¹¹⁷, F. Iltzsche⁴⁶, G. Introzzi^{68a,68b}, M. Iodice^{72a}, K. Iordanidou³⁸, V. Ippolito^{70a,70b},
 M.F. Isacson¹⁶⁹, N. Ishijima¹³⁰, M. Ishino¹⁶⁰, M. Ishitsuka¹⁶², W. Islam¹²⁶, C. Issever¹³², S. Istin¹⁵⁷,
 F. Ito¹⁶⁶, J.M. Iturbe Ponce^{61a}, R. Iuppa^{73a,73b}, A. Ivina¹⁷⁷, H. Iwasaki⁷⁹, J.M. Izen⁴², V. Izzo^{67a},
 P. Jacka¹³⁸, P. Jackson¹, R.M. Jacobs²⁴, V. Jain², G. Jäkel¹⁷⁹, K.B. Jakobi⁹⁷, K. Jakobs⁵⁰, S. Jakobsen⁷⁴,
 T. Jakoubek¹³⁸, D.O. Jamin¹²⁶, D.K. Jana⁹³, R. Jansky⁵², J. Janssen²⁴, M. Janus⁵¹, P.A. Janus^{81a},
 G. Jarlskog⁹⁴, N. Javadov^{77,ag}, T. Javůrek³⁵, M. Javurkova⁵⁰, F. Jeanneau¹⁴², L. Jeanty¹⁸, J. Jejelava^{156a,ah},
 A. Jelinskas¹⁷⁵, P. Jenni^{50,d}, J. Jeong⁴⁴, N. Jeong⁴⁴, S. Jézéquel⁵, H. Ji¹⁷⁸, J. Jia¹⁵², H. Jiang⁷⁶, Y. Jiang^{58a},
 Z. Jiang^{150,r}, S. Jiggins⁵⁰, F.A. Jimenez Morales³⁷, J. Jimenez Pena¹⁷¹, S. Jin^{15c}, A. Jinaru^{27b},
 O. Jinnouchi¹⁶², H. Jivan^{32c}, P. Johansson¹⁴⁶, K.A. Johns⁷, C.A. Johnson⁶³, W.J. Johnson¹⁴⁵,
 K. Jon-And^{43a,43b}, R.W.L. Jones⁸⁷, S.D. Jones¹⁵³, S. Jones⁷, T.J. Jones⁸⁸, J. Jongmanns^{59a},
 P.M. Jorge^{137a,137b}, J. Jovicevic^{165a}, X. Ju¹⁸, J.J. Junggeburth¹¹³, A. Juste Rozas^{14,aa}, A. Kaczmarzka⁸²,
 M. Kado¹²⁹, H. Kagan¹²³, M. Kagan¹⁵⁰, T. Kaji¹⁷⁶, E. Kajomovitz¹⁵⁷, C.W. Kalderon⁹⁴, A. Kaluza⁹⁷,
 S. Kama⁴¹, A. Kamenshchikov¹²¹, L. Kanjir⁸⁹, Y. Kano¹⁶⁰, V.A. Kantserov¹¹⁰, J. Kanzaki⁷⁹, B. Kaplan¹²²,
 L.S. Kaplan¹⁷⁸, D. Kar^{32c}, M.J. Kareem^{165b}, E. Karentzos¹⁰, S.N. Karpov⁷⁷, Z.M. Karpova⁷⁷,
 V. Kartvelishvili⁸⁷, A.N. Karyukhin¹²¹, L. Kashif¹⁷⁸, R.D. Kass¹²³, A. Kastanas¹⁵¹, Y. Kataoka¹⁶⁰,
 C. Kato^{58d,58c}, J. Katzy⁴⁴, K. Kawade⁸⁰, K. Kawagoe⁸⁵, T. Kawamoto¹⁶⁰, G. Kawamura⁵¹, E.F. Kay⁸⁸,
 V.F. Kazanin^{120b,120a}, R. Keeler¹⁷³, R. Kehoe⁴¹, J.S. Keller³³, E. Kellermann⁹⁴, J.J. Kempster²¹,
 J. Kendrick²¹, O. Kepka¹³⁸, S. Kersten¹⁷⁹, B.P. Kerševan⁸⁹, R.A. Keyes¹⁰¹, M. Khader¹⁷⁰,
 F. Khalil-Zada¹³, A. Khanov¹²⁶, A.G. Kharlamov^{120b,120a}, T. Kharlamova^{120b,120a}, E.E. Khoda¹⁷²,
 A. Khodinov¹⁶³, T.J. Khoo⁵², E. Khramov⁷⁷, J. Khubua^{156b}, S. Kido⁸⁰, M. Kiehn⁵², C.R. Kilby⁹¹,
 Y.K. Kim³⁶, N. Kimura^{64a,64c}, O.M. Kind¹⁹, B.T. King⁸⁸, D. Kirchmeier⁴⁶, J. Kirk¹⁴¹, A.E. Kiryunin¹¹³,
 T. Kishimoto¹⁶⁰, D. Kisielewska^{81a}, V. Kitali⁴⁴, O. Kivernyk⁵, E. Kladiva^{28b,*}, T. Klapdor-Kleingrothaus⁵⁰,
 M.H. Klein¹⁰³, M. Klein⁸⁸, U. Klein⁸⁸, K. Kleinknecht⁹⁷, P. Klimek¹¹⁹, A. Klimentov²⁹,
 R. Klingenberg^{45,*}, T. Klingl¹²⁴, T. Klioutchnikova³⁵, F.F. Klitzner¹¹², P. Kluit¹¹⁸, S. Kluth¹¹³,
 E. Kneringer⁷⁴, E.B.F.G. Knoop⁹⁹, A. Knue⁵⁰, A. Kobayashi¹⁶⁰, D. Kobayashi⁸⁵, T. Kobayashi¹⁶⁰,
 M. Kobel⁴⁶, M. Kocian¹⁵⁰, P. Kodys¹⁴⁰, P.T. Koenig²⁴, T. Koffas³³, E. Koffeman¹¹⁸, N.M. Köhler¹¹³,
 T. Koi¹⁵⁰, M. Kolb^{59b}, I. Koletsou⁵, T. Kondo⁷⁹, N. Kondrashova^{58c}, K. Köneke⁵⁰, A.C. König¹¹⁷,
 T. Kono⁷⁹, R. Konoplich^{122,an}, V. Konstantinides⁹², N. Konstantinidis⁹², B. Konya⁹⁴, R. Kopeliansky⁶³,
 S. Koperly^{81a}, K. Korcyl⁸², K. Kordas¹⁵⁹, G. Koren¹⁵⁸, A. Korn⁹², I. Korolkov¹⁴, E.V. Korolkova¹⁴⁶,
 N. Korotkova¹¹¹, O. Kortner¹¹³, S. Kortner¹¹³, T. Kosek¹⁴⁰, V.V. Kostyukhin²⁴, A. Kotwal⁴⁷,
 A. Koulouris¹⁰, A. Kourkouveli-Charalampidi^{68a,68b}, C. Kourkouvelis⁹, E. Kourlitis¹⁴⁶, V. Kouskoura²⁹,
 A.B. Kowalewska⁸², R. Kowalewski¹⁷³, T.Z. Kowalski^{81a}, C. Kozakai¹⁶⁰, W. Kozanecki¹⁴²,
 A.S. Kozhin¹²¹, V.A. Kramarenko¹¹¹, G. Kramberger⁸⁹, D. Krasnopevtsev^{58a}, M.W. Krasny¹³³,
 A. Krasznahorkay³⁵, D. Krauss¹¹³, J.A. Kremer^{81a}, J. Kretzschmar⁸⁸, P. Krieger¹⁶⁴, K. Krizka¹⁸,
 K. Kroeninger⁴⁵, H. Kroha¹¹³, J. Kroll¹³⁸, J. Kroll¹³⁴, J. Krstic¹⁶, U. Kruchonak⁷⁷, H. Krüger²⁴,
 N. Krumnack⁷⁶, M.C. Kruse⁴⁷, T. Kubota¹⁰², S. Kuday^{4b}, J.T. Kuechler¹⁷⁹, S. Kuehn³⁵, A. Kugel^{59a},
 F. Kuger¹⁷⁴, T. Kuhl⁴⁴, V. Kukhtin⁷⁷, R. Kukla⁹⁹, Y. Kulchitsky¹⁰⁵, S. Kuleshov^{144b}, Y.P. Kulinich¹⁷⁰,
 M. Kuna⁵⁶, T. Kunigo⁸³, A. Kupco¹³⁸, T. Kupfer⁴⁵, O. Kuprash¹⁵⁸, H. Kurashige⁸⁰, L.L. Kurchaninov^{165a},
 Y.A. Kurochkin¹⁰⁵, M.G. Kurth^{15d}, E.S. Kuwertz³⁵, M. Kuze¹⁶², A.K. Kvam¹⁴⁵, J. Kvita¹²⁷, T. Kwan¹⁰¹,
 A. La Rosa¹¹³, J.L. La Rosa Navarro^{78d}, L. La Rotonda^{40b,40a}, F. La Ruffa^{40b,40a}, C. Lacasta¹⁷¹,
 F. Lacava^{70a,70b}, J. Lacey⁴⁴, D.P.J. Lack⁹⁸, H. Lacker¹⁹, D. Lacour¹³³, E. Ladygin⁷⁷, R. Lafaye⁵,
 B. Laforge¹³³, T. Lagouri^{32c}, S. Lai⁵¹, S. Lammers⁶³, W. Lampl⁷, E. Lançon²⁹, U. Landgraf⁵⁰,
 M.P.J. Landon⁹⁰, M.C. Lanfermann⁵², V.S. Lang⁴⁴, J.C. Lange¹⁴, R.J. Langenberg³⁵, A.J. Lankford¹⁶⁸,
 F. Lanni²⁹, K. Lantzsch²⁴, A. Lanza^{68a}, A. Lapertosa^{53b,53a}, S. Laplace¹³³, J.F. Laporte¹⁴², T. Lari^{66a},
 F. Lasagni Manghi^{23b,23a}, M. Lassnig³⁵, T.S. Lau^{61a}, A. Laudrain¹²⁹, M. Lavorgna^{67a,67b}, A.T. Law¹⁴³,
 M. Lazzaroni^{66a,66b}, B. Le¹⁰², O. Le Dortz¹³³, E. Le Guirriec⁹⁹, E.P. Le Quilleuc¹⁴², M. LeBlanc⁷,
 T. LeCompte⁶, F. Ledroit-Guillon⁵⁶, C.A. Lee²⁹, G.R. Lee^{144a}, L. Lee⁵⁷, S.C. Lee¹⁵⁵, B. Lefebvre¹⁰¹,

M. Lefebvre¹⁷³, F. Legger¹¹², C. Leggett¹⁸, K. Lehmann¹⁴⁹, N. Lehmann¹⁷⁹, G. Lehmann Miotto³⁵,
W.A. Leight⁴⁴, A. Leisos^{159,x}, M.A.L. Leite^{78d}, R. Leitner¹⁴⁰, D. Lellouch¹⁷⁷, B. Lemmer⁵¹,
K.J.C. Leney⁹², T. Lenz²⁴, B. Lenzi³⁵, R. Leone⁷, S. Leone^{69a}, C. Leonidopoulos⁴⁸, G. Lerner¹⁵³,
C. Leroy¹⁰⁷, R. Les¹⁶⁴, A.A.J. Lesage¹⁴², C.G. Lester³¹, M. Levchenko¹³⁵, J. Levêque⁵, D. Levin¹⁰³,
L.J. Levinson¹⁷⁷, D. Lewis⁹⁰, B. Li¹⁰³, C-Q. Li^{58a,am}, H. Li^{58b}, L. Li^{58c}, M. Li^{15a}, Q. Li^{15d}, Q.Y. Li^{58a},
S. Li^{58d,58c}, X. Li^{58c}, Y. Li¹⁴⁸, Z. Liang^{15a}, B. Liberti^{71a}, A. Liblong¹⁶⁴, K. Lie^{61c}, S. Liem¹¹⁸,
A. Limosani¹⁵⁴, C.Y. Lin³¹, K. Lin¹⁰⁴, T.H. Lin⁹⁷, R.A. Linck⁶³, J.H. Lindon²¹, B.E. Lindquist¹⁵²,
A.L. Lioni⁵², E. Lipeles¹³⁴, A. Lipniacka¹⁷, M. Lisovyi^{59b}, T.M. Liss^{170,as}, A. Lister¹⁷², A.M. Litke¹⁴³,
J.D. Little⁸, B. Liu⁷⁶, B.L. Liu⁶, H.B. Liu²⁹, H. Liu¹⁰³, J.B. Liu^{58a}, J.K.K. Liu¹³², K. Liu¹³³, M. Liu^{58a},
P. Liu¹⁸, Y. Liu^{15a}, Y.L. Liu^{58a}, Y.W. Liu^{58a}, M. Livan^{68a,68b}, A. Lleres⁵⁶, J. Llorente Merino^{15a},
S.L. Lloyd⁹⁰, C.Y. Lo^{61b}, F. Lo Sterzo⁴¹, E.M. Lobodzinska⁴⁴, P. Loch⁷, T. Lohse¹⁹, K. Lohwasser¹⁴⁶,
M. Lokajicek¹³⁸, B.A. Long²⁵, J.D. Long¹⁷⁰, R.E. Long⁸⁷, L. Longo^{65a,65b}, K.A. Looper¹²³,
J.A. Lopez^{144b}, I. Lopez Paz¹⁴, A. Lopez Solis¹⁴⁶, J. Lorenz¹¹², N. Lorenzo Martinez⁵, M. Losada²²,
P.J. Lösel¹¹², A. Lösle⁵⁰, X. Lou⁴⁴, X. Lou^{15a}, A. Lounis¹²⁹, J. Love⁶, P.A. Love⁸⁷, J.J. Lozano Bahilo¹⁷¹,
H. Lu^{61a}, M. Lu^{58a}, N. Lu¹⁰³, Y.J. Lu⁶², H.J. Lubatti¹⁴⁵, C. Luci^{70a,70b}, A. Lucotte⁵⁶, C. Luedtke⁵⁰,
F. Luehring⁶³, I. Luise¹³³, L. Luminari^{70a}, B. Lund-Jensen¹⁵¹, M.S. Lutz¹⁰⁰, P.M. Luzi¹³³, D. Lynn²⁹,
R. Lysak¹³⁸, E. Lytken⁹⁴, F. Lyu^{15a}, V. Lyubushkin⁷⁷, H. Ma²⁹, L.L. Ma^{58b}, Y. Ma^{58b}, G. Maccarrone⁴⁹,
A. Macchiolo¹¹³, C.M. Macdonald¹⁴⁶, J. Machado Miguens^{134,137b}, D. Madaffari¹⁷¹, R. Madar³⁷,
W.F. Mader⁴⁶, A. Madsen⁴⁴, N. Madysa⁴⁶, J. Maeda⁸⁰, K. Maekawa¹⁶⁰, S. Maeland¹⁷, T. Maeno²⁹,
A.S. Maevskiy¹¹¹, V. Magerl⁵⁰, C. Maidantchik^{78b}, T. Maier¹¹², A. Maio^{137a,137b,137d}, O. Majersky^{28a},
S. Majewski¹²⁸, Y. Makida⁷⁹, N. Makovec¹²⁹, B. Malaescu¹³³, Pa. Malecki⁸², V.P. Maleev¹³⁵, F. Malek⁵⁶,
U. Mallik⁷⁵, D. Malon⁶, C. Malone³¹, S. Maltezos¹⁰, S. Malyukov³⁵, J. Mamuzic¹⁷¹, G. Mancini⁴⁹,
I. Mandić⁸⁹, J. Maneira^{137a}, L. Manhaes de Andrade Filho^{78a}, J. Manjarres Ramos⁴⁶, K.H. Mankinen⁹⁴,
A. Mann¹¹², A. Manousos⁷⁴, B. Mansoulie¹⁴², J.D. Mansour^{15a}, M. Mantoani⁵¹, S. Manzoni^{66a,66b},
G. Marceca³⁰, L. March⁵², L. Marchese¹³², G. Marchiori¹³³, M. Marcisovsky¹³⁸, C.A. Marin Tobon³⁵,
M. Marjanovic³⁷, D.E. Marley¹⁰³, F. Marroquim^{78b}, Z. Marshall¹⁸, M.U.F. Martensson¹⁶⁹,
S. Marti-Garcia¹⁷¹, C.B. Martin¹²³, T.A. Martin¹⁷⁵, V.J. Martin⁴⁸, B. Martin dit Latour¹⁷, M. Martinez^{14,aa},
V.I. Martinez Outschoorn¹⁰⁰, S. Martin-Haugh¹⁴¹, V.S. Martoiu^{27b}, A.C. Martyniuk⁹², A. Marzin³⁵,
L. Masetti⁹⁷, T. Mashimo¹⁶⁰, R. Mashinistov¹⁰⁸, J. Masik⁹⁸, A.L. Maslennikov^{120b,120a}, L.H. Mason¹⁰²,
L. Massa^{71a,71b}, P. Massarotti^{67a,67b}, P. Mastrandrea⁵, A. Mastroberardino^{40b,40a}, T. Masubuchi¹⁶⁰,
P. Mättig¹⁷⁹, J. Maurer^{27b}, B. Maček⁸⁹, S.J. Maxfield⁸⁸, D.A. Maximov^{120b,120a}, R. Mazini¹⁵⁵,
I. Maznas¹⁵⁹, S.M. Mazza¹⁴³, N.C. Mc Fadden¹¹⁶, G. Mc Goldrick¹⁶⁴, S.P. Mc Kee¹⁰³, A. McCarn¹⁰³,
T.G. McCarthy¹¹³, L.I. McClymont⁹², E.F. McDonald¹⁰², J.A. Mcfayden³⁵, G. Mchedlidze⁵¹,
M.A. McKay⁴¹, K.D. McLean¹⁷³, S.J. McMahon¹⁴¹, P.C. McNamara¹⁰², C.J. McNicol¹⁷⁵,
R.A. McPherson^{173,ae}, J.E. Mdhluli^{32c}, Z.A. Meadows¹⁰⁰, S. Meehan¹⁴⁵, T.M. Megy⁵⁰, S. Mehlhase¹¹²,
A. Mehta⁸⁸, T. Meideck⁵⁶, B. Meirose⁴², D. Melini^{171,h}, B.R. Mellado Garcia^{32c}, J.D. Mellenthin⁵¹,
M. Melo^{28a}, F. Meloni⁴⁴, A. Melzer²⁴, S.B. Menary⁹⁸, E.D. Mendes Gouveia^{137a}, L. Meng⁸⁸,
X.T. Meng¹⁰³, A. Mengarelli^{23b,23a}, S. Menke¹¹³, E. Meoni^{40b,40a}, S. Mergelmeyer¹⁹, C. Merlassino²⁰,
P. Mermod⁵², L. Merola^{67a,67b}, C. Meroni^{66a}, F.S. Merritt³⁶, A. Messina^{70a,70b}, J. Metcalfe⁶, A.S. Mete¹⁶⁸,
C. Meyer¹³⁴, J. Meyer¹⁵⁷, J-P. Meyer¹⁴², H. Meyer Zu Theenhausen^{59a}, F. Miano¹⁵³, R.P. Middleton¹⁴¹,
L. Mijović⁴⁸, G. Mikenberg¹⁷⁷, M. Mikesikova¹³⁸, M. Mikuž⁸⁹, M. Milesi¹⁰², A. Milic¹⁶⁴, D.A. Millar⁹⁰,
D.W. Miller³⁶, A. Milov¹⁷⁷, D.A. Milstead^{43a,43b}, A.A. Minaenko¹²¹, M. Miñano Moya¹⁷¹,
I.A. Minashvili^{156b}, A.I. Mincer¹²², B. Mindur^{81a}, M. Mineev⁷⁷, Y. Minegishi¹⁶⁰, Y. Ming¹⁷⁸, L.M. Mir¹⁴,
A. Mirto^{65a,65b}, K.P. Mistry¹³⁴, T. Mitani¹⁷⁶, J. Mitrevski¹¹², V.A. Mitsou¹⁷¹, A. Miucci²⁰,
P.S. Miyagawa¹⁴⁶, A. Mizukami⁷⁹, J.U. Mjörnmark⁹⁴, T. Mkrtchyan¹⁸¹, M. Mlynarikova¹⁴⁰, T. Moa^{43a,43b},
K. Mochizuki¹⁰⁷, P. Mogg⁵⁰, S. Mohapatra³⁸, S. Molander^{43a,43b}, R. Moles-Valls²⁴, M.C. Mondragon¹⁰⁴,
K. Mönig⁴⁴, J. Monk³⁹, E. Monnier⁹⁹, A. Montalbano¹⁴⁹, J. Montejo Berlingen³⁵, F. Monticelli⁸⁶,

S. Monzani^{66a}, N. Morange¹²⁹, D. Moreno²², M. Moreno Llácer³⁵, P. Morettini^{53b}, M. Morgenstern¹¹⁸, S. Morgenstern⁴⁶, D. Mori¹⁴⁹, M. Morii⁵⁷, M. Morinaga¹⁷⁶, V. Morisbak¹³¹, A.K. Morley³⁵, G. Mornacchi³⁵, A.P. Morris⁹², J.D. Morris⁹⁰, L. Morvaj¹⁵², P. Moschovakos¹⁰, M. Mosidze^{156b}, H.J. Moss¹⁴⁶, J. Moss^{150,o}, K. Motohashi¹⁶², R. Mount¹⁵⁰, E. Mountricha³⁵, E.J.W. Moyse¹⁰⁰, S. Muanza⁹⁹, F. Mueller¹¹³, J. Mueller¹³⁶, R.S.P. Mueller¹¹², D. Muenstermann⁸⁷, G.A. Mullier²⁰, F.J. Munoz Sanchez⁹⁸, P. Murin^{28b}, W.J. Murray^{175,141}, A. Murrone^{66a,66b}, M. Muškinja⁸⁹, C. Mwewa^{32a}, A.G. Myagkov^{121,ao}, J. Myers¹²⁸, M. Myska¹³⁹, B.P. Nachman¹⁸, O. Nackenhorst⁴⁵, K. Nagai¹³², K. Nagano⁷⁹, Y. Nagasaka⁶⁰, M. Nagel⁵⁰, E. Nagy⁹⁹, A.M. Nairz³⁵, Y. Nakahama¹¹⁵, K. Nakamura⁷⁹, T. Nakamura¹⁶⁰, I. Nakano¹²⁴, H. Nanjo¹³⁰, F. Napolitano^{59a}, R.F. Naranjo Garcia⁴⁴, R. Narayan¹¹, D.I. Narrias Villar^{59a}, I. Naryshkin¹³⁵, T. Naumann⁴⁴, G. Navarro²², R. Nayyar⁷, H.A. Neal^{103,*}, P.Y. Nechaeva¹⁰⁸, T.J. Neep¹⁴², A. Negri^{68a,68b}, M. Negrini^{23b}, S. Nektarijevic¹¹⁷, C. Nellist⁵¹, M.E. Nelson¹³², S. Nemecek¹³⁸, P. Nemethy¹²², M. Nessi^{35,f}, M.S. Neubauer¹⁷⁰, M. Neumann¹⁷⁹, P.R. Newman²¹, T.Y. Ng^{61c}, Y.S. Ng¹⁹, H.D.N. Nguyen⁹⁹, T. Nguyen Manh¹⁰⁷, E. Nibigira³⁷, R.B. Nickerson¹³², R. Nicolaidou¹⁴², J. Nielsen¹⁴³, N. Nikiforou¹¹, V. Nikolaenko^{121,ao}, I. Nikolic-Audit¹³³, K. Nikolopoulos²¹, P. Nilsson²⁹, Y. Ninomiya⁷⁹, A. Nisati^{70a}, N. Nishu^{58c}, R. Nisius¹¹³, I. Nitsche⁴⁵, T. Nitta¹⁷⁶, T. Nobe¹⁶⁰, Y. Noguchi⁸³, M. Nomachi¹³⁰, I. Nomidis¹³³, M.A. Nomura²⁹, T. Nooney⁹⁰, M. Nordberg³⁵, N. Norjoharuddeen¹³², T. Novak⁸⁹, O. Novgorodova⁴⁶, R. Novotny¹³⁹, L. Nozka¹²⁷, K. Ntekas¹⁶⁸, E. Nurse⁹², F. Nuti¹⁰², F.G. Oakham^{33,av}, H. Oberlack¹¹³, T. Obermann²⁴, J. Ocariz¹³³, A. Ochi⁸⁰, I. Ochoa³⁸, J.P. Ochoa-Ricoux^{144a}, K. O'Connor²⁶, S. Oda⁸⁵, S. Odaka⁷⁹, S. Oerdek⁵¹, A. Oh⁹⁸, S.H. Oh⁴⁷, C.C. Ohm¹⁵¹, H. Oide^{53b,53a}, M.L. Ojeda¹⁶⁴, H. Okawa¹⁶⁶, Y. Okazaki⁸³, Y. Okumura¹⁶⁰, T. Okuyama⁷⁹, A. Olariu^{27b}, L.F. Oleiro Seabra^{137a}, S.A. Olivares Pino^{144a}, D. Oliveira Damazio²⁹, J.L. Oliver¹, M.J.R. Olsson³⁶, A. Olszewski⁸², J. Olszowska⁸², D.C. O'Neil¹⁴⁹, A. Onofre^{137a,137e}, K. Onogi¹¹⁵, P.U.E. Onyisi¹¹, H. Oppen¹³¹, M.J. Oreglia³⁶, G.E. Orellana⁸⁶, Y. Oren¹⁵⁸, D. Orestano^{72a,72b}, E.C. Orgill⁹⁸, N. Orlando^{61b}, A.A. O'Rourke⁴⁴, R.S. Orr¹⁶⁴, B. Osculati^{53b,53a,*}, V. O'Shea⁵⁵, R. Ospanov^{58a}, G. Otero y Garzon³⁰, H. Otono⁸⁵, M. Ouchrif^{34d}, F. Ould-Saada¹³¹, A. Ouraou¹⁴², Q. Ouyang^{15a}, M. Owen⁵⁵, R.E. Owen²¹, V.E. Ozcan^{12c}, N. Ozturk⁸, J. Pacalt¹²⁷, H.A. Pacey³¹, K. Pachal¹⁴⁹, A. Pacheco Pages¹⁴, L. Pacheco Rodriguez¹⁴², C. Padilla Aranda¹⁴, S. Pagan Griso¹⁸, M. Paganini¹⁸⁰, G. Palacino⁶³, S. Palazzo^{40b,40a}, S. Palestini³⁵, M. Palka^{81b}, D. Pallin³⁷, I. Panagoulas¹⁰, C.E. Pandini³⁵, J.G. Panduro Vazquez⁹¹, P. Pani³⁵, G. Panizzo^{64a,64c}, L. Paolozzi⁵², T.D. Papadopoulou¹⁰, K. Papageorgiou^{9,k}, A. Paramonov⁶, D. Paredes Hernandez^{61b}, S.R. Paredes Saenz¹³², B. Parida¹⁶³, A.J. Parker⁸⁷, K.A. Parker⁴⁴, M.A. Parker³¹, F. Parodi^{53b,53a}, J.A. Parsons³⁸, U. Parzefall⁵⁰, V.R. Pascuzzi¹⁶⁴, J.M.P. Pasner¹⁴³, E. Pasqualucci^{70a}, S. Passaggio^{53b}, F. Pastore⁹¹, P. Pasuwan^{43a,43b}, S. Patariaia⁹⁷, J.R. Pater⁹⁸, A. Pathak^{178,1}, T. Pauly³⁵, B. Pearson¹¹³, M. Pedersen¹³¹, L. Pedraza Diaz¹¹⁷, R. Pedro^{137a,137b}, S.V. Peleganchuk^{120b,120a}, O. Penc¹³⁸, C. Peng^{15d}, H. Peng^{58a}, B.S. Peralva^{78a}, M.M. Perego¹⁴², A.P. Pereira Peixoto^{137a}, D.V. Perepelitsa²⁹, F. Peri¹⁹, L. Perini^{66a,66b}, H. Pernegger³⁵, S. Perrella^{67a,67b}, V.D. Peshekhonov^{77,*}, K. Peters⁴⁴, R.F.Y. Peters⁹⁸, B.A. Petersen³⁵, T.C. Petersen³⁹, E. Petit⁵⁶, A. Petridis¹, C. Petridou¹⁵⁹, P. Petroff¹²⁹, M. Petrov¹³², F. Petrucci^{72a,72b}, M. Pettee¹⁸⁰, N.E. Pettersson¹⁰⁰, A. Peyaud¹⁴², R. Pezoa^{144b}, T. Pham¹⁰², F.H. Phillips¹⁰⁴, P.W. Phillips¹⁴¹, M.W. Phipps¹⁷⁰, G. Piacquadio¹⁵², E. Pianori¹⁸, A. Picazio¹⁰⁰, M.A. Pickering¹³², R.H. Pickles⁹⁸, R. Piegai³⁰, J.E. Pilcher³⁶, A.D. Pilkington⁹⁸, M. Pinamonti^{71a,71b}, J.L. Pinfold³, M. Pitt¹⁷⁷, M.-A. Pleier²⁹, V. Pleskot¹⁴⁰, E. Plotnikova⁷⁷, D. Pluth⁷⁶, P. Podberezko^{120b,120a}, R. Poettgen⁹⁴, R. Poggi⁵², L. Poggioli¹²⁹, I. Pogrebnyak¹⁰⁴, D. Pohl²⁴, I. Pokharel⁵¹, G. Polesello^{68a}, A. Poley¹⁸, A. Policicchio^{70a,70b}, R. Polifka³⁵, A. Polini^{23b}, C.S. Pollard⁴⁴, V. Polychronakos²⁹, D. Ponomarenko¹¹⁰, L. Pontecorvo³⁵, G.A. Popeneciu^{27d}, D.M. Portillo Quintero¹³³, S. Pospisil¹³⁹, K. Potamianos⁴⁴, I.N. Potrap⁷⁷, C.J. Potter³¹, H. Potti¹¹, T. Poulsen⁹⁴, J. Poveda³⁵, T.D. Powell¹⁴⁶, M.E. Pozo Astigarraga³⁵, P. Pralavorio⁹⁹, S. Prell⁷⁶, D. Price⁹⁸, M. Primavera^{65a}, S. Prince¹⁰¹, N. Proklova¹¹⁰, K. Prokofiev^{61c}, F. Prokoshin^{144b}, S. Protopopescu²⁹, J. Proudfoot⁶, M. Przybycien^{81a},

A. Puri¹⁷⁰, P. Puzo¹²⁹, J. Qian¹⁰³, Y. Qin⁹⁸, A. Quadri⁵¹, M. Queitsch-Maitland⁴⁴, A. Qureshi¹, P. Rados¹⁰²,
 F. Ragusa^{66a,66b}, G. Rahal⁹⁵, J.A. Raine⁵², S. Rajagopalan²⁹, A. Ramirez Morales⁹⁰, T. Rashid¹²⁹,
 S. Raspopov⁵, M.G. Ratti^{66a,66b}, D.M. Rauch⁴⁴, F. Rauscher¹¹², S. Rave⁹⁷, B. Ravina¹⁴⁶, I. Ravinovich¹⁷⁷,
 J.H. Rawling⁹⁸, M. Raymond³⁵, A.L. Read¹³¹, N.P. Readioff⁵⁶, M. Reale^{65a,65b}, D.M. Rebuzzi^{68a,68b},
 A. Redelbach¹⁷⁴, G. Redlinger²⁹, R. Reece¹⁴³, R.G. Reed^{32c}, K. Reeves⁴², L. Rehnisch¹⁹, J. Reichert¹³⁴,
 D. Reikher¹⁵⁸, A. Reiss⁹⁷, C. Rembser³⁵, H. Ren^{15d}, M. Rescigno^{70a}, S. Resconi^{66a}, E.D. Resseguie¹³⁴,
 S. Rettie¹⁷², E. Reynolds²¹, O.L. Rezanova^{120b,120a}, P. Reznicek¹⁴⁰, E. Ricci^{73a,73b}, R. Richter¹¹³,
 S. Richter⁴⁴, E. Richter-Was^{81b}, O. Ricken²⁴, M. Ridel¹³³, P. Rieck¹¹³, C.J. Riegel¹⁷⁹, O. Rifki⁴⁴,
 M. Rijssenbeek¹⁵², A. Rimoldi^{68a,68b}, M. Rimoldi²⁰, L. Rinaldi^{23b}, G. Ripellino¹⁵¹, B. Ristic⁸⁷,
 E. Ritsch³⁵, I. Riu¹⁴, J.C. Rivera Vergara^{144a}, F. Rizatdinova¹²⁶, E. Rizvi⁹⁰, C. Rizzi¹⁴, R.T. Roberts⁹⁸,
 S.H. Robertson^{101,ae}, D. Robinson³¹, J.E.M. Robinson⁴⁴, A. Robson⁵⁵, E. Rocco⁹⁷, C. Roda^{69a,69b},
 Y. Rodina⁹⁹, S. Rodriguez Bosca¹⁷¹, A. Rodriguez Perez¹⁴, D. Rodriguez Rodriguez¹⁷¹,
 A.M. Rodríguez Vera^{165b}, S. Roe³⁵, C.S. Rogan⁵⁷, O. Røhne¹³¹, R. Röhrig¹¹³, C.P.A. Roland⁶³, J. Roloff⁵⁷,
 A. Romaniouk¹¹⁰, M. Romano^{23b,23a}, N. Rompotis⁸⁸, M. Ronzani¹²², L. Roos¹³³, S. Rosati^{70a},
 K. Rosbach⁵⁰, P. Rose¹⁴³, N-A. Rosien⁵¹, E. Rossi⁴⁴, E. Rossi^{72a,72b}, E. Rossi^{67a,67b}, L.P. Rossi^{53b},
 L. Rossini^{66a,66b}, J.H.N. Rosten³¹, R. Rosten¹⁴, M. Rotaru^{27b}, J. Rothberg¹⁴⁵, D. Rousseau¹²⁹, D. Roy^{32c},
 A. Rozanov⁹⁹, Y. Rozen¹⁵⁷, X. Ruan^{32c}, F. Rubbo¹⁵⁰, F. Rühr⁵⁰, A. Ruiz-Martinez¹⁷¹, Z. Rurikova⁵⁰,
 N.A. Rusakovich⁷⁷, H.L. Russell¹⁰¹, J.P. Rutherford⁷, E.M. Rüttinger^{44,m}, Y.F. Ryabov¹³⁵, M. Rybar¹⁷⁰,
 G. Rybkin¹²⁹, S. Ryu⁶, A. Ryzhov¹²¹, G.F. Rzehorz⁵¹, P. Sabatini⁵¹, G. Sabato¹¹⁸, S. Sacerdoti¹²⁹,
 H.F.W. Sadrozinski¹⁴³, R. Sadykov⁷⁷, F. Safai Tehrani^{70a}, P. Saha¹¹⁹, M. Sahinsoy^{59a}, A. Sahu¹⁷⁹,
 M. Saimpert⁴⁴, M. Saito¹⁶⁰, T. Saito¹⁶⁰, H. Sakamoto¹⁶⁰, A. Sakharov^{122,an}, D. Salamani⁵²,
 G. Salamanna^{72a,72b}, J.E. Salazar Loyola^{144b}, D. Salek¹¹⁸, P.H. Sales De Bruin¹⁶⁹, D. Salihagic¹¹³,
 A. Salnikov¹⁵⁰, J. Salt¹⁷¹, D. Salvatore^{40b,40a}, F. Salvatore¹⁵³, A. Salvucci^{61a,61b,61c}, A. Salzburger³⁵,
 J. Samarati³⁵, D. Sammel⁵⁰, D. Sampsonidis¹⁵⁹, D. Sampsonidou¹⁵⁹, J. Sánchez¹⁷¹,
 A. Sanchez Pineda^{64a,64c}, H. Sandaker¹³¹, C.O. Sander⁴⁴, M. Sandhoff¹⁷⁹, C. Sandoval²², D.P.C. Sankey¹⁴¹,
 M. Sannino^{53b,53a}, Y. Sano¹¹⁵, A. Sansoni⁴⁹, C. Santoni³⁷, H. Santos^{137a}, I. Santoyo Castillo¹⁵³,
 A. Santra¹⁷¹, A. Saprionov⁷⁷, J.G. Saraiva^{137a,137d}, O. Sasaki⁷⁹, K. Sato¹⁶⁶, E. Sauvan⁵, P. Savard^{164,av},
 N. Savic¹¹³, R. Sawada¹⁶⁰, C. Sawyer¹⁴¹, L. Sawyer^{93,al}, C. Sbarra^{23b}, A. Sbrizzi^{23a}, T. Scanlon⁹²,
 J. Schaarschmidt¹⁴⁵, P. Schacht¹¹³, B.M. Schachtner¹¹², D. Schaefer³⁶, L. Schaefer¹³⁴, J. Schaeffer⁹⁷,
 S. Schaepe³⁵, U. Schäfer⁹⁷, A.C. Schaffer¹²⁹, D. Schaile¹¹², R.D. Schamberger¹⁵², N. Scharmberg⁹⁸,
 V.A. Schegelsky¹³⁵, D. Scheirich¹⁴⁰, F. Schenck¹⁹, M. Schernau¹⁶⁸, C. Schiavi^{53b,53a}, S. Schier¹⁴³,
 L.K. Schildgen²⁴, Z.M. Schillaci²⁶, E.J. Schioppa³⁵, M. Schioppa^{40b,40a}, K.E. Schleicher⁵⁰, S. Schlenker³⁵,
 K.R. Schmidt-Sommerfeld¹¹³, K. Schmieden³⁵, C. Schmitt⁹⁷, S. Schmitt⁴⁴, S. Schmitz⁹⁷,
 J.C. Schmoeckel⁴⁴, U. Schnoor⁵⁰, L. Schoeffel¹⁴², A. Schoening^{59b}, E. Schopf²⁴, M. Schott⁹⁷,
 J.F.P. Schouwenberg¹¹⁷, J. Schovancova³⁵, S. Schramm⁵², A. Schulte⁹⁷, H-C. Schultz-Coulon^{59a},
 M. Schumacher⁵⁰, B.A. Schumm¹⁴³, Ph. Schune¹⁴², A. Schwartzman¹⁵⁰, T.A. Schwarz¹⁰³,
 Ph. Schwemling¹⁴², R. Schwienhorst¹⁰⁴, A. Sciandra²⁴, G. Sciolla²⁶, M. Scornajenghi^{40b,40a}, F. Scuri^{69a},
 F. Scutti¹⁰², L.M. Scyboz¹¹³, J. Searcy¹⁰³, C.D. Sebastiani^{70a,70b}, P. Seema¹⁹, S.C. Seidel¹¹⁶, A. Seiden¹⁴³,
 T. Seiss³⁶, J.M. Seixas^{78b}, G. Sekhniaidze^{67a}, K. Sekhon¹⁰³, S.J. Sekula⁴¹, N. Semprini-Cesari^{23b,23a},
 S. Sen⁴⁷, S. Senkin³⁷, C. Serfon¹³¹, L. Serin¹²⁹, L. Serkin^{64a,64b}, M. Sessa^{58a}, H. Severini¹²⁵, F. Sforza¹⁶⁷,
 A. Sfyrila⁵², E. Shabalina⁵¹, J.D. Shahinian¹⁴³, N.W. Shaikh^{43a,43b}, L.Y. Shan^{15a}, R. Shang¹⁷⁰, J.T. Shank²⁵,
 M. Shapiro¹⁸, A.S. Sharma¹, A. Sharma¹³², P.B. Shatalov¹⁰⁹, K. Shaw¹⁵³, S.M. Shaw⁹⁸,
 A. Shcherbakova¹³⁵, Y. Shen¹²⁵, N. Sherafati³³, A.D. Sherman²⁵, P. Sherwood⁹², L. Shi^{155,ar}, S. Shimizu⁷⁹,
 C.O. Shimmin¹⁸⁰, M. Shimojima¹¹⁴, I.P.J. Shipsey¹³², S. Shirabe⁸⁵, M. Shiyakova⁷⁷, J. Shlomi¹⁷⁷,
 A. Shmeleva¹⁰⁸, D. Shoaleh Saadi¹⁰⁷, M.J. Shochet³⁶, S. Shojaii¹⁰², D.R. Shope¹²⁵, S. Shrestha¹²³,
 E. Shulga¹¹⁰, P. Sicho¹³⁸, A.M. Sickles¹⁷⁰, P.E. Sidebo¹⁵¹, E. Sideras Haddad^{32c}, O. Sidiropoulou³⁵,
 A. Sidoti^{23b,23a}, F. Siegert⁴⁶, Dj. Sijacki¹⁶, J. Silva^{137a}, M. Silva Jr.¹⁷⁸, M.V. Silva Oliveira^{78a},

S.B. Silverstein^{43a}, L. Simic⁷⁷, S. Simion¹²⁹, E. Simioni⁹⁷, M. Simon⁹⁷, R. Simoniello⁹⁷, P. Sinervo¹⁶⁴, N.B. Sinev¹²⁸, M. Sioli^{23b,23a}, G. Siragusa¹⁷⁴, I. Siral¹⁰³, S.Yu. Sivoklov¹¹¹, J. Sjölin^{43a,43b}, P. Skubic¹²⁵, M. Slater²¹, T. Slavicek¹³⁹, M. Slawinska⁸², K. Sliwa¹⁶⁷, R. Slovak¹⁴⁰, V. Smakhtin¹⁷⁷, B.H. Smart⁵, J. Smiesko^{28a}, N. Smirnov¹¹⁰, S.Yu. Smirnov¹¹⁰, Y. Smirnov¹¹⁰, L.N. Smirnova¹¹¹, O. Smirnova⁹⁴, J.W. Smith⁵¹, M.N.K. Smith³⁸, M. Smizanska⁸⁷, K. Smolek¹³⁹, A. Smykiewicz⁸², A.A. Snesarev¹⁰⁸, I.M. Snyder¹²⁸, S. Snyder²⁹, R. Sobie^{173,ae}, A.M. Soffa¹⁶⁸, A. Soffer¹⁵⁸, A. Søggaard⁴⁸, D.A. Soh¹⁵⁵, G. Sokhranyi⁸⁹, C.A. Solans Sanchez³⁵, M. Solar¹³⁹, E.Yu. Soldatov¹¹⁰, U. Soldevila¹⁷¹, A.A. Solodkov¹²¹, A. Soloshenko⁷⁷, O.V. Solovyanov¹²¹, V. Solovyev¹³⁵, P. Sommer¹⁴⁶, H. Son¹⁶⁷, W. Song¹⁴¹, W.Y. Song^{165b}, A. Sopczak¹³⁹, F. Sopkova^{28b}, C.L. Sotiropoulou^{69a,69b}, S. Sottocornola^{68a,68b}, R. Soualah^{64a,64c,j}, A.M. Soukharev^{120b,120a}, D. South⁴⁴, B.C. Sowden⁹¹, S. Spagnolo^{65a,65b}, M. Spalla¹¹³, M. Spangenberg¹⁷⁵, F. Spanò⁹¹, D. Sperlich¹⁹, F. Spettel¹¹³, T.M. Spieker^{59a}, R. Spighi^{23b}, G. Spigo³⁵, L.A. Spiller¹⁰², D.P. Spiteri⁵⁵, M. Spousta¹⁴⁰, A. Stabile^{66a,66b}, R. Stamen^{59a}, S. Stamm¹⁹, E. Stanecka⁸², R.W. Stanek⁶, C. Stanescu^{72a}, B. Stanislaus¹³², M.M. Stanitzki⁴⁴, B. Stapf¹¹⁸, S. Stappes¹³¹, E.A. Starchenko¹²¹, G.H. Stark³⁶, J. Stark⁵⁶, S.H. Stark³⁹, P. Staroba¹³⁸, P. Starovoitov^{59a}, S. Stärz³⁵, R. Staszewski⁸², M. Stegler⁴⁴, P. Steinberg²⁹, B. Stelzer¹⁴⁹, H.J. Stelzer³⁵, O. Stelzer-Chilton^{165a}, H. Stenzel⁵⁴, T.J. Stevenson⁹⁰, G.A. Stewart³⁵, M.C. Stockton¹²⁸, G. Stoicea^{27b}, P. Stolte⁵¹, S. Stonjek¹¹³, A. Straessner⁴⁶, J. Strandberg¹⁵¹, S. Strandberg^{43a,43b}, M. Strauss¹²⁵, P. Strizenc^{28b}, R. Ströhmer¹⁷⁴, D.M. Strom¹²⁸, R. Stroynowski⁴¹, A. Strubig⁴⁸, S.A. Stucci²⁹, B. Stugu¹⁷, J. Stupak¹²⁵, N.A. Styles⁴⁴, D. Su¹⁵⁰, J. Su¹³⁶, S. Suchek^{59a}, Y. Sugaya¹³⁰, M. Suk¹³⁹, V.V. Sulin¹⁰⁸, M.J. Sullivan⁸⁸, D.M.S. Sultan⁵², S. Sultansoy^{4c}, T. Sumida⁸³, S. Sun¹⁰³, X. Sun³, K. Suruliz¹⁵³, C.J.E. Suster¹⁵⁴, M.R. Sutton¹⁵³, S. Suzuki⁷⁹, M. Svatos¹³⁸, M. Swiatlowski³⁶, S.P. Swift², A. Sydorenko⁹⁷, I. Sykora^{28a}, T. Sykora¹⁴⁰, D. Ta⁹⁷, K. Tackmann^{44,ab}, J. Taenzer¹⁵⁸, A. Taffard¹⁶⁸, R. Tafirout^{165a}, E. Tahirovic⁹⁰, N. Taiblum¹⁵⁸, H. Takai²⁹, R. Takashima⁸⁴, E.H. Takasugi¹¹³, K. Takeda⁸⁰, T. Takeshita¹⁴⁷, Y. Takubo⁷⁹, M. Talby⁹⁹, A.A. Talyshev^{120b,120a}, J. Tanaka¹⁶⁰, M. Tanaka¹⁶², R. Tanaka¹²⁹, B.B. Tannenwald¹²³, S. Tapia Araya^{144b}, S. Tapprogge⁹⁷, A. Tarek Abouelfadl Mohamed¹³³, S. Tarem¹⁵⁷, G. Tarna^{27b,e}, G.F. Tartarelli^{66a}, P. Tas¹⁴⁰, M. Tasevsky¹³⁸, T. Tashiro⁸³, E. Tassi^{40b,40a}, A. Tavares Delgado^{137a,137b}, Y. Tayalati^{34e}, A.C. Taylor¹¹⁶, A.J. Taylor⁴⁸, G.N. Taylor¹⁰², P.T.E. Taylor¹⁰², W. Taylor^{165b}, A.S. Tee⁸⁷, P. Teixeira-Dias⁹¹, H. Ten Kate³⁵, P.K. Teng¹⁵⁵, J.J. Teoh¹¹⁸, S. Terada⁷⁹, K. Terashi¹⁶⁰, J. Terron⁹⁶, S. Terzo¹⁴, M. Testa⁴⁹, R.J. Teuscher^{164,ae}, S.J. Thais¹⁸⁰, T. Theveneaux-Pelzer⁴⁴, F. Thiele³⁹, D.W. Thomas⁹¹, J.P. Thomas²¹, A.S. Thompson⁵⁵, P.D. Thompson²¹, L.A. Thomsen¹⁸⁰, E. Thomson¹³⁴, Y. Tian³⁸, R.E. Ticse Torres⁵¹, V.O. Tikhomirov^{108,ap}, Yu.A. Tikhonov^{120b,120a}, S. Timoshenko¹¹⁰, P. Tipton¹⁸⁰, S. Tisserant⁹⁹, K. Todome¹⁶², S. Todorova-Nova⁵, S. Todt⁴⁶, J. Tojo⁸⁵, S. Tokár^{28a}, K. Tokushuku⁷⁹, E. Tolley¹²³, K.G. Tomiwa^{32c}, M. Tomoto¹¹⁵, L. Tompkins^{150,r}, K. Toms¹¹⁶, B. Tong⁵⁷, P. Tornambe⁵⁰, E. Torrence¹²⁸, H. Torres⁴⁶, E. Torró Pastor¹⁴⁵, C. Tosciri¹³², J. Toth^{99,ad}, F. Touchard⁹⁹, D.R. Tovey¹⁴⁶, C.J. Treado¹²², T. Trefzger¹⁷⁴, F. Tresoldi¹⁵³, A. Tricoli²⁹, I.M. Trigger^{165a}, S. Trincaz-Duvoid¹³³, M.F. Tripiana¹⁴, W. Trischuk¹⁶⁴, B. Trocme⁵⁶, A. Trofymov¹²⁹, C. Troncon^{66a}, M. Trovatelli¹⁷³, F. Trovato¹⁵³, L. Truong^{32b}, M. Trzebinski⁸², A. Trzupek⁸², F. Tsai⁴⁴, J.C.-L. Tseng¹³², P.V. Tsiarshka¹⁰⁵, A. Tsirigotis¹⁵⁹, N. Tsirintanis⁹, V. Tsiskaridze¹⁵², E.G. Tskhadadze^{156a}, I.I. Tsukerman¹⁰⁹, V. Tsulaia¹⁸, S. Tsuno⁷⁹, D. Tsybychev^{152,163}, Y. Tu^{61b}, A. Tudorache^{27b}, V. Tudorache^{27b}, T.T. Tulbure^{27a}, A.N. Tuna⁵⁷, S. Turchikhin⁷⁷, D. Turgeman¹⁷⁷, I. Turk Cakir^{4b,v}, R. Turra^{66a}, P.M. Tuts³⁸, E. Tzovara⁹⁷, G. Ucchielli^{23b,23a}, I. Ueda⁷⁹, M. Ughetto^{43a,43b}, F. Ukegawa¹⁶⁶, G. Unal³⁵, A. Undrus²⁹, G. Unel¹⁶⁸, F.C. Ungaro¹⁰², Y. Unno⁷⁹, K. Uno¹⁶⁰, J. Urban^{28b}, P. Urquijo¹⁰², P. Urrejola⁹⁷, G. Usai⁸, J. Usui⁷⁹, L. Vacavant⁹⁹, V. Vacek¹³⁹, B. Vachon¹⁰¹, K.O.H. Vadla¹³¹, A. Vaidya⁹², C. Valderanis¹¹², E. Valdes Santurio^{43a,43b}, M. Valente⁵², S. Valentini^{23b,23a}, A. Valero¹⁷¹, L. Valéry⁴⁴, R.A. Vallance²¹, A. Vallier⁵, J.A. Valls Ferrer¹⁷¹, T.R. Van Daalen¹⁴, H. Van der Graaf¹¹⁸, P. Van Gemmeren⁶, J. Van Nieuwkoop¹⁴⁹, I. Van Vulpen¹¹⁸, M. Vanadia^{71a,71b}, W. Vandelli³⁵, A. Vaniachine¹⁶³, P. Vankov¹¹⁸, R. Vari^{70a}, E.W. Varnes⁷, C. Varni^{53b,53a}, T. Varol⁴¹, D. Varouchas¹²⁹, K.E. Varvell¹⁵⁴, G.A. Vasquez^{144b},

J.G. Vasquez¹⁸⁰, F. Vazeille³⁷, D. Vazquez Furelos¹⁴, T. Vazquez Schroeder¹⁰¹, J. Veatch⁵¹, V. Vecchio^{72a,72b}, L.M. Veloce¹⁶⁴, F. Veloso^{137a,137c}, S. Veneziano^{70a}, A. Ventura^{65a,65b}, M. Venturi¹⁷³, N. Venturi³⁵, V. Vercesi^{68a}, M. Verducci^{72a,72b}, C.M. Vergel Infante⁷⁶, C. Vergis²⁴, W. Verkerke¹¹⁸, A.T. Vermeulen¹¹⁸, J.C. Vermeulen¹¹⁸, M.C. Vetterli^{149,av}, N. Viaux Maira^{144b}, M. Vicente Barreto Pinto⁵², I. Vichou^{170,*}, T. Vickey¹⁴⁶, O.E. Vickey Boeriu¹⁴⁶, G.H.A. Viehhauser¹³², S. Viel¹⁸, L. Vigani¹³², M. Villa^{23b,23a}, M. Villaplana Perez^{66a,66b}, E. Vilucchi⁴⁹, M.G. Vinciter³³, V.B. Vinogradov⁷⁷, A. Vishwakarma⁴⁴, C. Vittori^{23b,23a}, I. Vivarelli¹⁵³, S. Vlachos¹⁰, M. Vogel¹⁷⁹, P. Vokac¹³⁹, G. Volpi¹⁴, S.E. von Buddenbrock^{32c}, E. Von Toerne²⁴, V. Vorobel¹⁴⁰, K. Vorobev¹¹⁰, M. Vos¹⁷¹, J.H. Vosseveld⁸⁸, N. Vranjes¹⁶, M. Vranjes Milosavljevic¹⁶, V. Vrba¹³⁹, M. Vreeswijk¹¹⁸, T. Šfiligoj⁸⁹, R. Vuillermet³⁵, I. Vukotic³⁶, T. Ženiš^{28a}, L. Živković¹⁶, P. Wagner²⁴, W. Wagner¹⁷⁹, J. Wagner-Kuhr¹¹², H. Wahlberg⁸⁶, S. Wahrenmund⁴⁶, K. Wakamiya⁸⁰, V.M. Walbrecht¹¹³, J. Walder⁸⁷, R. Walker¹¹², S.D. Walker⁹¹, W. Walkowiak¹⁴⁸, V. Wallangen^{43a,43b}, A.M. Wang⁵⁷, C. Wang^{58b,e}, F. Wang¹⁷⁸, H. Wang¹⁸, H. Wang³, J. Wang¹⁵⁴, J. Wang^{59b}, P. Wang⁴¹, Q. Wang¹²⁵, R.-J. Wang¹³³, R. Wang^{58a}, R. Wang⁶, S.M. Wang¹⁵⁵, W.T. Wang^{58a}, W. Wang^{15c,af}, W.X. Wang^{58a,af}, Y. Wang^{58a,am}, Z. Wang^{58c}, C. Wanotayaroj⁴⁴, A. Warburton¹⁰¹, C.P. Ward³¹, D.R. Wardrope⁹², A. Washbrook⁴⁸, P.M. Watkins²¹, A.T. Watson²¹, M.F. Watson²¹, G. Watts¹⁴⁵, S. Watts⁹⁸, B.M. Waugh⁹², A.F. Webb¹¹, S. Webb⁹⁷, C. Weber¹⁸⁰, M.S. Weber²⁰, S.A. Weber³³, S.M. Weber^{59a}, A.R. Weidberg¹³², B. Weinert⁶³, J. Weingarten⁴⁵, M. Weirich⁹⁷, C. Weiser⁵⁰, P.S. Wells³⁵, T. Wenaus²⁹, T. Wengler³⁵, S. Wenig³⁵, N. Wermes²⁴, M.D. Werner⁷⁶, P. Werner³⁵, M. Wessels^{59a}, T.D. Weston²⁰, K. Whalen¹²⁸, N.L. Whallon¹⁴⁵, A.M. Wharton⁸⁷, A.S. White¹⁰³, A. White⁸, M.J. White¹, R. White^{144b}, D. Whiteson¹⁶⁸, B.W. Whitmore⁸⁷, F.J. Wickens¹⁴¹, W. Wiedenmann¹⁷⁸, M. Wielers¹⁴¹, C. Wiglesworth³⁹, L.A.M. Wiik-Fuchs⁵⁰, A. Wildauer¹¹³, F. Wilk⁹⁸, H.G. Wilkens³⁵, L.J. Wilkins⁹¹, H.H. Williams¹³⁴, S. Williams³¹, C. Willis¹⁰⁴, S. Willocq¹⁰⁰, J.A. Wilson²¹, I. Wingerter-Seez⁵, E. Winkels¹⁵³, F. Winklmeier¹²⁸, O.J. Winston¹⁵³, B.T. Winter²⁴, M. Wittgen¹⁵⁰, M. Wobisch⁹³, A. Wolf⁹⁷, T.M.H. Wolf¹¹⁸, R. Wolff⁹⁹, M.W. Wolter⁸², H. Wolters^{137a,137c}, V.W.S. Wong¹⁷², N.L. Woods¹⁴³, S.D. Worm²¹, B.K. Wosiek⁸², K.W. Woźniak⁸², K. Wraight⁵⁵, M. Wu³⁶, S.L. Wu¹⁷⁸, X. Wu⁵², Y. Wu^{58a}, T.R. Wyatt⁹⁸, B.M. Wynne⁴⁸, S. Xella³⁹, Z. Xi¹⁰³, L. Xia¹⁷⁵, D. Xu^{15a}, H. Xu^{58a,e}, L. Xu²⁹, T. Xu¹⁴², W. Xu¹⁰³, B. Yabsley¹⁵⁴, S. Yacoob^{32a}, K. Yajima¹³⁰, D.P. Yallup⁹², D. Yamaguchi¹⁶², Y. Yamaguchi¹⁶², A. Yamamoto⁷⁹, T. Yamanaka¹⁶⁰, F. Yamane⁸⁰, M. Yamatani¹⁶⁰, T. Yamazaki¹⁶⁰, Y. Yamazaki⁸⁰, Z. Yan²⁵, H.J. Yang^{58c,58d}, H.T. Yang¹⁸, S. Yang⁷⁵, Y. Yang¹⁶⁰, Z. Yang¹⁷, W.-M. Yao¹⁸, Y.C. Yap⁴⁴, Y. Yasu⁷⁹, E. Yatsenko^{58c,58d}, J. Ye⁴¹, S. Ye²⁹, I. Yeletskikh⁷⁷, E. Yigitbasi²⁵, E. Yildirim⁹⁷, K. Yorita¹⁷⁶, K. Yoshihara¹³⁴, C.J.S. Young³⁵, C. Young¹⁵⁰, J. Yu⁸, J. Yu⁷⁶, X. Yue^{59a}, S.P.Y. Yuen²⁴, B. Zabinski⁸², G. Zacharis¹⁰, E. Zaffaroni⁵², R. Zaidan¹⁴, A.M. Zaitsev^{121,ao}, T. Zakareishvili^{156b}, N. Zakharchuk³³, J. Zalieckas¹⁷, S. Zambito⁵⁷, D. Zanzi³⁵, D.R. Zaripovas⁵⁵, S.V. Zeiβner⁴⁵, C. Zeitnitz¹⁷⁹, G. Zemaityte¹³², J.C. Zeng¹⁷⁰, Q. Zeng¹⁵⁰, O. Zenin¹²¹, D. Zerwas¹²⁹, M. Zgubič¹³², D.F. Zhang^{58b}, D. Zhang¹⁰³, F. Zhang¹⁷⁸, G. Zhang^{58a}, H. Zhang^{15c}, J. Zhang⁶, L. Zhang^{15c}, L. Zhang^{58a}, M. Zhang¹⁷⁰, P. Zhang^{15c}, R. Zhang^{58a}, R. Zhang²⁴, X. Zhang^{58b}, Y. Zhang^{15d}, Z. Zhang¹²⁹, P. Zhao⁴⁷, X. Zhao⁴¹, Y. Zhao^{58b,129,ak}, Z. Zhao^{58a}, A. Zhemchugov⁷⁷, Z. Zheng¹⁰³, D. Zhong¹⁷⁰, B. Zhou¹⁰³, C. Zhou¹⁷⁸, L. Zhou⁴¹, M.S. Zhou^{15d}, M. Zhou¹⁵², N. Zhou^{58c}, Y. Zhou⁷, C.G. Zhu^{58b}, H.L. Zhu^{58a}, H. Zhu^{15a}, J. Zhu¹⁰³, Y. Zhu^{58a}, X. Zhuang^{15a}, K. Zhukov¹⁰⁸, V. Zhulanov^{120b,120a}, A. Zibell¹⁷⁴, D. Zieminska⁶³, N.I. Zimine⁷⁷, S. Zimmermann⁵⁰, Z. Zinonos¹¹³, M. Zinser⁹⁷, M. Ziolkowski¹⁴⁸, G. Zobernig¹⁷⁸, A. Zoccoli^{23b,23a}, K. Zoch⁵¹, T.G. Zorbas¹⁴⁶, R. Zou³⁶, M. Zur Nedden¹⁹, L. Zwalinski³⁵.

¹Department of Physics, University of Adelaide, Adelaide; Australia.

²Physics Department, SUNY Albany, Albany NY; United States of America.

³Department of Physics, University of Alberta, Edmonton AB; Canada.

^{4(a)}Department of Physics, Ankara University, Ankara; ^(b)Istanbul Aydin University, Istanbul; ^(c)Division of

- Physics, TOBB University of Economics and Technology, Ankara; Turkey.
- ⁵LAPP, Université Grenoble Alpes, Université Savoie Mont Blanc, CNRS/IN2P3, Annecy; France.
- ⁶High Energy Physics Division, Argonne National Laboratory, Argonne IL; United States of America.
- ⁷Department of Physics, University of Arizona, Tucson AZ; United States of America.
- ⁸Department of Physics, University of Texas at Arlington, Arlington TX; United States of America.
- ⁹Physics Department, National and Kapodistrian University of Athens, Athens; Greece.
- ¹⁰Physics Department, National Technical University of Athens, Zografou; Greece.
- ¹¹Department of Physics, University of Texas at Austin, Austin TX; United States of America.
- ¹²(^a)Bahcesehir University, Faculty of Engineering and Natural Sciences, Istanbul; (^b)Istanbul Bilgi University, Faculty of Engineering and Natural Sciences, Istanbul; (^c)Department of Physics, Bogazici University, Istanbul; (^d)Department of Physics Engineering, Gaziantep University, Gaziantep; Turkey.
- ¹³Institute of Physics, Azerbaijan Academy of Sciences, Baku; Azerbaijan.
- ¹⁴Institut de Física d'Altes Energies (IFAE), Barcelona Institute of Science and Technology, Barcelona; Spain.
- ¹⁵(^a)Institute of High Energy Physics, Chinese Academy of Sciences, Beijing; (^b)Physics Department, Tsinghua University, Beijing; (^c)Department of Physics, Nanjing University, Nanjing; (^d)University of Chinese Academy of Science (UCAS), Beijing; China.
- ¹⁶Institute of Physics, University of Belgrade, Belgrade; Serbia.
- ¹⁷Department for Physics and Technology, University of Bergen, Bergen; Norway.
- ¹⁸Physics Division, Lawrence Berkeley National Laboratory and University of California, Berkeley CA; United States of America.
- ¹⁹Institut für Physik, Humboldt Universität zu Berlin, Berlin; Germany.
- ²⁰Albert Einstein Center for Fundamental Physics and Laboratory for High Energy Physics, University of Bern, Bern; Switzerland.
- ²¹School of Physics and Astronomy, University of Birmingham, Birmingham; United Kingdom.
- ²²Centro de Investigaciones, Universidad Antonio Nariño, Bogota; Colombia.
- ²³(^a)Dipartimento di Fisica e Astronomia, Università di Bologna, Bologna; (^b)INFN Sezione di Bologna; Italy.
- ²⁴Physikalisches Institut, Universität Bonn, Bonn; Germany.
- ²⁵Department of Physics, Boston University, Boston MA; United States of America.
- ²⁶Department of Physics, Brandeis University, Waltham MA; United States of America.
- ²⁷(^a)Transilvania University of Brasov, Brasov; (^b)Horia Hulubei National Institute of Physics and Nuclear Engineering, Bucharest; (^c)Department of Physics, Alexandru Ioan Cuza University of Iasi, Iasi; (^d)National Institute for Research and Development of Isotopic and Molecular Technologies, Physics Department, Cluj-Napoca; (^e)University Politehnica Bucharest, Bucharest; (^f)West University in Timisoara, Timisoara; Romania.
- ²⁸(^a)Faculty of Mathematics, Physics and Informatics, Comenius University, Bratislava; (^b)Department of Subnuclear Physics, Institute of Experimental Physics of the Slovak Academy of Sciences, Kosice; Slovak Republic.
- ²⁹Physics Department, Brookhaven National Laboratory, Upton NY; United States of America.
- ³⁰Departamento de Física, Universidad de Buenos Aires, Buenos Aires; Argentina.
- ³¹Cavendish Laboratory, University of Cambridge, Cambridge; United Kingdom.
- ³²(^a)Department of Physics, University of Cape Town, Cape Town; (^b)Department of Mechanical Engineering Science, University of Johannesburg, Johannesburg; (^c)School of Physics, University of the Witwatersrand, Johannesburg; South Africa.
- ³³Department of Physics, Carleton University, Ottawa ON; Canada.
- ³⁴(^a)Faculté des Sciences Ain Chock, Réseau Universitaire de Physique des Hautes Energies - Université

Hassan II, Casablanca;^(b)Centre National de l'Energie des Sciences Techniques Nucleaires (CNESTEN), Rabat;^(c)Faculté des Sciences Semlalia, Université Cadi Ayyad, LPHEA-Marrakech;^(d)Faculté des Sciences, Université Mohamed Premier and LPTPM, Oujda;^(e)Faculté des sciences, Université Mohammed V, Rabat; Morocco.

³⁵CERN, Geneva; Switzerland.

³⁶Enrico Fermi Institute, University of Chicago, Chicago IL; United States of America.

³⁷LPC, Université Clermont Auvergne, CNRS/IN2P3, Clermont-Ferrand; France.

³⁸Nevis Laboratory, Columbia University, Irvington NY; United States of America.

³⁹Niels Bohr Institute, University of Copenhagen, Copenhagen; Denmark.

^{40(a)}Dipartimento di Fisica, Università della Calabria, Rende;^(b)INFN Gruppo Collegato di Cosenza, Laboratori Nazionali di Frascati; Italy.

⁴¹Physics Department, Southern Methodist University, Dallas TX; United States of America.

⁴²Physics Department, University of Texas at Dallas, Richardson TX; United States of America.

^{43(a)}Department of Physics, Stockholm University;^(b)Oskar Klein Centre, Stockholm; Sweden.

⁴⁴Deutsches Elektronen-Synchrotron DESY, Hamburg and Zeuthen; Germany.

⁴⁵Lehrstuhl für Experimentelle Physik IV, Technische Universität Dortmund, Dortmund; Germany.

⁴⁶Institut für Kern- und Teilchenphysik, Technische Universität Dresden, Dresden; Germany.

⁴⁷Department of Physics, Duke University, Durham NC; United States of America.

⁴⁸SUPA - School of Physics and Astronomy, University of Edinburgh, Edinburgh; United Kingdom.

⁴⁹INFN e Laboratori Nazionali di Frascati, Frascati; Italy.

⁵⁰Physikalisches Institut, Albert-Ludwigs-Universität Freiburg, Freiburg; Germany.

⁵¹II. Physikalisches Institut, Georg-August-Universität Göttingen, Göttingen; Germany.

⁵²Département de Physique Nucléaire et Corpusculaire, Université de Genève, Genève; Switzerland.

^{53(a)}Dipartimento di Fisica, Università di Genova, Genova;^(b)INFN Sezione di Genova; Italy.

⁵⁴II. Physikalisches Institut, Justus-Liebig-Universität Giessen, Giessen; Germany.

⁵⁵SUPA - School of Physics and Astronomy, University of Glasgow, Glasgow; United Kingdom.

⁵⁶LPSC, Université Grenoble Alpes, CNRS/IN2P3, Grenoble INP, Grenoble; France.

⁵⁷Laboratory for Particle Physics and Cosmology, Harvard University, Cambridge MA; United States of America.

^{58(a)}Department of Modern Physics and State Key Laboratory of Particle Detection and Electronics, University of Science and Technology of China, Hefei;^(b)Institute of Frontier and Interdisciplinary Science and Key Laboratory of Particle Physics and Particle Irradiation (MOE), Shandong University, Qingdao;^(c)School of Physics and Astronomy, Shanghai Jiao Tong University, KLPPAC-MoE, SKLPPC, Shanghai;^(d)Tsung-Dao Lee Institute, Shanghai; China.

^{59(a)}Kirchhoff-Institut für Physik, Ruprecht-Karls-Universität Heidelberg, Heidelberg;^(b)Physikalisches Institut, Ruprecht-Karls-Universität Heidelberg, Heidelberg; Germany.

⁶⁰Faculty of Applied Information Science, Hiroshima Institute of Technology, Hiroshima; Japan.

^{61(a)}Department of Physics, Chinese University of Hong Kong, Shatin, N.T., Hong Kong;^(b)Department of Physics, University of Hong Kong, Hong Kong;^(c)Department of Physics and Institute for Advanced Study, Hong Kong University of Science and Technology, Clear Water Bay, Kowloon, Hong Kong; China.

⁶²Department of Physics, National Tsing Hua University, Hsinchu; Taiwan.

⁶³Department of Physics, Indiana University, Bloomington IN; United States of America.

^{64(a)}INFN Gruppo Collegato di Udine, Sezione di Trieste, Udine;^(b)ICTP, Trieste;^(c)Dipartimento di Chimica, Fisica e Ambiente, Università di Udine, Udine; Italy.

^{65(a)}INFN Sezione di Lecce;^(b)Dipartimento di Matematica e Fisica, Università del Salento, Lecce; Italy.

^{66(a)}INFN Sezione di Milano;^(b)Dipartimento di Fisica, Università di Milano, Milano; Italy.

^{67(a)}INFN Sezione di Napoli;^(b)Dipartimento di Fisica, Università di Napoli, Napoli; Italy.

- ^{68(a)}INFN Sezione di Pavia;^(b)Dipartimento di Fisica, Università di Pavia, Pavia; Italy.
- ^{69(a)}INFN Sezione di Pisa;^(b)Dipartimento di Fisica E. Fermi, Università di Pisa, Pisa; Italy.
- ^{70(a)}INFN Sezione di Roma;^(b)Dipartimento di Fisica, Sapienza Università di Roma, Roma; Italy.
- ^{71(a)}INFN Sezione di Roma Tor Vergata;^(b)Dipartimento di Fisica, Università di Roma Tor Vergata, Roma; Italy.
- ^{72(a)}INFN Sezione di Roma Tre;^(b)Dipartimento di Matematica e Fisica, Università Roma Tre, Roma; Italy.
- ^{73(a)}INFN-TIFPA;^(b)Università degli Studi di Trento, Trento; Italy.
- ⁷⁴Institut für Astro- und Teilchenphysik, Leopold-Franzens-Universität, Innsbruck; Austria.
- ⁷⁵University of Iowa, Iowa City IA; United States of America.
- ⁷⁶Department of Physics and Astronomy, Iowa State University, Ames IA; United States of America.
- ⁷⁷Joint Institute for Nuclear Research, Dubna; Russia.
- ^{78(a)}Departamento de Engenharia Elétrica, Universidade Federal de Juiz de Fora (UFJF), Juiz de Fora;^(b)Universidade Federal do Rio De Janeiro COPPE/EE/IF, Rio de Janeiro;^(c)Universidade Federal de São João del Rei (UFSJ), São João del Rei;^(d)Instituto de Física, Universidade de São Paulo, São Paulo; Brazil.
- ⁷⁹KEK, High Energy Accelerator Research Organization, Tsukuba; Japan.
- ⁸⁰Graduate School of Science, Kobe University, Kobe; Japan.
- ^{81(a)}AGH University of Science and Technology, Faculty of Physics and Applied Computer Science, Krakow;^(b)Marian Smoluchowski Institute of Physics, Jagiellonian University, Krakow; Poland.
- ⁸²Institute of Nuclear Physics Polish Academy of Sciences, Krakow; Poland.
- ⁸³Faculty of Science, Kyoto University, Kyoto; Japan.
- ⁸⁴Kyoto University of Education, Kyoto; Japan.
- ⁸⁵Research Center for Advanced Particle Physics and Department of Physics, Kyushu University, Fukuoka ; Japan.
- ⁸⁶Instituto de Física La Plata, Universidad Nacional de La Plata and CONICET, La Plata; Argentina.
- ⁸⁷Physics Department, Lancaster University, Lancaster; United Kingdom.
- ⁸⁸Oliver Lodge Laboratory, University of Liverpool, Liverpool; United Kingdom.
- ⁸⁹Department of Experimental Particle Physics, Jožef Stefan Institute and Department of Physics, University of Ljubljana, Ljubljana; Slovenia.
- ⁹⁰School of Physics and Astronomy, Queen Mary University of London, London; United Kingdom.
- ⁹¹Department of Physics, Royal Holloway University of London, Egham; United Kingdom.
- ⁹²Department of Physics and Astronomy, University College London, London; United Kingdom.
- ⁹³Louisiana Tech University, Ruston LA; United States of America.
- ⁹⁴Fysiska institutionen, Lunds universitet, Lund; Sweden.
- ⁹⁵Centre de Calcul de l'Institut National de Physique Nucléaire et de Physique des Particules (IN2P3), Villeurbanne; France.
- ⁹⁶Departamento de Física Teórica C-15 and CIAFF, Universidad Autónoma de Madrid, Madrid; Spain.
- ⁹⁷Institut für Physik, Universität Mainz, Mainz; Germany.
- ⁹⁸School of Physics and Astronomy, University of Manchester, Manchester; United Kingdom.
- ⁹⁹CPPM, Aix-Marseille Université, CNRS/IN2P3, Marseille; France.
- ¹⁰⁰Department of Physics, University of Massachusetts, Amherst MA; United States of America.
- ¹⁰¹Department of Physics, McGill University, Montreal QC; Canada.
- ¹⁰²School of Physics, University of Melbourne, Victoria; Australia.
- ¹⁰³Department of Physics, University of Michigan, Ann Arbor MI; United States of America.
- ¹⁰⁴Department of Physics and Astronomy, Michigan State University, East Lansing MI; United States of America.
- ¹⁰⁵B.I. Stepanov Institute of Physics, National Academy of Sciences of Belarus, Minsk; Belarus.

- ¹⁰⁶Research Institute for Nuclear Problems of Byelorussian State University, Minsk; Belarus.
- ¹⁰⁷Group of Particle Physics, University of Montreal, Montreal QC; Canada.
- ¹⁰⁸P.N. Lebedev Physical Institute of the Russian Academy of Sciences, Moscow; Russia.
- ¹⁰⁹Institute for Theoretical and Experimental Physics (ITEP), Moscow; Russia.
- ¹¹⁰National Research Nuclear University MEPhI, Moscow; Russia.
- ¹¹¹D.V. Skobeltsyn Institute of Nuclear Physics, M.V. Lomonosov Moscow State University, Moscow; Russia.
- ¹¹²Fakultät für Physik, Ludwig-Maximilians-Universität München, München; Germany.
- ¹¹³Max-Planck-Institut für Physik (Werner-Heisenberg-Institut), München; Germany.
- ¹¹⁴Nagasaki Institute of Applied Science, Nagasaki; Japan.
- ¹¹⁵Graduate School of Science and Kobayashi-Maskawa Institute, Nagoya University, Nagoya; Japan.
- ¹¹⁶Department of Physics and Astronomy, University of New Mexico, Albuquerque NM; United States of America.
- ¹¹⁷Institute for Mathematics, Astrophysics and Particle Physics, Radboud University Nijmegen/Nikhef, Nijmegen; Netherlands.
- ¹¹⁸Nikhef National Institute for Subatomic Physics and University of Amsterdam, Amsterdam; Netherlands.
- ¹¹⁹Department of Physics, Northern Illinois University, DeKalb IL; United States of America.
- ¹²⁰^(a)Budker Institute of Nuclear Physics and NSU, SB RAS, Novosibirsk;^(b)Novosibirsk State University Novosibirsk; Russia.
- ¹²¹Institute for High Energy Physics of the National Research Centre Kurchatov Institute, Protvino; Russia.
- ¹²²Department of Physics, New York University, New York NY; United States of America.
- ¹²³Ohio State University, Columbus OH; United States of America.
- ¹²⁴Faculty of Science, Okayama University, Okayama; Japan.
- ¹²⁵Homer L. Dodge Department of Physics and Astronomy, University of Oklahoma, Norman OK; United States of America.
- ¹²⁶Department of Physics, Oklahoma State University, Stillwater OK; United States of America.
- ¹²⁷Palacký University, RCPTM, Joint Laboratory of Optics, Olomouc; Czech Republic.
- ¹²⁸Center for High Energy Physics, University of Oregon, Eugene OR; United States of America.
- ¹²⁹LAL, Université Paris-Sud, CNRS/IN2P3, Université Paris-Saclay, Orsay; France.
- ¹³⁰Graduate School of Science, Osaka University, Osaka; Japan.
- ¹³¹Department of Physics, University of Oslo, Oslo; Norway.
- ¹³²Department of Physics, Oxford University, Oxford; United Kingdom.
- ¹³³LPNHE, Sorbonne Université, Paris Diderot Sorbonne Paris Cité, CNRS/IN2P3, Paris; France.
- ¹³⁴Department of Physics, University of Pennsylvania, Philadelphia PA; United States of America.
- ¹³⁵Konstantinov Nuclear Physics Institute of National Research Centre "Kurchatov Institute", PNPI, St. Petersburg; Russia.
- ¹³⁶Department of Physics and Astronomy, University of Pittsburgh, Pittsburgh PA; United States of America.
- ¹³⁷^(a)Laboratório de Instrumentação e Física Experimental de Partículas - LIP;^(b)Departamento de Física, Faculdade de Ciências, Universidade de Lisboa, Lisboa;^(c)Departamento de Física, Universidade de Coimbra, Coimbra;^(d)Centro de Física Nuclear da Universidade de Lisboa, Lisboa;^(e)Departamento de Física, Universidade do Minho, Braga;^(f)Departamento de Física Teórica y del Cosmos, Universidad de Granada, Granada (Spain);^(g)Dep Física and CEFITEC of Faculdade de Ciências e Tecnologia, Universidade Nova de Lisboa, Caparica; Portugal.
- ¹³⁸Institute of Physics, Academy of Sciences of the Czech Republic, Prague; Czech Republic.
- ¹³⁹Czech Technical University in Prague, Prague; Czech Republic.

- ¹⁴⁰Charles University, Faculty of Mathematics and Physics, Prague; Czech Republic.
- ¹⁴¹Particle Physics Department, Rutherford Appleton Laboratory, Didcot; United Kingdom.
- ¹⁴²IRFU, CEA, Université Paris-Saclay, Gif-sur-Yvette; France.
- ¹⁴³Santa Cruz Institute for Particle Physics, University of California Santa Cruz, Santa Cruz CA; United States of America.
- ¹⁴⁴(^a)Departamento de Física, Pontificia Universidad Católica de Chile, Santiago; (^b)Departamento de Física, Universidad Técnica Federico Santa María, Valparaíso; Chile.
- ¹⁴⁵Department of Physics, University of Washington, Seattle WA; United States of America.
- ¹⁴⁶Department of Physics and Astronomy, University of Sheffield, Sheffield; United Kingdom.
- ¹⁴⁷Department of Physics, Shinshu University, Nagano; Japan.
- ¹⁴⁸Department Physik, Universität Siegen, Siegen; Germany.
- ¹⁴⁹Department of Physics, Simon Fraser University, Burnaby BC; Canada.
- ¹⁵⁰SLAC National Accelerator Laboratory, Stanford CA; United States of America.
- ¹⁵¹Physics Department, Royal Institute of Technology, Stockholm; Sweden.
- ¹⁵²Departments of Physics and Astronomy, Stony Brook University, Stony Brook NY; United States of America.
- ¹⁵³Department of Physics and Astronomy, University of Sussex, Brighton; United Kingdom.
- ¹⁵⁴School of Physics, University of Sydney, Sydney; Australia.
- ¹⁵⁵Institute of Physics, Academia Sinica, Taipei; Taiwan.
- ¹⁵⁶(^a)E. Andronikashvili Institute of Physics, Iv. Javakhishvili Tbilisi State University, Tbilisi; (^b)High Energy Physics Institute, Tbilisi State University, Tbilisi; Georgia.
- ¹⁵⁷Department of Physics, Technion, Israel Institute of Technology, Haifa; Israel.
- ¹⁵⁸Raymond and Beverly Sackler School of Physics and Astronomy, Tel Aviv University, Tel Aviv; Israel.
- ¹⁵⁹Department of Physics, Aristotle University of Thessaloniki, Thessaloniki; Greece.
- ¹⁶⁰International Center for Elementary Particle Physics and Department of Physics, University of Tokyo, Tokyo; Japan.
- ¹⁶¹Graduate School of Science and Technology, Tokyo Metropolitan University, Tokyo; Japan.
- ¹⁶²Department of Physics, Tokyo Institute of Technology, Tokyo; Japan.
- ¹⁶³Tomsk State University, Tomsk; Russia.
- ¹⁶⁴Department of Physics, University of Toronto, Toronto ON; Canada.
- ¹⁶⁵(^a)TRIUMF, Vancouver BC; (^b)Department of Physics and Astronomy, York University, Toronto ON; Canada.
- ¹⁶⁶Division of Physics and Tomonaga Center for the History of the Universe, Faculty of Pure and Applied Sciences, University of Tsukuba, Tsukuba; Japan.
- ¹⁶⁷Department of Physics and Astronomy, Tufts University, Medford MA; United States of America.
- ¹⁶⁸Department of Physics and Astronomy, University of California Irvine, Irvine CA; United States of America.
- ¹⁶⁹Department of Physics and Astronomy, University of Uppsala, Uppsala; Sweden.
- ¹⁷⁰Department of Physics, University of Illinois, Urbana IL; United States of America.
- ¹⁷¹Instituto de Física Corpuscular (IFIC), Centro Mixto Universidad de Valencia - CSIC, Valencia; Spain.
- ¹⁷²Department of Physics, University of British Columbia, Vancouver BC; Canada.
- ¹⁷³Department of Physics and Astronomy, University of Victoria, Victoria BC; Canada.
- ¹⁷⁴Fakultät für Physik und Astronomie, Julius-Maximilians-Universität Würzburg, Würzburg; Germany.
- ¹⁷⁵Department of Physics, University of Warwick, Coventry; United Kingdom.
- ¹⁷⁶Waseda University, Tokyo; Japan.
- ¹⁷⁷Department of Particle Physics, Weizmann Institute of Science, Rehovot; Israel.
- ¹⁷⁸Department of Physics, University of Wisconsin, Madison WI; United States of America.

¹⁷⁹Fakultät für Mathematik und Naturwissenschaften, Fachgruppe Physik, Bergische Universität Wuppertal, Wuppertal; Germany.

¹⁸⁰Department of Physics, Yale University, New Haven CT; United States of America.

¹⁸¹Yerevan Physics Institute, Yerevan; Armenia.

^a Also at Borough of Manhattan Community College, City University of New York, NY; United States of America.

^b Also at California State University, East Bay; United States of America.

^c Also at Centre for High Performance Computing, CSIR Campus, Rosebank, Cape Town; South Africa.

^d Also at CERN, Geneva; Switzerland.

^e Also at CPPM, Aix-Marseille Université, CNRS/IN2P3, Marseille; France.

^f Also at Département de Physique Nucléaire et Corpusculaire, Université de Genève, Genève; Switzerland.

^g Also at Departament de Física de la Universitat Autònoma de Barcelona, Barcelona; Spain.

^h Also at Departamento de Física Teórica y del Cosmos, Universidad de Granada, Granada (Spain); Spain.

ⁱ Also at Departamento de Física, Instituto Superior Técnico, Universidade de Lisboa, Lisboa; Portugal.

^j Also at Department of Applied Physics and Astronomy, University of Sharjah, Sharjah; United Arab Emirates.

^k Also at Department of Financial and Management Engineering, University of the Aegean, Chios; Greece.

^l Also at Department of Physics and Astronomy, University of Louisville, Louisville, KY; United States of America.

^m Also at Department of Physics and Astronomy, University of Sheffield, Sheffield; United Kingdom.

ⁿ Also at Department of Physics, California State University, Fresno CA; United States of America.

^o Also at Department of Physics, California State University, Sacramento CA; United States of America.

^p Also at Department of Physics, King's College London, London; United Kingdom.

^q Also at Department of Physics, St. Petersburg State Polytechnical University, St. Petersburg; Russia.

^r Also at Department of Physics, Stanford University; United States of America.

^s Also at Department of Physics, University of Fribourg, Fribourg; Switzerland.

^t Also at Department of Physics, University of Michigan, Ann Arbor MI; United States of America.

^u Also at Dipartimento di Fisica E. Fermi, Università di Pisa, Pisa; Italy.

^v Also at Giresun University, Faculty of Engineering, Giresun; Turkey.

^w Also at Graduate School of Science, Osaka University, Osaka; Japan.

^x Also at Hellenic Open University, Patras; Greece.

^y Also at Horia Hulubei National Institute of Physics and Nuclear Engineering, Bucharest; Romania.

^z Also at II. Physikalisches Institut, Georg-August-Universität Göttingen, Göttingen; Germany.

^{aa} Also at Institutio Catalana de Recerca i Estudis Avancats, ICREA, Barcelona; Spain.

^{ab} Also at Institut für Experimentalphysik, Universität Hamburg, Hamburg; Germany.

^{ac} Also at Institute for Mathematics, Astrophysics and Particle Physics, Radboud University Nijmegen/Nikhef, Nijmegen; Netherlands.

^{ad} Also at Institute for Particle and Nuclear Physics, Wigner Research Centre for Physics, Budapest; Hungary.

^{ae} Also at Institute of Particle Physics (IPP); Canada.

^{af} Also at Institute of Physics, Academia Sinica, Taipei; Taiwan.

^{ag} Also at Institute of Physics, Azerbaijan Academy of Sciences, Baku; Azerbaijan.

^{ah} Also at Institute of Theoretical Physics, Ilia State University, Tbilisi; Georgia.

^{ai} Also at Instituto de Física Teórica de la Universidad Autónoma de Madrid; Spain.

^{aj} Also at Istanbul University, Dept. of Physics, Istanbul; Turkey.

^{ak} Also at LAL, Université Paris-Sud, CNRS/IN2P3, Université Paris-Saclay, Orsay; France.

- al* Also at Louisiana Tech University, Ruston LA; United States of America.
- am* Also at LPNHE, Sorbonne Université, Paris Diderot Sorbonne Paris Cité, CNRS/IN2P3, Paris; France.
- an* Also at Manhattan College, New York NY; United States of America.
- ao* Also at Moscow Institute of Physics and Technology State University, Dolgoprudny; Russia.
- ap* Also at National Research Nuclear University MEPhI, Moscow; Russia.
- aq* Also at Physikalisches Institut, Albert-Ludwigs-Universität Freiburg, Freiburg; Germany.
- ar* Also at School of Physics, Sun Yat-sen University, Guangzhou; China.
- as* Also at The City College of New York, New York NY; United States of America.
- at* Also at The Collaborative Innovation Center of Quantum Matter (CICQM), Beijing; China.
- au* Also at Tomsk State University, Tomsk, and Moscow Institute of Physics and Technology State University, Dolgoprudny; Russia.
- av* Also at TRIUMF, Vancouver BC; Canada.
- aw* Also at Università di Napoli Parthenope, Napoli; Italy.
- * Deceased